12-2023

Computational Study About Noncovalent Bonding Systems Involving Halogen, Chalcogen and Pnicogen Bonds

Jia Lu
Utah State University, jia.lu@usu.edu

COMPUTATIONAL STUDY ABOUT NONCOVALENT BONDING SYSTEMS INVOLVING HALOGEN, CHALCOGEN AND PNICOGEN BONDS

by

Jia Lu

A thesis submitted in partial fulfillment
of the requirements for the degree

of

MASTER OF SCIENCE

in

Chemistry

Approved:

Steve Scheiner, Ph.D. Major Professor	Tianbiao Liu, Ph.D. Committee Member
Tuan Trinh, Ph.D. Committee Member	David Britt, Ph.D. Committee Member

D. Richard Cutler, Ph.D.
Vice Provost of Graduate Studies

UTAH STATE UNIVERSITY
Logan, Utah

2023

ABSTRACT

The Computational Study about Noncovalent Bonding Systems Involving Halogen, Chalcogen and Pnicogen Bonds

by

Jia Lu, Master of Science

Utah State University, 2023

Major Professor: Dr. Steve Scheiner
Department: Chemistry and Biochemistry

After hydrogen bonds (B-H···B) are well studied and understood by scientists and researchers, halogen bonds (R-X···B) have drawn attention due to the similarities in bonding format and geometries. However, it is not straightforward to understand how the overall negative halogen atoms interact with the electronegative chemical group, which is usually a Lewis base until scientists proved the existence of the σ-hole, which is the positive region surrounding the halogen atom X directly opposite the R group. This thesis included 6 projects which first analyzed and compared halogen bonds, chalcogen bonds, pnicogen bonds with hydrogen bonds in steric repulsion, monomer deformation and rearrangement, displacement of Molecular Electrostatic Potential maxima by lone pairs, and the complete absence due to opposite position of σ-bonds. Then the research was extended to the halogen transfer in symmetric (between two same molecules) and asymmetric systems (between two different molecules). In either case, the potential contains a single symmetric well for short halogen bond length and transferred to a double well when the distance was increased. Furthermore, the partial transfer of halogen

as bridging atom between two molecules are calculated. The degree of halogen transfer to form an ion pair is small even when a strong acid is combined with a strong base.

Then the research focused on the analysis on the relationship between energetics and IR spectra, NMR shielding compared among halogen, chalcogen and pnicogen bonds. Atomic charges and electron density shifts are also calculated to accomplish the through study of this project. The last but not lease project is to extend Badger-Bauer rules from hydrogen bonds to halogen, chalcogen and pnicogen bonds. Badger-Bauer rules states the spectroscopic change were linearly related to the bond strength of hydrogen bonds. The theory extension will improve the understanding of bond strength of a specific bond in the complicated systems by detecting the spectroscopic change.

(177 pages)

PUBLIC ABSTRACT

The Computational Study about Noncovalent Bonding Systems Involving Halogen, Chalcogen and Pnicogen Bonds

Jia Lu

First terms used in this thesis are introduced and defined as follows. In the periodic table, the elements in the 17th column are named halogen including fluorine (F), chlorine (Cl), bromine (Br) and iodine (I). The elements in the 16th column are named chalcogen including oxygen (O), sulfur (S), selenium (Se) and tellurium (Te). The elements in the 15th column are named pnicogen including nitrogen (N), phosphorus (P), arsenic (As) and antimony (Sb).

After hydrogen bonds (B-H···B) are well studied and understood by scientists and researchers, halogen bonds (R-X···B) have drawn attention due to the similarities in bonding format and geometries. However, it is not straightforward to understand how the overall negative halogen atoms interact with the electronegative chemical group, which is usually a Lewis base until scientists proved the existence of the positive region surrounding the halogen atom X directly opposite the R group by Molecular Electrostatic Potential analysis. This thesis studied the detailed structural, geometric and spectroscopic features quantitatively by computational chemistry. The research studied the halogen transfer in symmetric (between two same molecules) and asymmetric systems (between two different molecules). In either case, the potential contains a single symmetric well for short halogen bond length and transferred to a double well when the distance was increased. Furthermore, the partial transfer calculations of halogen as bridging atom

between two molecules suggests the degree of halogen transfer to form an ion pair is small even when a strong acid is combined with a strong base.

Moreover, the thesis extended the application of Badger-Bauer rules from hydrogen bonds to halogen, chalcogen and pnicogen bonds. Badger-Bauer rules states the spectroscopic change were linearly related to the bond strength of hydrogen bonds. The theory extension will improve the understanding of bond strength of a specific bond in the complicated systems by detecting the spectroscopic change.

ACKNOWLEDGMENTS

This thesis and my academic research are possibly made and inspired by all the awesome and nice people I met in my life as a graduate student.

First of all, my sincerest appreciation was expressed to my academic advisor and Major Professor Steve Scheiner, an amazing advisor and professional scientist. He is an outstanding advisor who supported me strongly over my entire program. I learned a lot whenever I have a conversation with him. He provided me with tons of great ideas, inspirations and encouragements to develop my academic research. His wisdom and kindness not only offered effective and useful suggestions about my research but also warmed my life and teach me valuable life experiences especially in the most difficult time. It has been a great blessing for me to have him as my academic advisor over the past few years. He is always by my side to help me walk through the tough road of scientific research. He is an exceptional person, advisor and teacher.

Second, I'd like to extend my sincere gratitude to my committee members: Prof. Tianbiao Liu, Prof. Tuan Trinh and Prof. David Britt. They all offered valuable comments, enlightening guidance, fruitful discussions, strong support and encouragement. Moreover, many thanks to Cindy Weatbrook, my graduate program coordinator. She is such a nice and responsible person to help me smooth the procedure of my graduation. Also her big and bright smiles always warm my life. I'm grateful for Buckley Banham who provides instant technical support and Tia Lawrence, who assisted me with organizing meetings and presentations. During my time at Utah State University, I appreciate I have been supported by the National Science Foundation under Grant

No. 1954310 to Prof. Steve Scheiner and I feel honored to be hired as a Teaching Assistant (TA) in the Department of Chemistry and Biochemistry. This experience provided me with the great opportunities to learn teaching skills and make friends with students. I feel very proud when my students enjoyed my teaching and were grateful with my help. I really appreciate Dr. Douglas Harris and Dr. Robert Alumbaugh, the professors in charge of the course of my TA position. They taught me great teaching skills and to treat the students with patience.

I would like to extend my appreciation to my family who is the most cherished present for me, to my mother, Shaohui Deng and my father, Zhong Lu. Family supports me to finish my thesis emotionally. I love them so much.

Jia Lu

CONTENTS

Page

LIST OF TABLES

Page

LIST OF FIGURES

Page

CHAPTER 1 INTRODUCTION

1.1 Bonds definition

Chemistry is a scientific subject based on the experiments and empirical experience. However, as the theories and new concepts and tools are developed significantly, considering the time consuming and uncertainty of the experiments, computational chemistry turns up to a competitive and effective tool to study the chemistry theory and provides useful and reliable proofs, exploration and inspirations to experiments. Quantum chemistry provides various accurate and efficient tools that applies the concept of molecular orbitals (MOs). MOs are applied for calculations and quantitative values on different properties of chemical systems by delocalizing over the whole molecule.

First terms used in this thesis are introduced and defined as follows. In the periodic table, the elements in the 17^{th} column are named halogen including fluorine (F), chlorine (Cl), bromine (Br) and iodine (I). The elements in the 16^{th} column are named chalcogen including oxygen (O), sulfur (S), selenium (Se) and tellurium (Te). The elements in the 15^{th} column are named pnicogen including nitrogen (N), phosphorus (P), arsenic (As) and antimony (Sb). The bonds formed by these elements are named as halogen (XB), chalcogen (YB) and pnicogen bonds (ZB) with a bond type R-A$\cdots$B, where A=X, Y, Z, R is Lewis acid and B is Lewis base. A hypervalent molecule is an example of exception from the octet rule, a molecule surrounding by multiple groups, which obviously bears more than eight electrons in the valence shells.

Gilbert Lewis proposed the molecule model that shared electron-pair to form

chemical covalent bonds in 1916[1], before the quantum chemistry was developed. Lewis built a classic model to predict structures which are still considered the most successful and generally adopted theory of chemical bonding now based on the experimental chemical data only available at that time. The Lewis model described atoms shared the electron pairs to form chemical bonds and lone pairs.

1.2 Computational Methods

Quantum calculations were performed at the Møller–Plesset perturbation theory to second order (MP2)[2] level or with the M06-2X variant[3] of DFT using the Gaussian-09[4] program suit. The basis set, aug-cc- pVDZ was executed to all the atoms except the fourth row atoms in the periodic table, I, Te and Sb, which were calculated by the aug-cc-pVDZ-PP pseudopotential[5, 6] which take account of relativistic effects. The effectiveness and accuracy of this level of theory has been proved by a great deal of previous studies[7-16] of relevant systems. All the geometries studied were fully optimized with or without constrained conditions and checked by frequencies to confirm they were true minima.

The binding energy, E_b, is calculated by the energy difference between the sum of the energies of fully-optimized monomers and the complex, which was corrected for basis set superposition error via the counterpoise procedure[17-19] to eliminate superposition error. The interaction energy E_{int} is defined as the energy difference between the complex and all the optimized monomers which are within the context of the geometries in the optimized complex. In this way, this value refers to the interaction between the monomers which was deformed into the structures that was adopted ultimately in the complex. Therefore, the binding and interaction energy is different considering the deformed energy of each monomer changing from the fully-optimized structure to that

adopted in the optimized complex.

Analysis on molecular electrostatic potentials around each molecule were evaluated by the Multiwfn program[20] to figure out the maxima and minima on the isodensity electrostatic surface referring to ρ =0.001 au. Natural bonding orbital (NBO) analysis introduced by Weinhold[21, 22] proves to be one of the most useful and popular techniques analyzing the chemical interactions and charge distribution. NBO refers to the localized orbitals that depicts the bonding pattern of electron pairs in molecules which are defined in Lewis model. The AIMALL program[23] is applied to analyze the topology of the electron density[24, 25] of the molecules along the generated bond paths between atoms.

1.3 Badger-Bauer rules

It was discovered[26-28] that the hydrogen bond (HB) formation of a AH···D bond caused a red shift of the ν(AH) vibrational frequency relative to the monomer. Badger-Bauer rules[29] states the infrared spectroscopy (IR) changes have a linear correlation with the bond strength of the hydrogen bonds. It would be meaningful to extend these rules to halogen, chalcogen and pnicogen bonds, as well as consider whether NMR chemical shift will have a linear relationship to the bond strength. Does the frequency of the R-A stretching mode (where A=X, Y, and Z) shift to red and is this shift linearly related to the bond strength considering the similarities between HB and XB, YB, ZB?

This thesis answered the previous questions and focus on the quantitative analysis of the halogen, chalcogen and pnicogen interactions under certain conditions with the comparison to hydrogen bonds considering the similarities between those interactions. These kinds of bonds become more and more essential in various chemical and biological

systems. Hence, it is important to understand such interactions from a fundamental and theoretical point of view. This thesis is able to offer interpretation and intuitive pictures of structures, electronic and spectroscopic properties of various chemical systems and inspirations to the related future study. Such interaction analysis contributes to understanding how and why such interactions are formed and how the interaction is different under certain conditions.

CHAPTER 2 HALOGEN, CHALCOGEN, AND PNICOGEN BONDING INVOLVING HYPERVALENT ATOMS[a]

2.1 Introduction

Researchers have concentrated on the hydrogen bond (HB) [28, 30-33] over the past several decades to provide useful and through insights into the bonding nature. Although it was considered as one of the special bonds in chemistry, lots of recent work has proved that there exists a great amount of similar noncovalent bonding interactions[34-38]. The substitute of the bridging proton in HB by other electronegative atoms on the right side of the periodic table produces similar interactions. This kind of interactions are named after the family of the bridging atom, for instance, halogen, chalcogen, pnicogen or tetrel bond, which has many mutual features. From principles, the HB forms by a Coulombic interaction between the partially positive donor H and the partially negative region of the acceptor H atom. This is true for the cousins of HB, but with a wrinkle. Different from the H with a positive charge, the electronegative atoms are featured by a general negative charge. However, after analyzing the detailed distribution of the potential surrounding the halogen atom X[39, 40] in a halogen bond R-X, there is a positive charge region on halogen atom X across from the R group. This positive region is characterized as a σ-hole[41, 42], and attracts the negative charge on a surrounding nucleophile. Like the HB case, the halogen bond(XB) is not only held together by pure electrostatic attraction, but is also supplemented by attractions of electronic redistributions with various rubrics, for

[a] Coauthored by Steve Scheiner and Jia Lu. Reproduced from *Chem. Eur. J. 2018, 24, 8167-8177* with permission.

instance, orbital mixing, charge transfer, polarization, etc. It's worth of studying the details of all these added dispersive attractions.

The reasoning that exists in hydrogen bond and halogen bond can be generalized to other noncovalent bond with slight differences. While there is single σ-hole connected to the halogen atoms, other atoms such as chalcogen, pnicogen are characteristically associated with more than one σ-hole. So they are quite inclined to form hypervalent bond which involves a lot of covalent bonds.

2.2 Computational methods

Theoretical methods and modern computational skills provide a powerful tool for chemistry research, which can analyze the bond strength quantitatively and offer reference values for experiments.

Quantum calculations were performed at the Møller–Plesset perturbation theory to second order (MP2)[2] level using the Gaussian-09[4] program suit. The basis set, aug-cc-pVDZ was executed to all the atoms except the fourth row atoms in the periodic table, I, Te and Sb, which were calculated by the aug-cc-pVDZ-PP pseudopotential[5, 6] which take account of relativistic effects. The effectiveness and accuracy of this level of theory has been proved by a great deal of previous studies[7-16] of relevant systems.

All the geometries studied were fully optimized with or without constrained conditions and checked by frequencies to confirm they were true minima. The binding energy, E_b, is calculated by the energy difference between the sum of the energies of fully-optimized monomers and the complex, which was corrected for basis set superposition error via the counterpoise procedure[17-19]. The interaction energy E_{int} is defined as the energy difference between the complex and all the optimized monomers

which are within the context of the geometries in the optimized complex. In this way, this value refers to the interaction between the monomers which was deformed into the structures that was adopted ultimately in the complex. Therefore, the binding and interaction energy is different considering the deformed energy of each monomer changing from the fully-optimized structure to that adopted in the optimized complex. Analysis on molecular electrostatic potentials around each molecule were evaluated by the Multiwfn program[20] to figure out the maxima and minima on the isodensity electrostatic surface referring to ρ =0.001 au. Charge transfer was analyzed via the Natural Bond Orbital (NBO) technique[43]. Bond paths between atoms were elucidated by the AIM formalism using the AIMALL program[23] to analyze the topology of the electron density[24, 25] of the molecules. The total decomposition interaction energy was completed by the symmetry-adapted perturbation theory (SAPT) method[44, 45], with the calculation of the MOLPRO program[46].

2.3 Results and discussion

2.3.1 Perfluorinated Lewis Acids

The optimized geometries of the complexes of the various perfluorinated molecules with NH_3 are displayed in Table 2-1 which clearly shows the different sorts of structures. The XF_5 monomers with their lone pair on the central atom adopt a square pyramidal shape which persists in the complex. So there is a competition of sorts in terms of the preferred site for an approaching nucleophile. On one hand the lone pair that sits opposite the apical F atom would tend to repel the nucleophile. But a position opposite the apical X-F bond would have a tendency for a positive region of the

Molecular Electrostatic Potential (MEP) as the electronegative F atom sucks electron density out of this area, in a so-called σ-hole. In the case of IF_5, the lone pair predominates, and the σ-hole appears 135 ºfrom the F-I axis, a distortion of 45 ºfrom where it would be located in the absence of the I lone pair. It is for this reason that the NH_3 is also removed from a position directly opposite the apical F, with a θ(FI··N) angle of 145 º. This same deviation of the MEP maximum from linearity appears also in ClF_5 and BrF_5, and in almost the same amount, with respective angles of 147 °and 142 ° respectively. It is therefore interesting to see in Figure 2-1 that the effect of this displacement of the σ-hole has no effect on ClF_5··NH_3 where the N is precisely opposite the apical F. (More on this system below.) There is more of an influence for the Br analogue but the 168 °(F-Br··N) angle is still much closer to linearity than would be indicated by the σ-hole. Perhaps the growing influence of the σ-hole position with larger X atom reflects the larger magnitude of $V_{s,max}$, which is collected in the last column of Table 2-1.

As the central halogen atom grows in size one sees that the intermolecular R(X··N) distance elongates quite significantly from 2.07 to 2.91 Å. As may be seen in Table 2-1, the shortness of the R(Cl··N) distance is reflected in a much stronger binding energy than for the other two halogen atoms. The density at the X··N bond critical point is likewise much larger for Cl, as are the NBO measures of halogen bond strength. E(2) in Table 2-1 refers to the transfer from the N lone pair to the σ*(X-F) antibonding orbital of the apical F atom. There is also some transfer into the other σ*(X-F) orbitals of the other F atoms, denoted E(2)* in Table 2-1. In the case of ClF_5, the former is quite large, and the latter only amounts to a total of 0.99 kcal/mol for the two secondary interactions.

But the situation is quite different for X=Br and I, where the total secondary transfers are cumulatively larger than that involving the apical F. Nonetheless, by all measures the Cl··N halogen bond is quite a bit stronger than that for the two heavier halogens. This trend is opposite to that which would have been predicted based upon the intensity of the σ-hole, listed as Vs,max , evaluated at ρ=0.001 au, in the penultimate column of Table 2-1. This quantity increases in the order Cl < Br < I, which fulfills expectations based upon electronegativity and polarizability. But its behavior contrary to halogen bond strength demonstrates that this aspect of the MEP is a poor indicator.

Part of the explanation of this deviation arises because the Cl··N bond has some of the hallmarks of a covalent bond, at least in part. Its bond length of 2.067 Å is only slightly longer than the F-Cl bonds which all exceed 1.8 Å. The large density at its bond critical point of 0.11 au approaches that of true covalent bonds, only 0.03 au smaller than the same quantities for the Cl-F bonds. The formation of this bond also induces a good deal of distortion of the ClF_5 monomer. There is a very large 30 kcal/mol difference between the binding and interaction energies in this complex which is due to the monomer deformation energy which stretches the Cl-F bonds by more than 0.1 Å upon forming the complex with NH_3. The incipient Cl-N bond also causes the four F atoms in the pyramid base to move outward, away from the apical F, by 9 °. This sort of motion toward the Cl-N bond would be consistent with a picture wherein the bulky Cl lone pair is pulled and constricted as it engages in a covalent bond with N, thereby reducing its repulsions with the four Cl-F bonds. None of the above are true of the complexes of NH_3 with BrF_5 and IF_5, which retain their noncovalent halogen bond character.

Turning next to chalcogen atoms Y, one can envision either a hexavalent or

tetravalent bonding situation. The YF_6 atoms will have no Y lone pairs while there will be one such pair in YF_4. The YF_6 molecule will take on an octahedral shape so be unable to develop a σ-hole directly opposite any F atom. Instead, each such hole appears on a face of the octahedron, equally spaced between three F atoms. It is therefore to this point which a nucleophile is attracted, as illustrated in Figure 2-1. But partly due to the congested nature of this area, coupled with the fairly small values of $V_{s,max}$, less than 40 kcal/mol, the N is unable to approach the Y atom very closely, with R(Y··N) distances all close to 4 Å. The shortest distance is associated with Y=Te. Indeed it is only for this large Y atom that there is any evidence of a chalcogen bond at all. Both SF_6 and SeF_6 are bonded to NH_3 via a pair of NH··F H-bonds, as indicated by both AIM and NBO. While AIM does not register a true chalcogen bond for TeF_6, there is some NBO evidence. While there is no single Te-F bond directly opposite the N, there are three such bonds, which are partially opposite. The cumulative E(2) for transfer into these three σ*(Te-F) antibonds sums to 0.33 kcal/mol, and NBO shows no indication of a NH··F HB. The transition from H-bonds to a chalcogen bond on going from Se to Te is aided by the intensification of $V_{s,max}$ which rises to 38 kcal/mol for the larger atom. But in any case, the interaction between NH_3 and the hexafluorinated chalcogens, whether H-bond or chalcogen bond, is very weak, never exceeding 1 kcal/mol. Note, however, that if three of the F atoms of TeF_6 are replaced by H, the situation changes. The σ-hole on the H_3 face of the TeF_3H_3 molecule doubles in magnitude, and the N is pulled in to R(Te··N)=3.165 Å. The binding energy climbs up to 7.6 kcal/mol, and both NBO and AIM verify the presence of a true chalcogen bond, with only minimal H-bond contribution. It is worth stressing that the NH_3 approaches the Te directly, forgoing the

possibility of an approach along a TeH bond axis which could potentially result in a strong and linear TeH··N H-bond.

The alteration from hexavalent to tetravalent chalcogen produces a YF_4 monomer which contains a Y lone pair. The monomer thus adopts a "see-saw" geometry which includes a pair of axial F atoms, and two of the three equatorial sites are occupied by F atoms. There are thus openings in the equatorial plane where a nucleophile might approach Y. At the same time the NH_3 needs to avoid the Y lone pair which also lies in the equatorial plane. The σ-holes for YF_4 do indeed avoid the Y lone pair, lying 13 ºfrom a position directly opposite each of the equatorial F atoms. It is this avoidance of the lone pair that causes the F-Y··N angles in Figure 2-1 to all be somewhat less than 180 º. This deviation from F-Y··N linearity is smallest for SF_4 and increases as the chalcogen atom is enlarged. The intermolecular distance is at a maximum for Y=S, diminishes for Se, and then increases a small amount for Te. Some of the other measures of the chalcogen bond strength also reflect this trend with E(2) and ρ_{BCP} at their maxima for Se. On the other hand, the quickly rising values of E(2)* suggest that the secondary transfers into the three other Y-F antibonding orbitals are partly responsible for the similarly precipitous S < Se < Te increase in binding energy from 6.6 to 16.0 kcal/mol. It might be noted that a similar order pertains to $V_{s,max}$, evaluated at ρ=0.001 au. The difference between E_b and E_{int} reflects the deformation energy that occurs as the two monomers approach. While only 1.3 kcal/mol for SF_4, it grows with enlarging chalcogen atom, to 5.6 and 6.2 kcal/mol for SeF_4 and TeF_4, respectively. In other words, the deformation energy increases as the chalcogen bond gets stronger.

One might think that the MEP on the van der Waals surface of the monomer,

approximated by a density of 0.001 au, is a poor indicator of the incipient bonding that occurs at much closer interatomic distance. Another choice would be the density at the bond critical point, which occurs roughly halfway between the bonding atoms. $V_{s,max}$ was thus recomputed for each monomer, on the isodensity surface corresponding to ρ_{BCP} of each complex listed in Table 2-1. Lying much closer to the nuclei, these maxima displayed in the final column of Table 2-1 are of course much more positive. Nonetheless, they share many of the same trends as the 0.001 au maxima in the preceding column. The largest values are associated with the pnicogen bonds, and the smallest with the YF_6 chalcogen bonds. On the other hand, the maxima evaluated at the bond critical points do not necessarily increase with the size of the central atom, as witness the halogen and pnicogen atoms.

Decomposition of the total interaction energy into its various components can offer additional insight into the nature of the bonding. SAPT decomposition of three sample complexes are compiled in Table 2-2. As the strength of the complex grows in the order halogen < chalcogen < pnicogen bond, so do their various components. ES is the dominant attractive term, followed by induction, and then by dispersion, except for $BrF_5\cdots NH_3$ where the two latter components are nearly equal. The concept of decomposition is a questionable one, however, when the two subunits are close to one another. The $AsF_5\cdots NH_3$ dimer, with a R(As··N) distance of only 2.1 Å, is a prime example. The exaggerated electrostatic and induction components, on the order of 100 kcal/mol, serves as a caution, as does the total SAPT interaction energy of -95 kcal/mol, twice that computed by the standard supermolecule approach.

Of all the interactions considered here, the pnicogen bonds to the pentavalent ZF_5

molecules are the strongest. The binding energy of $SbF_5\cdots NH_3$ reaches up to nearly 40 kcal/mol. The intermolecular distances reflect this bond strength, between 1.9 and 2.2 Å. The strengths of these bonds are reflected also in the AIM values of ρ_{BCP} which exceed 0.1 au in several cases, matched only by the halogen bond in $ClF_5\cdot\cdot NH_3$. The binding energy rises quickly along with the size of the pnicogen atom, as does the intensity of the σ-hole. On the other hand, the trends in some of the other quantities do not reflect these trends. For example, ρ_{BCP} is smallest for Z=Sb as is E(2). It might also be noted that the auxiliary E(2)* quantities for the four other Z-F antibonds are quite large for these pnicogen bonds, eclipsing the primary E(2). Another important issue for the ZF_5 systems is the magnitude of the monomer rearrangement upon complexation. Without any lone pair, the monomer adopts a pure trigonal bipyramid shape. As may be seen in Figure 2-1, in order to accommodate the NH_3, the monomer rearranges into a square pyramid shape. In the case of SbF_5, for example, this rearrangement costs 9.47 kcal/mol. This deformation energy is even larger for the smaller pnicogens, 16.3 and 22.7 kcal/mol for the Br and Cl analogues, respectively. Addition of these deformation energies to the binding energies in Table 2-1 yields a pure interaction energy, between pre-deformed monomers. These interaction energies are quite large, nearly 50 kcal/mol, and surprisingly insensitive to the nature of the pnicogen atom or to the magnitude of its σ-hole.

2.3.2 SeF_nH_{6-n}

Relations between MEP maxima and equilibrium geometries:

As was shown above, the replacement of several F atoms of TeF_6 by H produces some substantial changes in the complexation process with NH_3. An intensification of

the σ-hole occurs, in particular in the H_3 face of the octahedron. It is this positive region which draws in the base, and thereby forms a strong chalcogen bond. It is of some importance that the base eschews formation of a TeH··N HB in place of this chalcogen bond, nor does one see any NH··F HBs. This result brings to the fore the fundamental issue of how the replacement of highly electronegative atoms by H might affect the ability of the central atom to engage in a chalcogen bond. At what point do YH··N HBs take precedence over such a bond? And might these substitutions induce the formation of one or more NH··F HBs as a replacement for a chalcogen bond.

In order to thoroughly examine this question, the octahedral SeH_6 molecule was taken as a starting point, and then variable numbers of H atoms were replaced by F, all the way up to perfluorinated SeF_6. For each molecule, all maxima on the MEP was identified. Then NH_3 was added and the potential energy surface of the ensuing heterodimer was searched for all energy minima. The types of noncovalent interaction that hold together each dimer were characterized and quantified, and the geometries of the minima related to the location and intensities of MEP maxima.

As F atoms replace H one by one, on the SeH_6 molecule, there can be a number of different conformers. The two F atoms on SeF_2H_4 can be placed either anti or cis to one another, respectively disposed roughly 180 °or 90 °to one another within the octahedral geometry of the molecule. The three F atoms in SeF_3H_3 can all be within 90 °of one another, denoted cis,cis, or one pair can be anti, with the third F cis to both of them, here referred to as anti,cis. When there are more F than H atoms, it becomes more convenient for the notation to refer to the latter, wherein the two H atoms in the cis,cis conformation of SeF_4H_2 can either be anti or cis to one another.

Due to the octahedral structure of SeF_nH_{6-n}, the position directly opposite any particular substituent is occupied by another, precluding the possibility of strict σ-holes opposite any given Se-X/H bond. Most of the locations of $V_{s,max}$ then occur on one of the octahedral faces, denoted by the three atoms on that face. For example, the FH_2 face of $SeFH_5$ is situated between these three atoms, and there are four such faces, all equivalent to one another. There are also four equivalent H_3 faces on this same molecule. In some cases, there is a maximum in the MEP that occurs not on a face of three substituents, but rather between just two substituents. For example, the anti SeF_2H_4 molecule has four equivalent $V_{s,max}$ points in the equatorial SeH_4 plane, each located between a pair of H atoms, so are designated as H_2. Finally, in some cases, there is a maximum along an extension of a Se-F or Se-H covalent bond, i.e. on a vertex of the octahedron, denoted respectively as F or H.

The locations of each maximum are reported in Table 2-3, including both the value of $V_{s,max}$ and its distance from the central Se where appropriate. The last two columns are related to the equilibrium geometry of the $SeF_nH_{6-n}\cdots NH_3$ dimer that correlates with the particular maximum, wherever such correlations can be drawn. These dimers are illustrated in Figure 2-2. The first row of Table 2-3 shows for example, that there is only one minimum on the surface of $SeF_0H_6\cdots NH_3$, wherein the base lies along the H_3 face of the acid, as depicted in Figure 2-2a. The equilibrium R(Se··N) separation is 3.387 Å, and the binding energy of this complex is 0.93 kcal/mol. Replacement of one H atom of SeH_6 by F leads to two types of maxima on the MEP. There is one on each of the four H_3 faces and a single maximum along the extension of the SeH_a bond where the a subscript designates a position axial to the single F atom. The value of $V_{s,max}$ for the

former is 29.45 kcal/mol, a bit higher than the 22.83 kcal/mol for the latter. One equilibrium structure (Figure 2-2c) conforms nicely to the H_3 maximum, bound by 3.63 kcal/mol. The second MEP maximum also relates to an equilibrium structure, in this case bound by a SeH··N HB. This geometry is bound by less than the former, 2.48 vs 3.63 kcal/mol. But it is instructive to note that the most strongly bound dimer of all does not relate to a maximum in the MEP. This structure, shown in Figure 2-2b, is bound primarily by a NH··F HB, with smaller supplements from a pair of SeH··N HBs (see below for more detailed analysis). The geometry of this structure places the N atom on a FH_2 face but as Table 2-3 makes clear, there is no MEP maximum on this face.

The anti configuration of SeF_2H_4 contains a single type of MEP maximum between each pair of H atoms in the equatorial plane. That maximum corresponds to the single equilibrium dimer with NH_3, although a NH··F attraction pulls the NH_3 out of the HSeH plane, toward a FH_2 face, as displayed in Figure 2-2d. The cis geometry of SeF_2H_4 is also characterized by a single MEP maximum, which occurs in the H_3 face (Figure 2-2e). Although $V_{s,max}$ for this conformation is quite a bit larger than that for the cis geometry, the binding energy of 5.45 kcal/mol is only slightly larger than 4.37 kcal/mol for the anti configuration. Equilibrium structures were also sought for the FH_2 and F_2H faces of cis SeF_2H_4, but none were found, consistent with the absence of MEP maxima on those faces.

SeF_3H_3 can appear as either anti,cis or cis,cis combinations of the three F atoms. The former arrangement yields only a single MEP maximum on the HSeH bisector. But rather than appear as an equilibrium SeF_3H_3··NH_3 dimer, placement of the base along this position results in a proton transfer to an $SeF_3H_2^-$··NH_4^+ ion pair. The cis,cis structure

displays two separate types of MEP maximum. The first lies in the H_3 face, and is quite positive, with $V_{s,max}$ = 64.43 kcal/mol. The binding energy of the associated dimer in Figure 2-2f is correspondingly large: at -7.25 kcal/mol it represents the most tightly bound dimer of all those considered here. There is a second maximum in the F_3 face, but its $V_{s,max}$ is quite negative, so it is no surprise to see no corresponding equilibrium geometry. On the other hand, there are two equilibrium heterodimers for cis,cis SeF_3H_3 that are unconnected to any MEP maximum. The NH_3 approaches the F_2H and FH_2 faces in these two geometries (Figure 2-2g and Figure 2-2h) which are both bound by nearly 6 kcal/mol.

With respect to SeF_4H_2, the anti arrangement of the two H atoms yields a MEP maximum only on the extension of the two SiH bonds. Placement of the NH_3 in this position results in a transfer of the proximate proton directly to the NH_3, yielding the ion pair. When the two H atoms are cis to one another, a MEP maximum appears between them. Its high $V_{s,max}$ again results in a strongly bound dimer (Figure 2-2i) of 7.02 kcal/mol. The other maximum, on the F_3 face, is negative so unsurprisingly does not yield a stable dimer of the desired type, but instead rearranges to have a H atom of the NH_3 face the F atoms, engaging in a pair of NH··F HBs, as illustrated in Figure 2-2j.

There are three MEP maxima when only a single H atom is left on SeF_5H. The most intense occurs along the SeH axis, and another on each F_3 face. But placement of a NH_3 in either position results in a proton transfer to an ion pair. When NH_3 is placed coincident with a F_2H face, no minimum can be located. The eight equivalent MEP maxima on SeF_6 on each F_3 face are fairly positive in sign, with $V_{s,max}$=24.38 kcal/mol, but the ensuing dimer in Figure 2-2k is bound by less than 1 kcal/mol. The weak maxima

found along the SeF axes of both SeF_5H and SeF_6 do not yield minima either.

Analysis of Attractive Forces:

A cursory inspection of the dimer geometries in Figure 2-2 leads to questions as to the precise nature of the bonding in each. The roughly C_{3v} structure of the $SeF_6\cdot\cdot NH_3$ complex in Figure 2-2a, for example, could lead one to surmise the presence of a Se··N chalcogen bond, or one or more SeH··N HBs, or some combination thereof. The same could be said of many of the other equilibrium geometries in Figure 2-2. As the geometries of these dimers do not immediately and unambiguously point to a single type of attractive force in each, it becomes important to analyze the source of binding. As in the former cases, both AIM and NBO are used for this purpose. In the case of a Se chalcogen bond, it is typical to observe NBO charge transfer from the nonbonding lone pair of the Lewis base to a σ*(Se-R) antibonding orbital of the Lewis acid, where R is situated directly opposite the approaching base. Due to the octahedral structure of the SeF_nH_{6-n} molecules considered here, the NH_3 cannot lie directly opposite any one Se-R bond so this transfer will generally involve three such bonds, those that are most nearly opposite the N.

The pertinent NBO and AIM parameters are contained in Figure 2-2. Blue lines are drawn between atoms that are connected by an AIM bond path, along with the interatomic distance in Å (in black). The value of the density at each bond critical point ($x10^4$ au) is displayed alongside this path, in blue. The red number refers to the NBO value of E(2) (x100 kcal/mol) wherever there is charge transfer from the N lone pair to the appropriate σ* antibonding orbital. The large black number represents the binding energy of each dimer, and the green number refers to the value of $V_{s,max}$ on the Lewis

acid which the NH_3 is approaching, when such a maximum is present.

Taking SF_6··NH_3 in Figure 2-2a as an example, there are AIM bond paths from the N to two of the H atoms on SF_6, indicating a pair of SeH··N HBs. ρ_{BCP} is equal to 0.0085 au for each of these bonds, and there is a small $N_{lp} \rightarrow \sigma^*$(Se-H) charge transfer energy of 0.09 kcal/mol for each. (The latter two values are only displayed for one of these two equivalent bonds to avoid needless clutter of the figure.) There is discrepancy between the two methods with respect to a possible Se··N chalcogen bond. Whereas there is no AIM bond path between these two atoms, NBO indicates 0.27 kcal/mol of charge transfer from the N lone pair to the antibonding orbitals of the three Se-H bonds that are turned away from the N. Note that altogether these three interactions account for a total binding energy of less than 1 kcal/mol, consistent with their weakness, as well as the small value of $V_{s,max}$ of only 12.3 kcal/mol.

Neither AIM nor NBO suggest a chalcogen bond in Figure 2-1b where the two molecules are held together primarily by a NH··F HB which, with ρ_{BCP}=0.0153 au and E(2)=4.01 kcal/mol, is a rather strong one. This interaction is supplemented by a pair of reasonably strong SeH··N HBs, for a total binding energy of 4.06 kcal/mol. Neither AIM nor NBO suggest the presence of a chalcogen bond, which is not surprising in light of both the orientation of the NH_3 lone pair away from the Se, and the absence of a MEP maximum on the FH_2 face of the $SeFH_5$ molecule. The H_3 face of this same molecule contains a MEP maximum of magnitude 29 kcal/mol, so the geometry of the complex in Figure 2-1c turns the NH_3 lone pair more in line with the Se atom. Nonetheless, the Se··N chalcogen bond remains weak, with E(2) equal to only 0.44 kcal/mol, and no AIM bond path. Like the other geometry of this dimer, there are a pair of SeH··N HBs that

help stabilize it. It should be noted that the SFH_5 molecule also shows a MEP maximum along the Se-H axis (directly opposite Se-F), which leads to a geometry with a linear SeH··N HB and no hint of a chalcogen bond. However, this structure is not quite as stable as the two illustrated in Figure 2-2.

The anti SeF_2H_4 complex with NH_3 in Figure 2-2d contains three HBs, all of moderate strength, supplemented by what appears to be only a weak chalcogen bond. The cis configuration of this same acid, however, is characterized by a fairly intense σ-hole of 48.3 kcal/mol on its H_3 face which induces the NH_3 to turn its lone pair toward the Se, forming a Se··N chalcogen bond, measured by NBO E(2)=0.99 kcal/mol, as indicated in Figure 2-2e. Note that this value of E(2) exceeds the 0.79 kcal/mol for the SeH··N HB, but it is only the latter that is characterized by an AIM bond path.

Turning next to trisubstituted SeF_3H_3 the anti,cis conformer has a MEP maximum between each pair of H atoms, which is fairly intense at 48.7 kcal/mol. However, there is no equilibrium geometry of the dimer that corresponds to this position. The cis,cis conformer is interesting for a number of reasons. The three F atoms on cis-SeF_3H_3 intensify the σ-hole on its H_3 face to 64 kcal/mol, leading to what is probably the strongest chalcogen bond of those examined here, with R(Se··N)=3.11 Å and E(2)=2.25 kcal/mol. It is in this structure in Figure 2-2f that AIM for the first time confirms the presence of a chalcogen bond, with ρ_{BCP}=0.0118 au. With some supplementation by three SeH··N HBs, the total binding energy rises to 7.25 kcal/mol. (Note, however, that the latter HBs are manifested only in AIM, with no evidence of the NBO charge transfer that is characteristic of such bonds.) The other two structures involve the F_2H and FH_2 faces of SeF_3H_3 in Figure 2-2g and Figure 2-2h, but it is worth emphasizing that neither

of these faces contains a MEP maximum. Both of these complexes depend almost exclusively on HBs, with only weak indications of a chalcogen bond. And both are bound less tightly than is the chalcogen-bonded structure in Figure 2-2f. There is a maximum on the F_3 face of this molecule, but $V_{s,max}$ is quite negative so it is not surprising that there is no equilibrium geometry to which it corresponds.

The anti geometry of SeF_4H_2 contains a MEP maximum only along each SeH bond and does not lead to a minimum on the potential energy surface. The large value of $V_{s,max}$ on the HSeH bisector of the cis monomer better orients the NH_3 lone pair in Figure 2-2i, and E(2) for the chalcogen bond exceeds 1 kcal/mol. After supplementation by a pair of moderately strong SeH··N HBs, the binding energy reaches 7.02 kcal/mol. Considering the MEP maximum on the F_3 face, its negative value leads to a rearrangement to the bifurcated HB configuration in Figure 2-2j, bound by only 1.14 kcal/mol. As indicated in Table 2-3, the only $V_{s,max}$ of any consequence for SeF_5H occurs along the Se-H bond extension, so no stable dimer of the sort that might contain a chalcogen bond is present. The perfluorinated SeF_6 displays a MEP maximum on each of its F_3 faces which attracts the NH_3 molecule to this area. The complex does not contain a chalcogen bond, but instead relies for its weak attraction on a pair of distorted NH··F HBs. Note in Figure 2-2k that these bonds are so weak that there is little indication of their presence via NBO analysis.

2.4 Conclusions

In summary, the pentavalent ZF_5 molecules engage in the strongest interactions with NH_3. These pnicogen bond energies range between 25 and 37 kcal/mol, despite their burden of a substantial monomer deformation energy as ZF_5 converts from a trigonal

bipyramid to a square pyramid shape. When these distortions are factored in, the interaction energies between pre-deformed monomers are even larger, ranging up to 48 kcal/mol, and might even be characterized as partial covalent bonds. The chalcogen bonds involving tetravalent central atoms are not as strong but not weak by any means, covering the 6.6 - 16.0 kcal/mol range. Like the pnicogen bonds, these chalcogen bonds also strengthen as the central atom is enlarged. Halogen bonds involving XF_5 show an unusual pattern in that it is the lightest X=Cl atom which displays the strongest bond, with both Br and I roughly half that magnitude. By far the weakest of all are the interactions between hexavalent YF_6 and NH_3. In fact, these interactions would probably not even be categorized as chalcogen bonds at all, but are bound primarily by weak NH··F H-bonds. The presence of a lone pair on the central atom affects the position and magnitude of σ-holes, and influences angular characteristics of the complexes to a varying degree.

While the intensity and location of maxima on the MEP offer some guidance as to geometries and strengths of noncovalent bonds, they represent a clearly imperfect marker. On one hand, $V_{s,max}$ increases as the central atom grows in size for any central atom type, as does the binding energy. But in terms of comparison of the various bond types, there are some misleading patterns. For example, even though the YF_4 σ-holes are comparable to those for ZF_5, the binding and interaction energies of the former with NH_3 are very much smaller than those of the latter. The steric crowding in the octahedral YF_6 molecules prevent formation of significant chalcogen bonds, even when $V_{s,max}$ achieves a respectable magnitude as in TeF_6. But this problem can be countered to some extent by replacing three of the F atoms by H, which reduces steric repulsion and doubles the value

of $V_{s,max}$.

The additional substituents connected with hypervalency do more than simply crowd the central atom and potentially obstruct the path of a base toward it. The molecular geometries place σ-bonds directly opposite one another, which block the development of σ-holes. Lone pairs adopt positions that can either conflict directly with a σ-hole, displace it from its normally preferred direction, or weaken its intensity. Each of the hypervalent systems displays unique properties in this regard. In the case of halogen bonds, the base is able to approach the central halogen atom of XF_5 opposite the apical F atom of the square pyramidal molecule to engage in a reasonably strong halogen bond. This direction presents a conflict in that the X lone pair would produce a negative MEP, while a positive potential is associated with the XF antibonding orbital. As a result the MEP maxima are shifted away from the linear direction by 33 °, 37 °, and 45 ° respectively for Cl, Br, and I. The competition between these two effects is dependent upon the nature of the X atom. The θ (FX··N) angle varies from 180° for Cl, to 168° for Br, and 145 ° for I. In other words, the base is drawn closer toward the linear FX··N direction than would be the case if it were fully controlled by the $V_{s,max}$ position. There is little need for the spacious square pyramid to alter its shape to accommodate the base so the XB forms with very little deformation energy.

The Y lone pair in YF_4 lies in the equatorial plane, but not directly opposite any of the F-S bonds, so consequently only nudges the $V_{s,max}$ 12-15 ° from lying directly opposite these bonds. This deviation is reflected in the nonlinearity of the YF_4··NH_3 dimers, which again grows stronger along with the size of the central atom. As in the previous case, not much rearrangement is required to accommodate the base, so the

deformation energies are modest. The ZF_5 molecules undergo the most severe deformation, shifting their structure from trigonal bipyramid to square planar. Z has no lone pairs, so the base is free to approach directly opposite the apical F atom, with θ(FZ··N)=180°. Since the intermolecular steric interactions are small, the deformation energy arises from the internal rearrangement. It is in the YF_6 cases where intermolecular steric crowding is dominant. The fairly rigid octahedral shape prevents the F atoms from getting out of the way of the approaching base, which keeps the intermolecular distance long and the binding energies minimal, despite reasonably large values of $V_{s,max}$.

In connection with the interchange of F and H substituents, there are clear patterns seen when the H atoms of SeH_6 are replaced one by one by the much more electronegative F. The NH_3 is generally able to approach within bonding distance of the Lewis acid, despite the latter's crowded octahedral structure. The bonding is quite weak for SeH_6 but builds quickly as the H atoms are progressively replaced by F. The peak occurs when the NH_3 approaches the H_3 face of SeF_3H_3 where the N lone pair can transfer charge into three σ*(Se-F) antibonding orbitals in an unambiguous chalcogen bond. The strength of this interaction is aided by a rather intense MEP maximum that also lies on the H_3 face. Due to the congested nature of these acids, there are few dimer geometries which contain only a single type of attractive interaction. The aforementioned SeF_3H_3 complex, for example, also contains elements of three weaker SeH··N HBs. On that same line, the strongest interactions generally involve the approach of the NH_3 toward the H atoms of the Lewis acid, whether that involves SeH··N HBs or a bona fide Se··N chalcogen bond. It is this region which generally provides the most

positive MEP, although a number of stable dimers occur where there is no MEP maximum at all. These cases tend to invoke one or more NH··F HBs as the N lone pair turns away from the electronegative F atoms, leaving the NH_3 protons to better approach the latter.

Not all MEP maxima lead to equilibrium geometries, nor is such a maximum necessary for such a structure to arise. In the $SeFH_5$ case for example, its most stable dimer with NH_3 is not connected to a maximum in the MEP. The same can be said of the cis,cis conformer of SeF_3H_3, where two of the three optimized dimers, with binding energies in excess of 5 kcal/mol, do not have a corresponding $V_{s,max}$. Conversely, the anti,cis conformation of this same SeF_3H_3 displays a single MEP maximum, but no associated equilibrium structure. In some cases, the optimization beginning with the appropriate chalcogen bond led instead to SeH··N or NH··F HBs, or some combination thereof.

There are other studies in the literature that offer a means of testing the validity of the calculations presented here. Most of the prior work dealing with noncovalent interactions of hypervalent atoms concerns halogen bonds. Theoretical calculations suggested that halogen bond strengths involving trivalent X were roughly equivalent to their monovalent analogues. Like our own study of XF_5, these authors also noted secondary NBO charge transfer to the antibonding orbitals that are peripheral to the X··N axis. As in our own calculations, the base deviates significantly from a position directly opposite the apical F atom of BrF5.

In conclusion, hypervalency presents the study of noncovalent interactions with additional complexity. Issues related to steric repulsion, monomer deformation and

rearrangement, displacement of MEP maxima by lone pairs, or complete absence thereof due to opposite placement of σ-bonds, must all be considered. Depending on the particular combination of these factors, the noncovalent bond may be eliminated, whereas this bond can be strengthened in others.

Table 2-1. Equilibrium geometries, energetics, and other properties of complexes of AF_n with NH_3.

AF_n[a]	R Å	$-E_b$ kcal/mol	$-E_{int}$ kcal/mol	ρ_{BCP} au	E(2) kcal/mol	E(2)*,[b] kcal/mol	$V_{s,max}(\rho=0.001)$ kcal/mol	$V_{s,max}(\rho_{BCP})$ kcal/mol
halogen (1)								
ClF_5	2.067	16.93	46.82	0.1130	217.92	0.99/2	45.1	680.2
BrF_5	2.713	8.56	9.42	0.0310	3.84	5.69/4	53.6	259.2
IF_5	2.912	9.36	9.79	0.0243	2.01	5.54/2	64.2	272.5
chalcogen (0)								
SF_6	3.976	0.25	0.57	0.0039[c]	0	0.28/2[e]	17.0	41.6
SeF_6	3.974	0.62	0.66	0.0041[c]	0	0.33/2[e]	24.4	59.2
TeF_6	3.764	1.04	1.40	0.0064[d]	0.33/3	0	38.1	118.2
TeF_3H_3	3.165	7.57	7.76	0.0126	3.15/3	0.36/3[e]	70.0	176.8
chalcogen (1)								
SF_4	2.573	6.62	7.97	0.0337	14.69	3.71/1	50.7	273.5
SeF_4	2.354	10.99	15.64	0.0579	42.75	12.63/3	60.9	486.5
TeF_4	2.404	16.00	22.23	0.0574	31.66	24.05/3	69.0	552.5
pnicogen (0)								
PF_5	1.915	24.98	47.64	0.1056	38.04	95.32/4	48.0	1377.1
AsF_5	2.014	31.55	47.84	0.1027	33.74	98.43/4	60.5	934.2
SbF_5	2.204	37.46	46.93	0.0785	29.83	86.59/4	82.5	728.1

[a]number of lone pairs on central atom in parentheses

[b]Total charge transfer into peripheral antibonds, with number of such bonds after /

[c]average of $\rho(N\cdot\cdot F)$ and two $\rho(H\cdot\cdot F)$

[d]each of 3 $\rho(N\cdot\cdot F)$

[e]$F_{lp}\rightarrow\sigma^*(NH)$

Table 2-2. SAPT contributions to total interaction energy (kcal/mol) of Lewis acids with NH_3.

AF_n	ES	EX	IND[a]	DISP[b]	total
BrF_5	-22.84	25.87	-4.31	-4.91	-6.19
SeF_4	-53.53	68.20	-23.07	-8.96	-17.37
AsF_5	-117.59	135.15	-99.82	-13.20	-95.47

[a]includes exchange-induction term

[b]includes exchange-dispersion term

Table 2-3. Locations and values of MEP maxima surrounding SeFnH6-n, and equilibrium intermolecular separation and binding energy of complexes of each with NH3.

F	H		face	$V_{s,max}$ kcal/mol	R(Se-V) Å	R(Se-N) Å	$-E_b$ kcal/mol	bonding source
0	6		H_3	12.33	2.164	3.387	0.93	2 SeH··N
1	5		FH_2	No max	-	3.350	4.06	2 SeH··N NH··F
			H_3	29.45	2.148	3.332	3.63	2 SeH··N
			H_a	22.83	-		2.48	SeH··N
2	4	anti	H_2	28.90	2.239	3.280	4.37	2 SeH··N NH··F
		cis	H_3	48.29	2.106	3.246	5.45	SeH··N
3	3	anti, cis	H_2	48.68	2.181	no min		3 SeH··N
		cis, cis	H_3	64.43	2.036	3.110	7.25	
			F_2H	No max		3.306	5.74	SeH··N 2 NH··F
			FH_2	No max		3.289	5.63	2 SeH··N NH··F
			F_3	-22.66		no min		
4	2	anti	H	49.35		no min		
		cis	H_2	61.36	2.139	3.174	7.02	2 SeH··N
			F_3	-4.10	2.245	-	1.14	bif NH-F
5	1		F_3	11.37	2.168	no min		
			H	55.93		no min		
			F	-6.79		no min		
6	0		F_3	24.38	1.719	3.976	0.62	2 NH··F N··F
			F	0.58		no min		

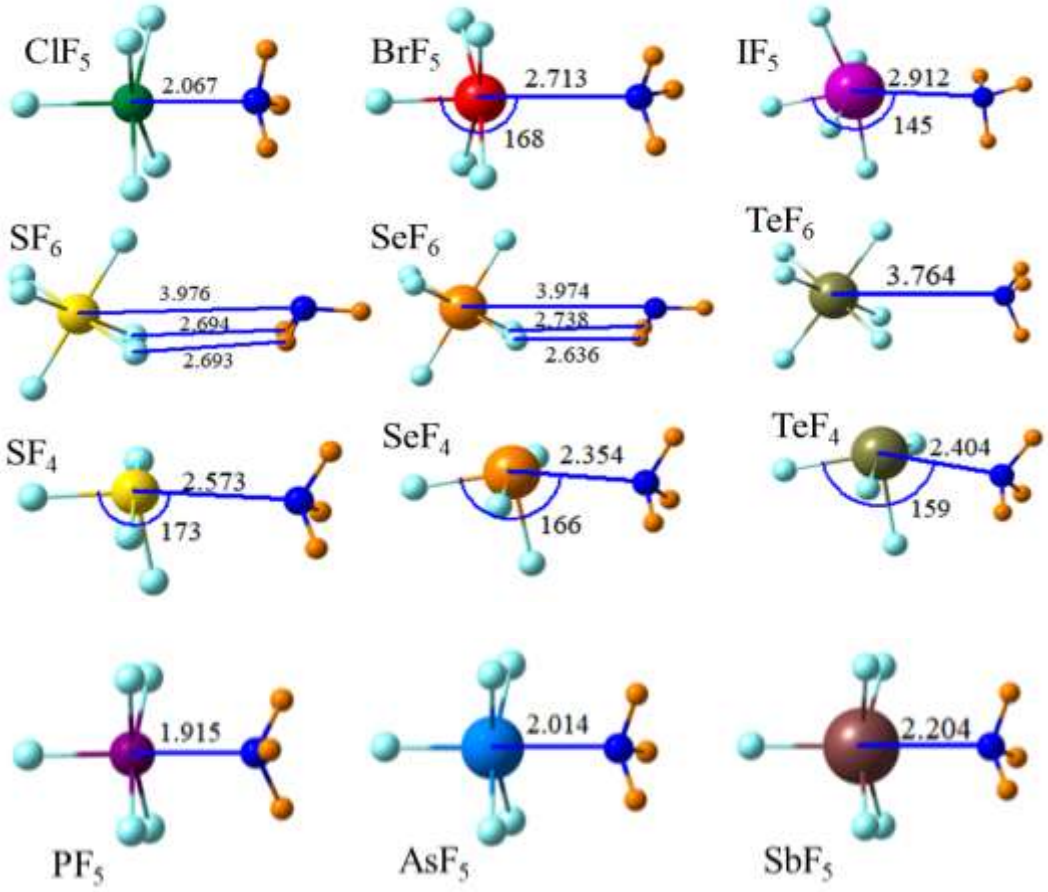

Figure 2-1. Equilibrium geometries of indicated molecules with NH3. Distances in Å, angles in degrees.

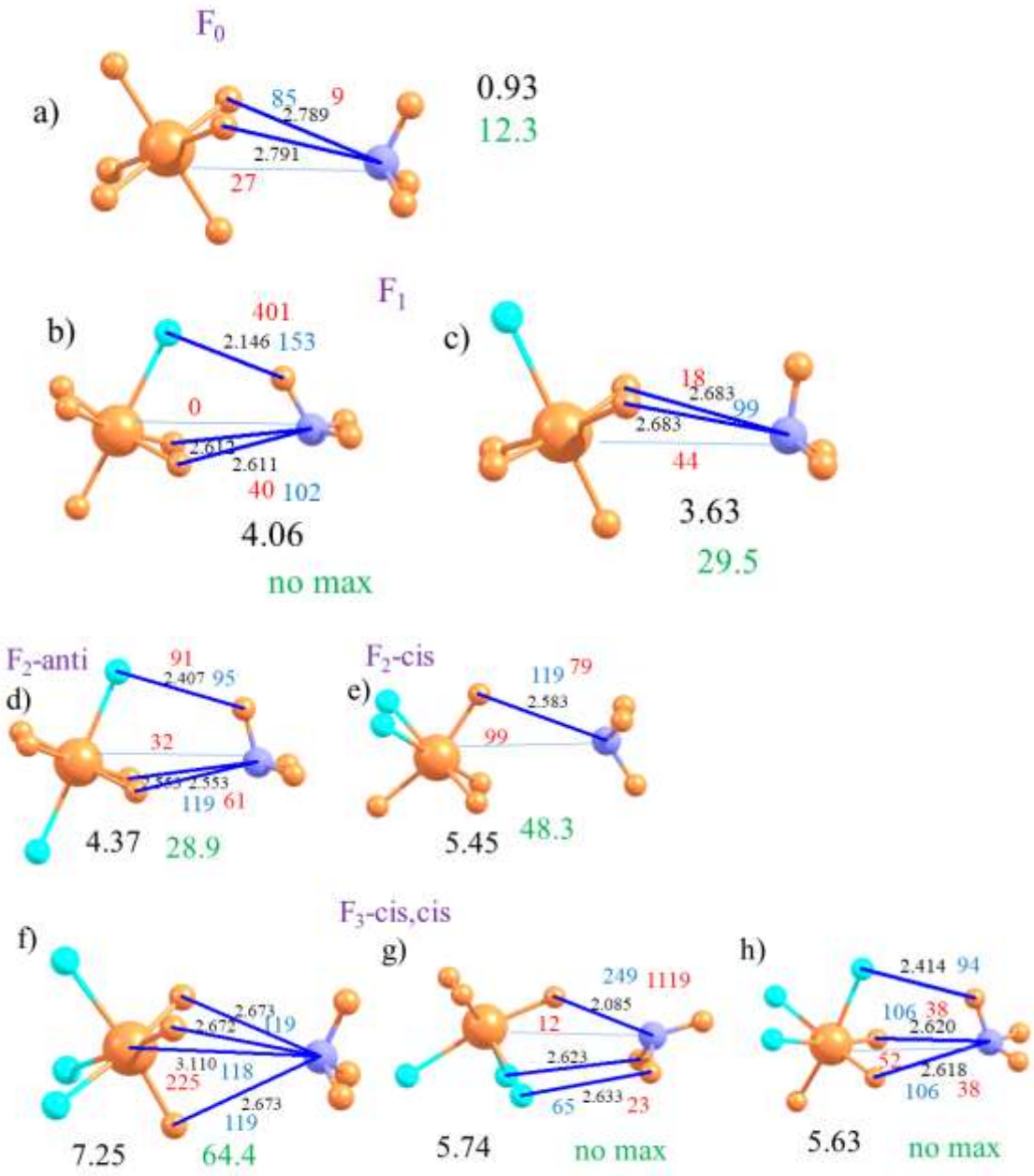
F0
a)
85
9
2.789
2.791
27
0.93
12.3
F1
b)
401
2.146
153
0
2.613
2.611
40
102
4.06
no max
c)
18
2.683
99
2.683
44
3.63
29.5
F2-anti
d)
91
2.407
95
32
2.553
119
61
4.37
28.9
F2-cis
e)
119
79
2.583
99
5.45
48.3
F3-cis,cis
f)
2.673
2.672
119
3.110
118
225
2.673
119
7.25
64.4
g)
249
1119
2.085
12
2.623
65
2.633
23
5.74
no max
h)
2.414
94
106
38
2.620
52
2.618
106
38
5.63
no max

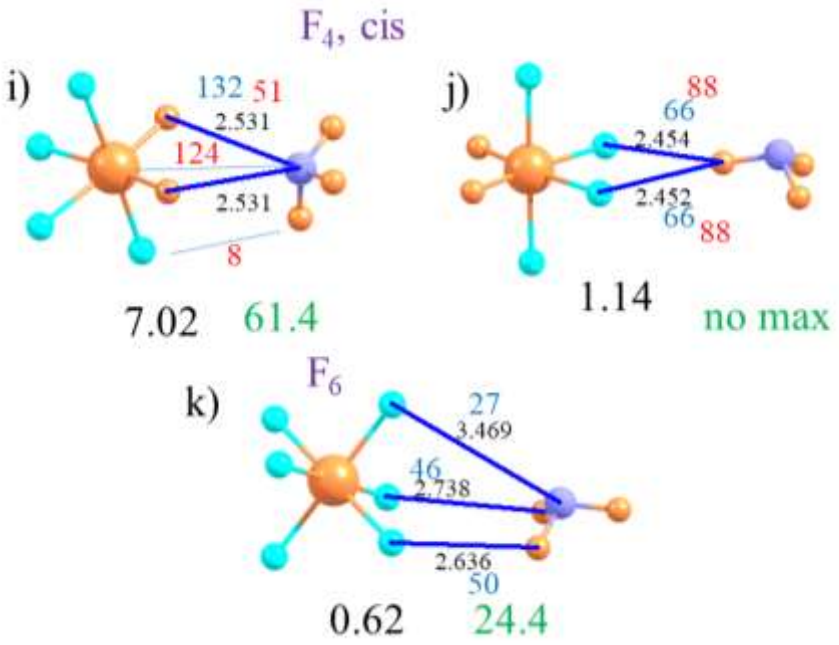

Figure 2-2. Equilibrium geometries of complexes of NH_3 with SeF_nH_{6-n}. Distance in Å as black numbers shown for interactions marked by an AIM bond critical point, with ρBCP in blue (104 au). NBO values of E(2) (102 kcal/mol) shown in red. Large black number refers to binding energy (kcal/mol), and large green number to the value of Vs,max (kcal/mol) at the site nearest the N position (if such a maximum exists in that region).

CHAPTER 3 COMPARISON OF HALOGEN WITH PROTON TRANSFER. SYMMETRIC AND ASYMMETRIC SYSTEMS[b]

3.1 Introduction

One of the simplest and most prevalent elementary reactions in chemistry involves the transfer of a proton from one molecular entity to another. This process underlies all of acid-base chemistry, and is an integral component of countless catalytic and enzymatic reactions. Its importance has motivated an enormous body of research into its most fundamental aspects[47-49].

The influence of the pK of the two competing groups on the transfer energetics is well understood, as is the effect of the geometry of the H-bond connecting them [50-55]. The relationship between transfer energetics and kinetics has become clearer, as has the contribution made by quantum mechanical tunneling of the light proton [56-58].

Recent years have witnessed the growing recognition of an analogue to H-bonding, wherein the central proton is replaced by any of several halogen atoms X [59, 60]. Although at first sight counterintuitive that a highly electronegative halogen, with its partial negative atomic charge, might act as a bridge to a nucleophile, this paradox is resolved by consideration of the spatial distribution of electron density around this atom. A polar flattening and depletion of the density along the extension of the R-X bond produces a region of positive potential, which is commonly referred to as a σ-hole, which can in turn attract an electrophile [61-63]. Study of the halogen bond (XB) has yielded a

[b] Coauthored by Jia Lu and Steve Scheiner. Reproduced from *Chemical Physics Letters 2019, 731, 136593* with permission.

great deal of insight [64-67] into the source of their intrinsic strength, rivaling that of its H-bond cousin, and how it is affected by the identity of the halogen atom, its substituents, and its spectroscopic and geometric signature[68-72].

Just as the bridging proton of a HB can transfer between the two participating units, one can in principle imagine the same sort of a transfer of a halogen atom within a XB. And indeed, given the many similarities between these two noncovalent bonds, it would be surprising if such a transfer were not possible. There is in fact ample precedent for the idea of a transfer of a halogen ion or atom between species. In 2001, Grinblat et al [73] had reviewed prior findings and pointed out similarities between proton and halogen transfer. They then went on to provide comprehensive kinetic data on the transfer of a Br atom between a pair of anions. After noting that the Br transfer is much faster than that of a proton, they questioned the validity of invoking nucleophilicity as a guiding principle in these processes. The transfer of the larger I atom was later documented [74] by crystal and computational data, with some sensitivity observed for the nature of the donor and acceptor groups.

There have been a series of computational studies of halogen bonding [75-80] wherein the halogen atom in question went beyond simply forming such a bond, but seemed to transfer, at least partially, from one molecular entity to the other. One work [75] noted this transfer is facilitated if the X is shared by atoms more electronegative than C, and that Br seemed to transfer more quickly than does Cl. When placed between a pair of N atoms [81], I favored a symmetric position, equally shared between the donor and acceptor. Indeed, NMR and calculations found such a symmetric position was favored for a number of systems involving pyridine units [82], in clear contrast to the asymmetric

proton position in analogous H-bonded complexes, which was confirmed for X=I as well [83]. Indeed, this symmetric I position seems quite general as varying substituents on the pyridine units [84] does not change the situation. A later work confirmed these findings [85] but also presented evidence that F behaves in an opposite manner, favoring an asymmetric position. The latter idea has been countered by the finding [86, 87] of symmetric fluoronium ions. However, the situation may change when both the donor and acceptor groups lie on the same molecule, as shown [88] by recent NMR and computational data that indicate a preference for an asymmetric X position. Calculations [89] have confirmed the dominance of symmetric single-well XT potentials, at least for the idealized transfer between NH_3 subunits, and considered how the distance between donor and acceptor groups might play into the situation.

There are a number of important and fundamental questions that remain unanswered. At what point does a symmetric single-well halogen transfer (XT) potential transition to a double-well potential? What is the energy barrier separating the two X positions, and how is this barrier affected by the length of the XB? Do the properties of the X transfer depend upon the identity of the X atom, i.e. Cl vs Br vs I, and if so, how? How is a symmetric X transfer between a pair of identical subunits modified in an asymmetric system when these two units differ from one another? How do the various facets of the XT process differ from the better understood proton transfer?

The current work is designed to answer these questions in a detailed and systematic fashion by application of quantum chemical methods. Symmetric ($A\text{-}X^+\text{-}A$) systems are first constructed composed of identical A subunits. The R(A··A) distance is held to a series of constant XB lengths so as to monitor when the XT potential transforms

from single to double well, and how quickly the barrier rises as this distance is elongated. Asymmetry is introduced into the system by way of different A subunits, in order to determine its influence on the XT properties. All of these properties are compared to the same quantities of the proton transfer process by replacing X by H.

3.2 Computational methods

Both symmetric and asymmetric systems were selected to examine the H or X transfer. Symmetric systems consisted of a pair of first-row atom hydride molecules sharing a H or X cation $(H_nA\text{-}X\text{-}AH_n)^+$ (A= C, N, or O, n=2, or 3, and X= H, Cl, Br or I). When fully optimized, most of these systems led to a fully symmetric geometry wherein the X ion lies midway between the two A atoms. The intermolecular R(A··A) distance was then stretched to a variety of lengths, and held fixed while the central X was allowed to move between them, optimizing all parameters other than the chosen R, tracing out a transfer potential. As described below, for stretches of R(A··A) beyond a certain critical length, the transfer potential alters its shape from a central single well, to a double-well potential, with an energy barrier $E^\dagger$ separating these two equivalent wells. As an example asymmetric system, with two different molecules competing for the central ion, $(H_3N\text{-}X\text{-}H_2O)^+$ was chosen. Whether of single or double-well shape, this potential will not be symmetric regardless of the selected R(N··O) intermolecular distance.

Quantum calculations made use of the Gaussian-09 program [90] at the second-order Møller–Plesset (MP2) level. The aug-cc-pVDZ basis set was employed for all atoms with the exception of I for which the aug-cc-pVDZ-PP pseudopotential was used so as to incorporate relativistic effects. The reliability of such methods applied in similar systems is supported by previous work [91-95]. Geometries were optimized with certain

restrictions applied as detailed below.

3.3 Results and discussion

The energy barriers separating the two equivalent minima in the transfer potentials of the $(H_3N\text{-}X\text{-}NH_3)^+$ systems are displayed in Figure 3-1. The intersection of each curve with the abscissa indicates the transition from single to double well potential. So for example, the transfer potential for $(H_3N\text{-}H\text{-}NH_3)^+$ contains a single symmetric well for R(N··N) < 2.5 Å, while this transition occurs for the much longer 5.2 Å for $(H_3N\text{-}I\text{-}NH_3)^+$. In fact, this transition point corresponds to the size of the central ion: H < Cl < Br < I. In each case, the barrier grows quickly as the N atoms are further separated. This growth is roughly linear with R(N··N), with correlation coefficients (in orange in Figure 3-1) all exceeding 0.99. The slopes of the curves in Figure 3-1 are displayed in blue, and are roughly 30 kcal/mol-Å for the halogen ions; the larger slope of 46 kcal/mol-Å portrays a sharper rise for a central proton. These curves are very nearly parallel to one another, with slopes of roughly 30 kcal/mol-Å for the halogen transfer systems, but with a somewhat faster growth for H.

Analogous data are presented in Figure 3-2 for the corresponding interoxygen transfer in $(H_2O\text{-}X\text{-}OH_2)^+$. These data fit similar patterns as in Figure 3-1 in that there is a roughly linear growth of $E^\dagger$ with R. There are certain differences as well. In the first place, the transition from single to double well potential occurs at slightly shorter intermolecular distances for the oxygen systems. The barrier rises a bit more slowly for $(H_2O\text{-}I\text{-}OH_2)^+$ and $(H_2O\text{-}Br\text{-}OH_2)^+$ than for the inter-nitrogen transfers, although there are no significant differences noted for X=H or Cl.

This pattern continues for the $(H_3C\text{-}H\text{-}CH_3)^+$ system, as illustrated by the

resemblance of Figure 3-3 to Figure 3-1 and Figure 3-2. The chief difference lies in the slopes of the curves which are a bit more gradual in the C-systems, for all central ions X^+. The transition point where a double-well potential collapses into a single well occurs at a somewhat longer intermolecular distance for the intercarbon system. This transition occurs, for example, at roughly 2.5 A for $(H_3N\text{-}H\text{-}NH_3)^+$ and $(H_2O\text{-}H\text{-}OH_2)^+$, but at 3.0 Å for the C-analogue.

Whereas the NH_3 and OH_2 monomers each represent a closed-shell molecule, the two CH_3 entities each comprise an open-shell radical. So it would be sensible to consider not only the closed-shell singlet $(H_3C\text{-}H\text{-}CH_3)^+$ but also a triplet state. In doing so, however, there are substantial changes in geometry. For example, the central proton drifts well off of the C···C axis, allowing the single electron on each CH_3 unit to unite into a covalent C-C bond. Ignoring this tendency, and forcing the central proton to remain along the intermolecular C--C axis, leads to transfer barriers depicted in Figure 3-4. One again sees a rapid rise of barrier with stretched R(C--C), but with reduced slopes relative to the corresponding singlet state situation. Finally, the proton transfer between a pair of anionic CH_3^- units would involve no unpaired electrons, so a singlet state would be sufficient. The barrier for this transfer is exhibited in Figure 3-8 where it rises quite linearly with R(C--C). The slope of this increase is nearly identical to that seen in Figure 3-3 for the corresponding $(H_3C\text{-}X\text{-}CH_3)^+$ cation.

One can glean some insight into the distinction between proton and halogen transfer by comparison of Figure 3-5 and Figure 3-6, which respectively illustrate the barriers for H^+ and Cl^+ transfer. Figure 3-5 shows that for any given intermolecular distance R, the proton transfer barriers rise steadily in the order: CHC << NHN < OHO,

i.e. a clear separation between the three curves. This pattern is altered in the case of Cl transfers. The OClO curve remains to the left of NClN, but the CClC curve is hardly distinguishable from NClN. In other words, while the intercarbon proton transfer is much lower than that between a pair of N atoms, the same cannot be said for the Cl^+ transfer where there is only a slight difference, and that only at longer distances. Diagrams corresponding to Br and I transfer are presented in Figure 3-9 and Figure 3-10 look much like Figure 3-6, indicating that Figure 3-6 is representative of halogen transfers in general.

The systems examined above are all fully symmetric with identical groups serving as donor and acceptor. On the other hand, most systems which participate in H or halogen bonds will lack this high level of symmetry, so it is important to determine how the asymmetry introduced by the use of different models for the donor and acceptor will influence the transfer potential. This sort of asymmetry was modeled here by placing NH_3 and OH_2 within the system, and allow them to compete for the bridging proton or halogen within the $(H_3N\text{-}X\text{-}OH_2)^+$ complex. As is evident in Figure 3-7, the Cl^+ transfer potential is likewise highly asymmetric, and the most stable position of the Cl^+ is covalently attached to the NH_3 subunit on the left side of the potential. This preference is true for any intermolecular R(N··O) distance. Indeed, it is only for intermolecular distances exceeding 5.2 Å that there is even a second minimum at all, corresponding to the transferred $(H_3N\cdot\cdot ClOH_2)^+$ structure. This secondary minimum is quite a bit higher in energy than $(H_3NCl\cdot\cdot OH_2)^+$ by some 50 kcal/mol. As R increases beyond 5.3 Å, the Cl-transfer barrier begins to rise. For R=5.6 Å, for example, the barrier that the Cl^+ would have to surpass in order to transfer back to the NH_3 from the OH_2 (right to left) is some

12 kcal/mol. The transfer potentials for the other halogen atoms Br and I in Figure 3-11 and Figure 3-12 look very much like those in Figure 3-7. The only real difference is the R(N··O) at which the second minimum occurs in the transfer potentials. As mentioned above, this critical distance is 5.3 Å, which increases up to 5.6 Å for Br, and 6.0 Å for I.

The data presented above refer to "rigid" transfers wherein the distance between the non-halogen atoms, viz. O, N, or C, are held fixed as the halogen atom moves between them. Of interest also is the situation when there is no such restriction, as would be the case for the free ions, untethered to any macromolecular skeleton. The distance between the two heavy atoms in the fully optimized ions are presented in Table 4-1 where it may first be noted that these distances become longer in the order H < Cl < Br < I, i.e. consistent with radius of the central unit. In terms of the dependence upon the identity of the atoms sharing the halogen, this distance increases rather quickly in the cations from O to N to C, wherein the $(H_3C{\cdot\cdot}X{\cdot\cdot}CH_3)^+$ system is considered in its triplet state. However, this distance is very much shorter if the system is forced into its singlet state. (These distances must be considered in the light of the full geometry. Unlike the other systems considered here, the fully optimized geometry of the singlet $(H_3C{\cdot\cdot}X{\cdot\cdot}CH_3)^+$ places the X well off of the central C··C axis.) The situation changes when the central cation is sandwiched between a pair of closed-shell CH_3^- anions. As noted in the penultimate column of Table 4-1, the H-bond distance is quite long at 3.558 Å, but the halogen bonded complexes are a bit shorter than for the corresponding cationic triplet. Turning to the asymmetric system in the last column, the R(N··O) distances are comparable to the N··N distances in the symmetric cations.

When placed in the context of the energy barriers in the figures, it becomes clear

that most of the systems considered here are characterized by a single-well H/X transfer potential. That is, a second minimum appears in the potential only when the two units are pulled sufficiently apart from their optimized close intermolecular contact. One exception is the H-bonded $(H_3N{\cdot\cdot}H{\cdot\cdot}NH_3)^+$ which contains two minima separated by a very small barrier. Systems with a larger barrier separating the two wells are the X-bonded triplet $(H_3C{\cdot\cdot}X{\cdot\cdot}CH_3)^+$ cations.

3.4 Conclusions

The transfer of a halogen atom within an X-bonded complex shows strong parallels with proton transfer in the analogous H-bonded systems. In either case, the potential contains a single symmetric well for short H or X-bond length, which transitions to a double well for longer distance. As the latter continues to grow, the barrier climbs quickly, increasing by approximately 3 kcal/mol for each 0.1 Å elongation. The point at which this transition from single to double well potential occurs is roughly proportional to the radius of the transferring atom: H << Cl < Br < I. Transfer between O atoms requires surmounting a higher barrier than internitrogen transfer at a given XB length, and the transfer between C atoms is lowest of all. In terms of an asymmetric system, the halogen atom prefers association with N over O. A second minimum corresponding to $(H_3N{\cdots}XOH_2)^+$ occurs only for long R(N··O) , and this second minimum remains much higher in energy than the preferred $(H_3NX{\cdots}OH_2)^+$ configuration.

Table 3-1. X-bond lengths (Å) in fully optimized geometries

	O··X··O+	N··X··N^+	C··X··C^+ (triplet)	C··X··C^+ (singlet)	C··X··C^- (singlet)	N··X··O^+
X=H	2.399	2.717[a]	3.063	1.944	3.558 [a]	2.707
X=Cl	3.955	4.070	4.850[a]	2.861	4.518	4.184
X=Br	4.168	4.286	4.990[a]	2.996	4.657	4.309
X=I	4.510	4.631	5.238[a]	3.216	4.857	4.613

[a] double-well potential

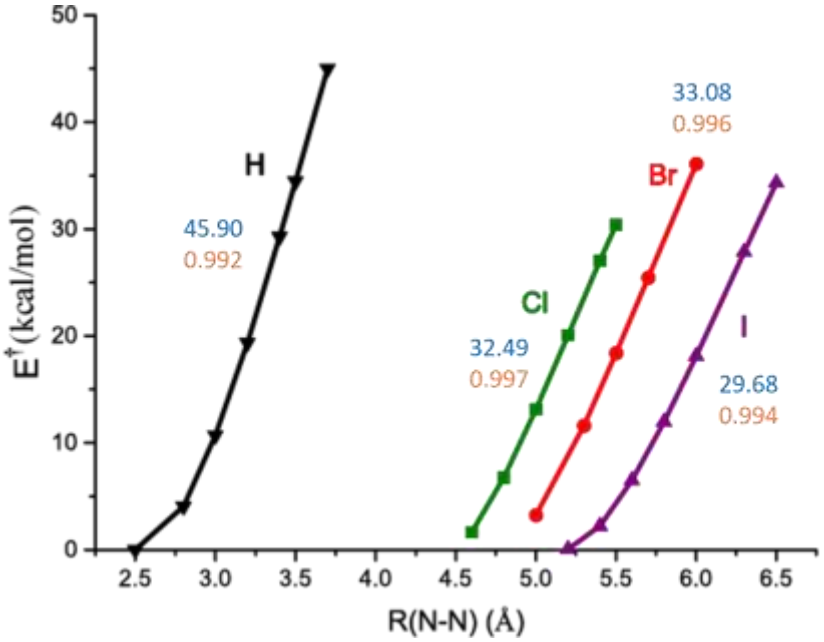

Figure 3-1. Calculated energy barrier $E^{\dagger}$ for proton and halogen transfer in symmetric system $(H_3N\text{-}X\text{-}NH_3)^+$ (X= H, Cl, Br or I) in terms of intermolecular distance R(N-N). Slopes of fit to linear relationship are shown as blue numbers (kcal/mol-Å) and the corresponding correlation coefficients are in orange.

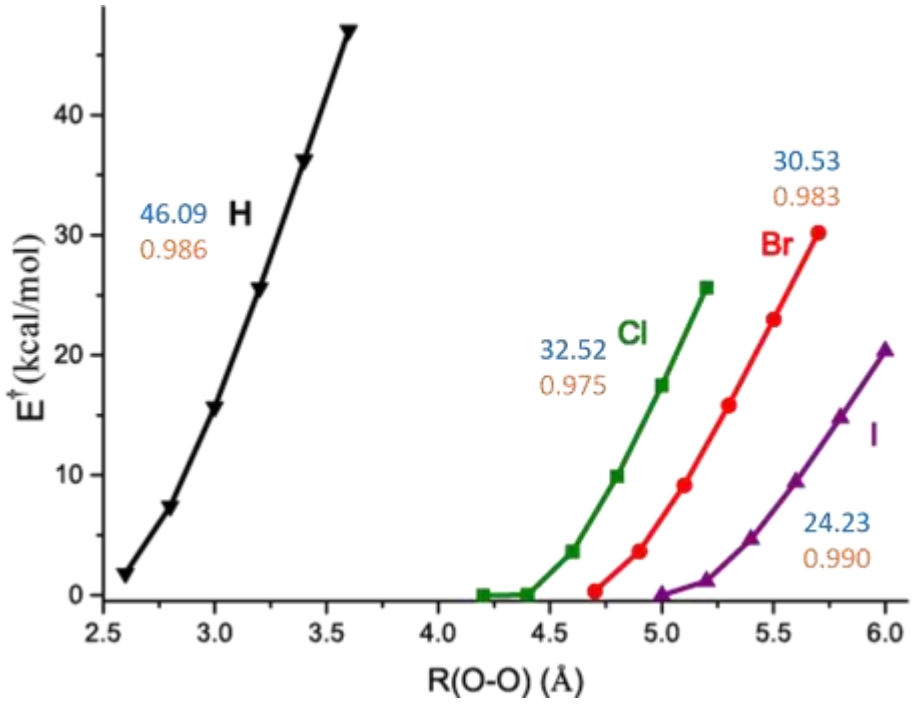

Figure 3-2. Energy barrier $E^{\dagger}$ for proton and halogen transfer in symmetric system $(H_2O\text{-}X\text{-}OH_2)^+$ (X= H, Cl, Br or I). Slopes of fit to linear relationship are shown as blue numbers (kcal/mol-Å) and the corresponding correlation coefficients are in orange.

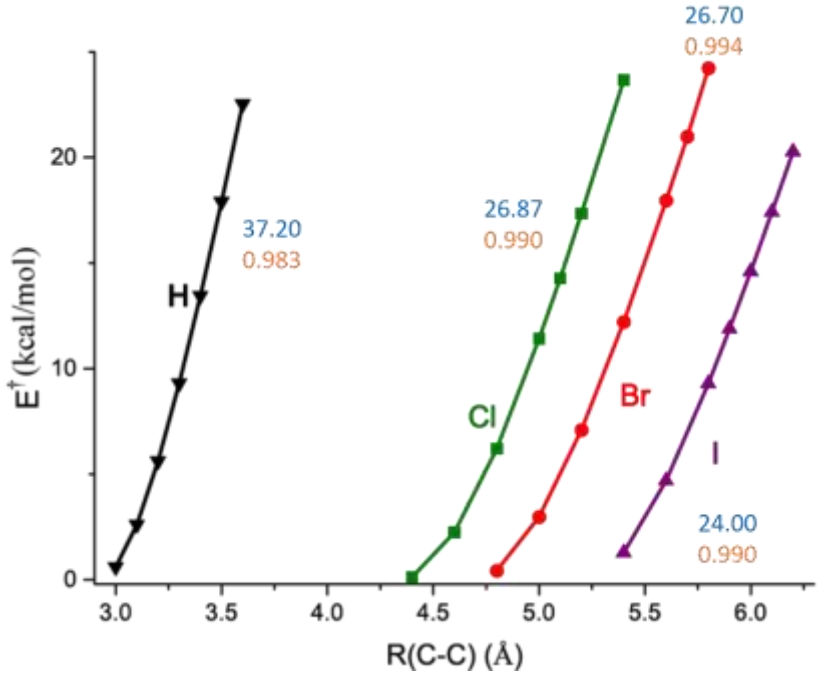

Figure 3-3. Energy barrier $E^{\dagger}$ for proton and halogen transfer in symmetric singlet system $(H_3C\text{-}X\text{-}CH_3)^+$ (X= H, Cl, Br or I). Slopes of fit to linear relationship are shown as blue numbers (kcal/mol-Å) and the corresponding correlation coefficients are in orange.

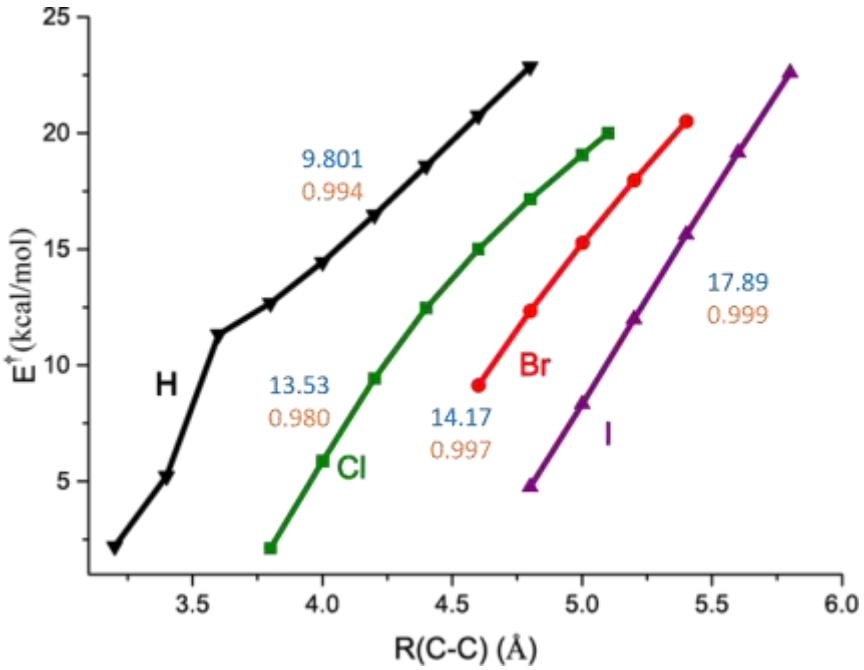

Figure 3-4. Energy barrier $E^{\dagger}$ for proton and halogen transfer in triplet $(H_3C\text{-}X\text{-}CH_3)^+$ (X= H, Cl, Br or I). Slopes of fit to linear relationship are shown as blue numbers (kcal/mol-Å) and the corresponding correlation coefficients are in orange.

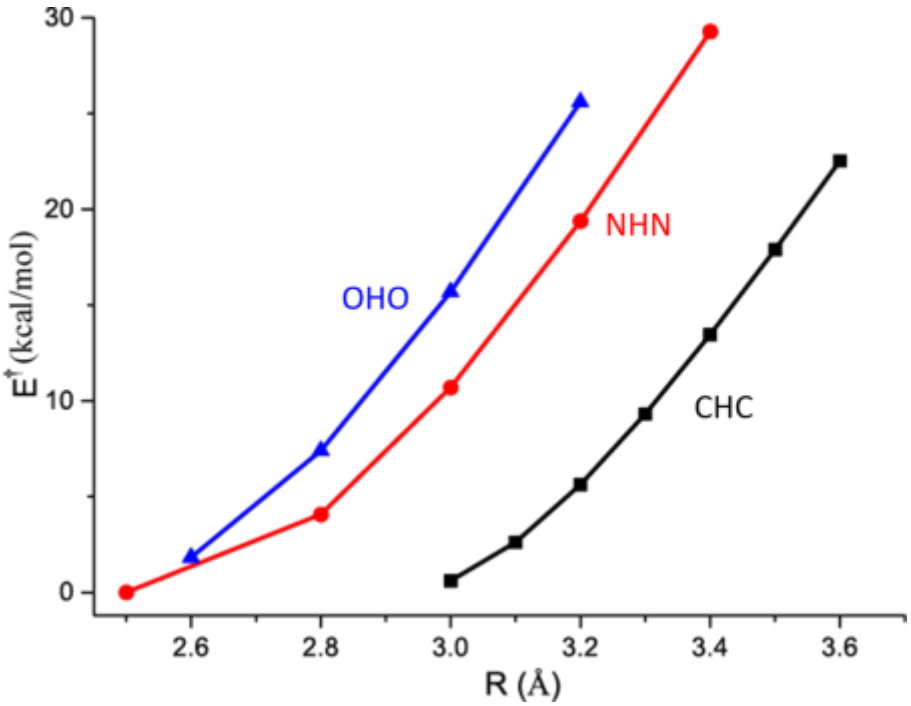

Figure 3-5. Proton transfer barrier $E^{\dagger}$ in $(H_nA\text{-}H\text{-}AH_n)^+$, all singlet states.

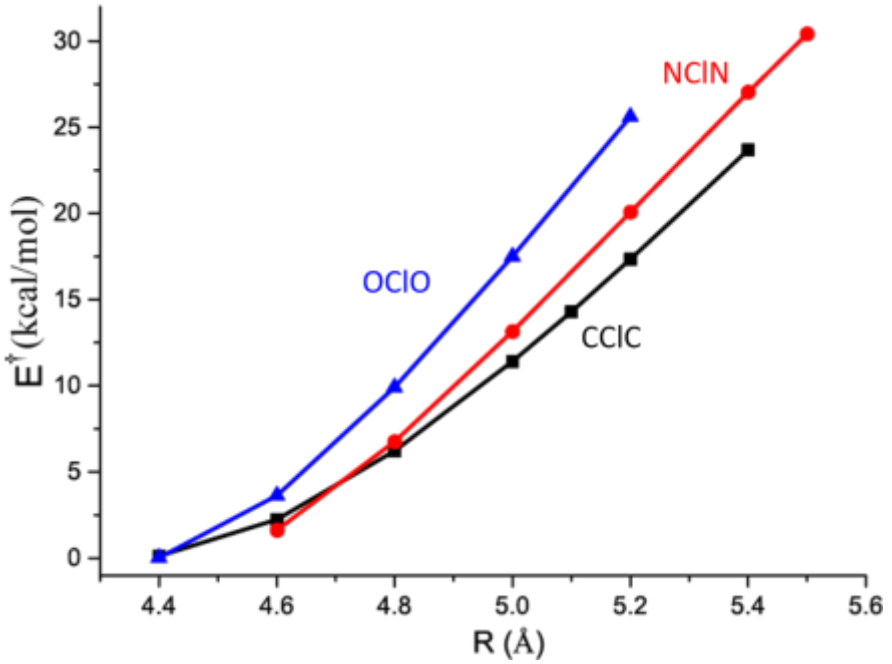

Figure 3-6. Cl transfer barrier $E^{\dagger}$ in $[H_nA\text{-}Cl\text{-}AH_n]^+$, all singlet states.

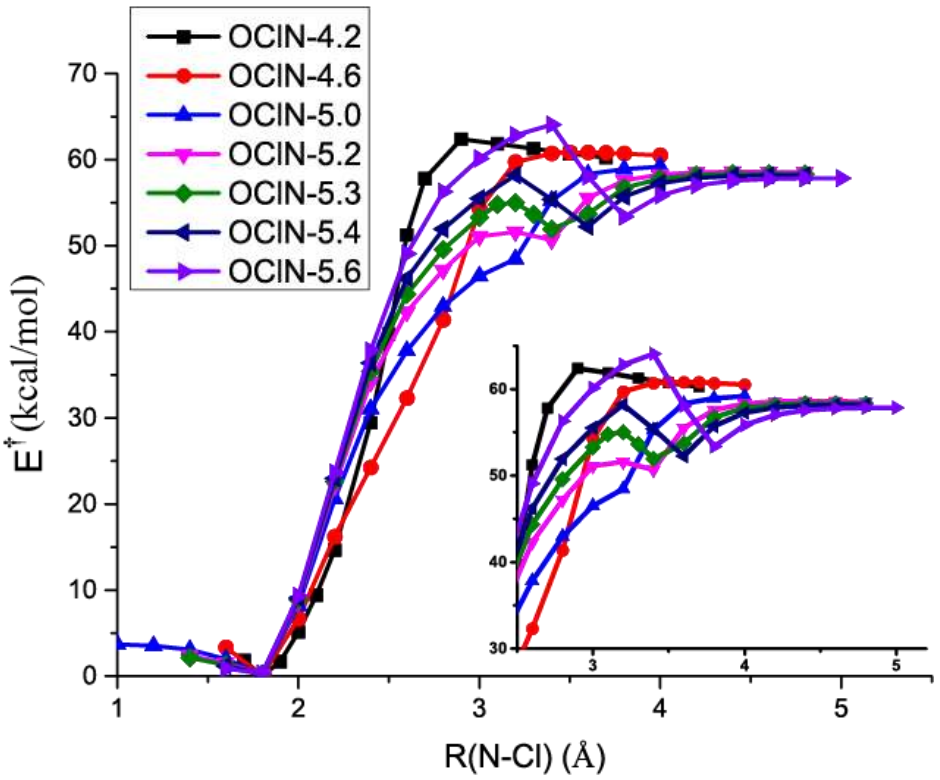

Figure 3-7. Energy barriers for Cl transfer from N to O in asymmetric system $(H_3N\text{-}Cl\text{-}OH_2)^+$.

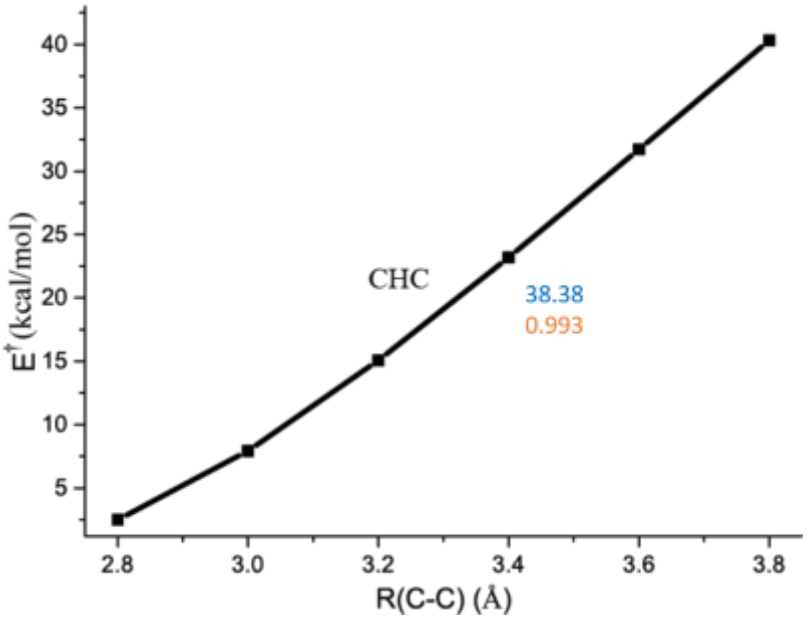

Figure 3-8. Energy barrier $E^{\dagger}$ for proton transfer in anionic $(H_3C\text{-}X\text{-}CH_3)^-$. Slope of fit to linear relationship is shown as blue number (kcal/mol-Å) and the corresponding correlation coefficient is in orange.

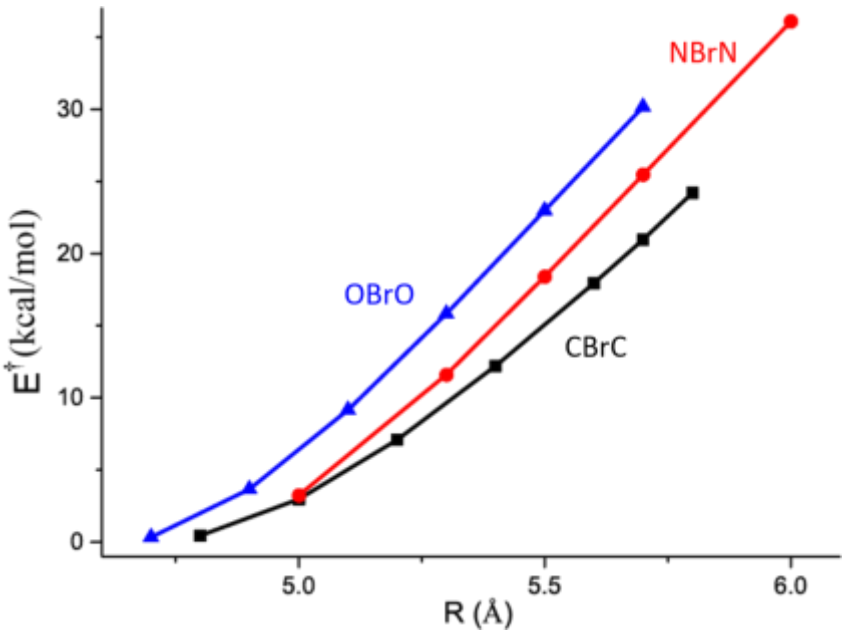

Figure 3-9. Br transfer barrier $E^{\dagger}$ in $[H_nA\text{-}Br\text{-}AH_n]^+$, all singlet states.

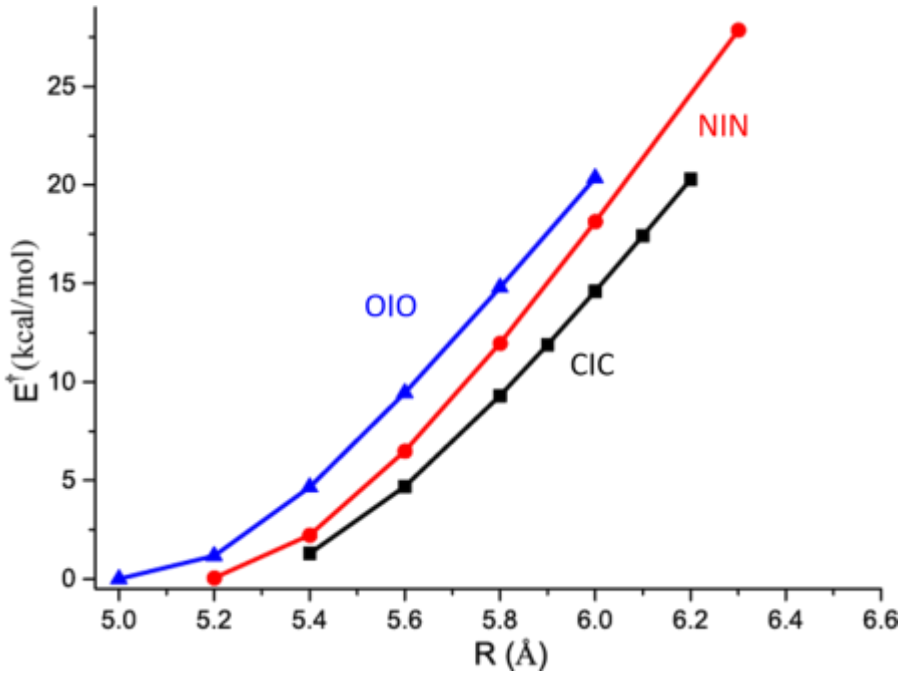

Figure 3-10. I transfer barrier $E^{\dagger}$ in $[H_nA\text{-}I\text{-}AH_n]^+$, all singlet states.

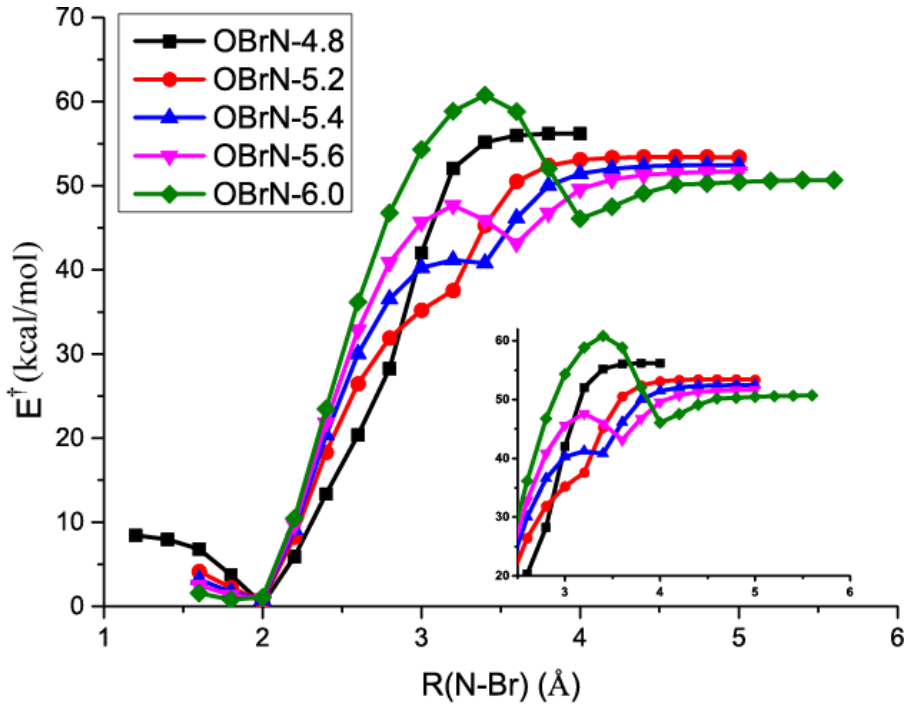

Figure 3-11. Energy barriers for Br transfer from N to O in asymmetric system $(H_3N\text{-}Br\text{-}OH_2)^+$.

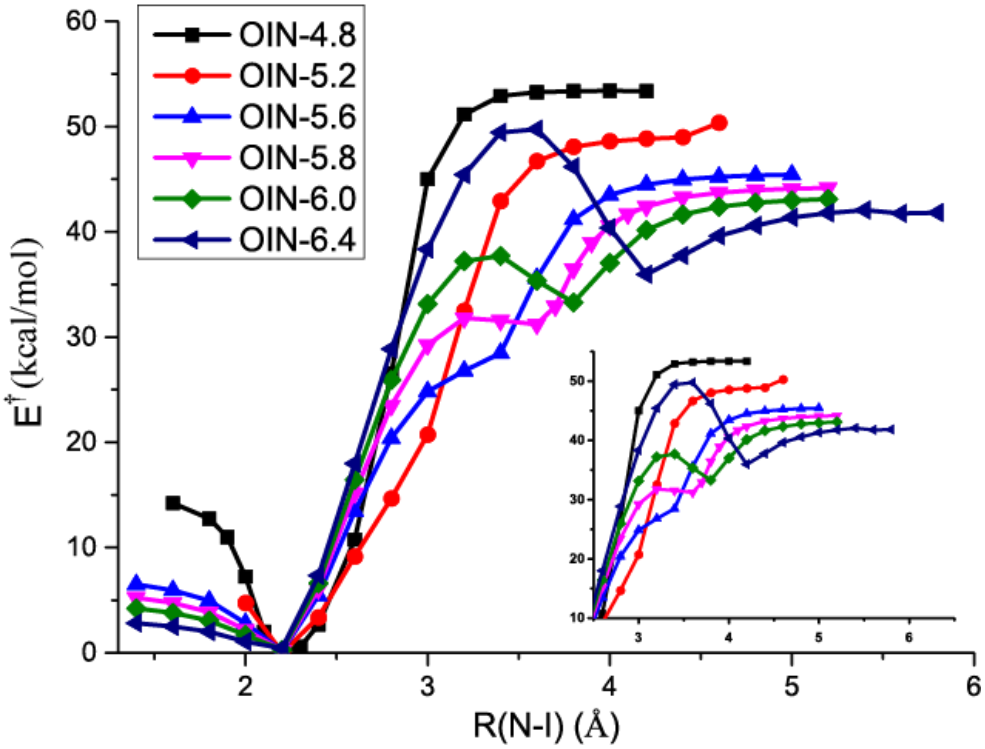

Figure 3-12. Energy barriers for I transfer from N to O in asymmetric system $(H_3N\text{-}I\text{-}OH_2)^+$.

CHAPTER 4 PARTIAL TRANSFER OF BRIDGING ATOM IN HALOGEN-BONDED COMPLEXES[c]

4.1 Introduction

There are many diverse aspects of the H-bond that have generated a good deal of study over the years[96-99]. The H-bond is a directional phenomenon in that the proton prefers a location close to the axis between the proton donor and acceptor atoms. Angular deviations from this configuration are energetically costly, and have direct implications on the properties of the bond. The effect of H-bond formation upon the IR and NMR spectra of the constituent subunits has served as a crucial signpost of the presence of H-bonds, and their strength. The dynamic formation, breakage, and rescrambling of H-bonds is an integral component of solvation.

One of the more interesting issues concerned with H-bond formation is the position adopted by the bridging proton. It is almost a universal observation that the A-H covalent bond is stretched upon complexation with a base B to form the AH···B H-bond (with some exceptions that have come to be called blue-shifting H-bonds [100-104]). But the degree of this stretch is quite variable. In certain cases, the proton can adopt a position roughly midway between the A and B subunits in what is alternately called a low-barrier or very strong H-bond [105-108]. Other acid/base combinations can lead to a double-well proton transfer potential where not only the AH··B but also the A··HB configuration represents a minimum[50-53, 109-114]. These two configurations will generally have different

[c] Coauthored by Jia Lu and Steve Scheiner. Reproduced from *Computational and Theoretical Chemistry 2021, 1204, 113398* with permission.

energies from one another, and the latter structure is the result of a proton transfer within the confines of the H-bond. If the energy barrier separating these two minima is sufficiently low, the situation can best be represented as a dynamic and rapid equilibrium between the two minima, where the transition between them is assisted by quantum mechanical tunneling [58, 115, 116]. The study of the proton transfer process has generated a rich and complex body of knowledge with relevance to chemistry and biology that continues to this day.

Recent years have witnessed the rediscovery of the halogen bond, which in many ways parallels the H-bond except that the bridging H of the Lewis acid unit is replaced by Cl, Br, or I [63, 117-127]. The continuing exploration of the properties of the halogen bond has reiterated its similarity to the H-bond, including directionality and substituent effects, as well as the similarity of the fundamental forces of which they are both comprised.

Given these parallels it is perhaps not surprising that certain elements of the proton transfer of H-bonds have begun to emerge within the framework of halogen bonds as well. Whether X refers to H or a halogen atom, interaction with a Lewis base leads to stretching of the A-X bond, which can be quite substantial in certain instances [76, 123, 128-134], consistent with the idea of at least a partial transfer.

Previous calculations by this group [135] have elucidated the governing principles of halogen transfer in the context of a cationic system where the X^+ is shifting between a pair of neutral molecules, and found strong similarities with proton transfer. These symmetric transfer potentials are of single-well character when the halogen bond is short, but evolve to double wells for longer intermolecular separation.

The earlier work, however, left unsolved the situation when the entire system is

neutral. The transfer of a X^+ within the $AX\cdot\cdot B$ system would generate a $A^{-}\cdot\cdot X^{+}B$ ion pair. Many years of study of the H-bond have led to some basic understanding of what it might take for a proton to transfer within the context of a neutral system. It would be of fundamental interest to determine how such criteria might be modified in the parallel case of the halogen bond. Does the larger size of the halogen as compared to a proton, and its greater diffusion of positive charge, permit an easier transfer? Can such a transition to an ion pair occur within the gas phase, or is a solvent or crystal environment required? Elucidation of the rules for halogen transfer would have far-reaching implications for such fields as pharmaceuticals, many of which participate in halogen bonds in certain environments.

The current work attempts to address this issue in a systematic fashion to answer the following questions. Are there any acid/base pairs where the halogen would spontaneously transfer across to the base? And for what sort of pair might the ion pair represent even a metastable equilibrium? How does formation of the complex alter the position of the bridging halogen? How are the halogen transfer properties related to other aspects of the complex, e.g. the binding energy or the native halogen acidity and basicity of the partner monomers? In order to address these questions, a full range of acids and bases are considered. The acids place the halogen on a C, N or O atom for purposes of comparison, and two different bases are considered with substantially different strength. The Cl, Br, and I halogen atoms are all considered as bridging halogen atom, and the results are compared with those obtained with the parallel H-bonds.

4.2 Computational methods

A diverse set of Lewis acid molecules was chosen so as to present a wide

spectrum in the data set. The halogen/hydrogen atom was bonded to C in F_3CX where X refers to either H, Cl, Br, or I. The three F substituents provide maximal acidity to this C-acid. At the opposite end of the continuum, FX places the bridging atom on F. N is used as the X donor atom in F_2NX, and O-acids are represented by FOX and F_2NOX. As bases, NMe_3 is a strong neutral nucleophile due in part to the three electron-releasing methyl group substituents. Electron-withdrawing Cl makes NCl_3 a much weaker base.

Ab initio calculations were run in the framework of the Gaussian 09 set of programs [136]. All geometries were fully optimized and minima verified as containing all real frequencies. The aug-cc-pVDZ basis set applied here includes polarization and diffuse functions, and its reliability has been documented in numerous prior studies [92, 137-139]. Relativistic effects related to I were included by use of the aug-cc-pVDZ-PP pseudopotential [5] for this fourth-row atom. Electron correlation was incorporated through the MP2 protocol. The binding energy, E_b, was computed as the difference in energy between the dimer and the sum of the energies of monomers in their fully optimized structure, and is reported here as a positive quantity.

4.3 Results and discussion

The intrinsic force with which the various units hold onto the X^+ (where X refers to either H or a halogen) may be encapsulated by the energy required to separate the latter from the unit which will be left behind. In the case of the neutral Lewis acids, this quantity refers to the deprotonation energy, or its analogue for any of the other halonium ions:

$$RX \rightarrow R^- + X^+ \qquad (1)$$

while the amine (Am) cations revert to a neutral molecule upon losing X^+.

$AmX^+ \rightarrow Am + X^+$ (2)

These deprotonation energies and their analogous halogen quantities (all denoted here generically as dehalogenation energies) are listed in Table 4-1 where several trends are in evidence. Regarding the proton, removal from the C atom is most difficult, requiring 383 kcal/mol, followed by F, N and then O. Replacing the F substituent of FOH by the NF_2 group of F_2NOH eases the proton loss by some 76 kcal/mol, making F_2NOH the most acidic of molecules considered here.

Replacement of the bridging H by a halogen atom leaves most of these trends intact with one exception. The dehalogenation of FX is considerably easier than either F_2NX or FOX, in contrast to the relatively high deprotonation energy of FH. Removal of X^+ becomes progressively less endothermic as the halogen atom grows in size: Cl > Br > I. The lowest dehalogenation energy of 188 kcal/mol is associated with F_2NOI. The deprotonation energies are larger than the analogous quantities for removal of the halogens, with the single exception of F_3CX. This trend may be due in part to the high energy required to remove all electrons from H, leaving only a bare proton in the gas phase. There is a second factor dealing with the intrinsic bond enthalpies. For example, the average bond enthalpy of a O-H bond is twice that of a O-Cl bond, and likewise for N-H vs N-Cl.

The last two rows of Table 4-1 refer to the two amine bases. Due to the electron-withdrawing capacity of Cl, it is much easier for Cl_3N to accommodate the excess electron density that accrues upon removal of X^+ as compared to Me_3N, so the values are much smaller in Table 4-1 for the former. The nature of the X atom plays an important part in the calculated dehalogenation energies of the bases. Just as in the case of the

acids, the Cl → Br → I replacements cause a progressive reduction in these quantities for the two amines as well.

The competition between the acid and the base for the central X^+ is based in large part on the relative forces with which each hold on to this cation. It is clear from Table 4-1 that the deprotonation and dehalogenation energies of the Lewis acids are all larger than the energy required to separate X^+ from the base. This distinction is even true for the strongest acid F_2NOX when paired with the base Me_3N with the stronger hold on X^+.

In order to understand the transfer properties of the bridging ion, each of the five Lewis acids in Table 4-1 was paired with each of the two bases to form an acid-X^+-base complex. Several examples of such complexes are displayed in Figure 3-1 for illustrative purposes. The binding energy of each such dimer, relative to the neutral pair RX + NR'_3, is reported in Table 4-2. These quantities are uniformly much larger for NMe_3 as compared to its less basic NCl_3 analogue. The binding energy rises along with halogen atomic size Cl < Br < I, conforming to the diminishing dehalogenation energy of Table 4-1. This trend is also consonant with the well documented ability of larger halogen atoms to engage in stronger halogen bonds. The largest complexation energy occurs for FX, followed by FOX, F_2NX, and then by F_3CX. With the exception of the proton-bound systems, this same ordering of acids causes a progressive diminution in the dehalogenation energies, again buttressing the idea that stronger acids engage in more tightly held complexes with a base. Overall, the binding strength is enhanced by both stronger acid and stronger base.

Within each of the complexes, the proton/halogen transfer potential contains a single minimum, wherein X adopts a position between the acid and the N atom of the

amine base. This equilibrium position is characterized in Table 4-3 in terms of its stretch away from its bond length within the monomer. In other words, the H atom within F_3C-H--NMe_3 has moved 0.003 Å further from the C than in the isolated F_3CH monomer. With respect to the base, the central H is located 1.162 Å further from the N than in Me_3NH^+. That is, the bridging H has stretched only a small amount away from the acid and remains quite a distance from the base. The third row of Table 4-3 presents the ratio of these two stretches, in this case 0.003/1.162 = 0.0026. This $\Delta r_a/\Delta r_b$ ratio can be taken as a simple measure of the degree of X transfer. A 1:1 ratio of 1.0 would thus refer to what may be considered a half-transfer wherein the bridging X has stretched equal amounts from the acid as from the base.

There are some interesting trends in Table 4-3. Regarding first the stretches of X^+ away from the acid caused by the NMe_3 base, it is Cl that usually elongates the most, followed by Br and then I (with the exception of F_2NBr where r(N-Br) lengthens the most). The proton moves away from the acid unit by the smallest amount, when compared to the halogens. There is an opposite trend for Δr_b which shrinks as the halogen atom grows larger. When these two trends are combined, the degree of transfer $\Delta r_a/\Delta r_b$ diminishes along the Cl > Br > I >>H order, again with the exception of CF_3X. The switching of the NMe_3 nucleophile to its less basic NCl_3 congener strongly reduces Δr_a while enlarging Δr_b. The combined effect is a lowering of the degree of transfer, not surprising in light of the lesser basicity of NCl_3. With regard to comparisons amongst the various acids, there is essentially no transfer at all for the F_3CX acids, with the $\Delta r_a/\Delta r_b$ ratio never exceeding 0.003. On the other end of the spectrum, the FX acid is subject to the highest partial transfer, with $\Delta r_a/\Delta r_b$ reaching up to as high as 0.54. Just below FX on

this scale is FOX, followed by F_2NX.

Some of these patterns can be reconciled with the data in Table 4-1. The reluctance of F_3CX to shift its X is consistent with its large deprotonation/dehalogenation energies in Table 4-1. Likewise, the ability of FX to shift its X toward the base is consistent with its small dehalogenation energies. The difficulty in generating much proton transfer in the complexes compares favorably with the higher deprotonation energies. The particularly small dehalogenation energies of F_2NOX cannot be realized in the X transfer as this molecule decomposes upon addition of NMe_3. And of course the smaller transfers toward the NCl_3 base are consonant with the much smaller energy required to remove X^+ from NCl_3X^+. On the other hand, reading across a row of Table 4-1 shows reductions in dehalogenation energy for larger X, leading to an expectation of easier X transfer. But the $\Delta r_a/\Delta r_b$ trends in Table 4-3 run counter to this expectation, as it is Cl which is generally transferred to the highest degree.

Table 4-2 had shown that the binding energies are largest for X=I and smallest for X=Cl or H, depending upon specific acid. FX forms the strongest complexes and F_3CX the weakest; NMe_3 is bound more strongly than is NCl_3. There is a rule of thumb proposed several times over the years, that an intermolecular H-bond will strengthen as the proton affinities of the two subunits competing for the bridging proton come closer together. In fact, a near equilibration of these two quantities has been proposed to lead to a single-well transfer potential, with the proton nearly midway between these two subunits, in what has sometimes been called [105-108] a very strong hydrogen bond (VSHB). It was considered intriguing to test out this idea in the more general context of halogen X^+ transfers. Figure 4-2 displays the binding energies of the various dimers in terms of

the difference in H^+/X^+ affinity between the acid and base groups. While there does appear to be some indication of the interaction strengthening toward the left of the figure as the two affinities approach one another, there is a great deal of spread in the data.

Another idea tested here is whether the degree of H^+/X^+ transfer is related to the affinity difference. These two measures are plotted against one another in Figure 4-3. Clearly, the large affinity differences on the right side of Figure 4-3 are reflected in only miniscule shifts of the bridging ion position. The transfer measure does increase toward the left as the affinity difference becomes smaller, at least in a general sense. However, this increase is highly scattered with certain systems showing precious little transfer even for small affinity differences. One can conclude then that the trend toward affinity equilibration exerts only a modest, and inconsistent, strengthening of the bond or shift of the central ion.

The clearest correlation arises between the binding energy and degree of transfer. As seen in Figure 4-4, strengthening of the intermolecular bond leads to a progressive increase in the transfer, albeit with a fair amount of scatter. The linear relationship between these two quantities is characterized by a modest correlation coefficient R^2 of 0.79. This correlation may be interpreted to suggest that as the force with which the acid pulls in on the base increases, there is a certain reactive force that pulls the central ion toward the base. On the other hand, this overall correlation may be misleading. For most of the acids on an individual level, viz. FX, F_2NX, and FOX, the degree of transfer diminishes in the order Cl>Br>I when complexed with NMe_3, while the binding energies increase in this same order.

Another quantity, and one with particular connection with possible experimental

measurements, is the stretching frequency of the A-X bond. In the context of H-bonds, the red shift induced in this band has been of immense value in assessing H-bond strength. The shifts in this frequency are reported in Table 4-4 where several trends are in evidence. Most of these quantities are negative, consistent with a red shift. The principal exceptions involve the C-X bonds of the F_3CX acids where a small blue shift occurs. Such a blue shift has been seen on numerous occasions [100-103] in connection with CH H-bonds, particularly with sp^3 hybridization of the C [140] which is the case here. The shifts in Table 4 are much larger for the H-bonds, which is due in part to the much smaller mass of the H nucleus. Indeed, the magnitude of these red shifts declines along with increasing X mass: H >> Cl > Br > I. With respect to the individual Lewis acids, the red shifts diminish in the order FX > FOX > F_2NX. This is the same order as that observed in Table 4-3 for degree of proton transfer, as well as the complexation energies in Table 4-2. Note finally that the frequency shifts are much larger for the stronger NMe_3 base than for NCl_3.

The results described above highlight the difficulty of transferring a proton or halogen ion within the respective noncovalent bonds. Recent calculations have shown that this process can be aided by cooperativity in the form of other noncovalent interactions. Formation of an external tetrel bond, for example, can push a proton along an internal H-bond [141] between N and O, or between two O atoms [142], where the transfer would otherwise not occur.

4.4 Conclusions

Enlarging the halogen atom from Cl to Br to I progressively lowers the dehalogenation energy of the A-X acid, and also reduces that of the BX^+ base. Whether

X = H or halogen, it is difficult to stretch the A-X bond by very much toward a base in the context of an incipient transfer, as such a transfer would lead to an energetically disfavored ion pair. Cl undergoes the highest degree of transfer within most of these complexes, followed by Br and then I; the proton is more resistant to transfer. Higher degrees of partial transfer are generally favored by lowering the affinity of the anionic acid unit toward the bridging ion, and raising the affinity of the base, although this is not always the case. This transfer is also enhanced by a stronger interaction energy between the acid and the base within the complex in the general case, but this rule is violated for a constant acid unit. The A-I molecule engages in the strongest halogen bonds with a base, followed by Br and then Cl, with H roughly comparable to Cl. The shifts in the frequency of the A-X bond stretch also conform closely to the patterns of proton transfer and bond strength.

Table 4-1. Energy (kcal/mol) required to remove X^+ from indicated subunit (see Reactions 1 and 2)

	H^+	Cl^+	Br^+	I^+
F_3CX	383.02	391.01	347.94	297.49
FX	370.13	320.09	293.71	263.36
F_2NX	367.61	355.99	319.00	275.28
FOX	365.61	334.30	302.72	265.74
F_2NOX	289.53	257.13	222.93	188.23
Me_3NX^+	233.64	214.67	181.20	141.75
Cl_3NX^+	175.68	151.21	120.09	85.80

Table 4-2. Binding Energies of Complexes (kcal/mol)

	NMe_3				NCl_3			
	H^+	Cl^+	Br^+	I^+	H^+	Cl^+	Br^+	I^+
F_3CX	7.05	5.35	9.08	13.28	3.79	3.18	4.58	5.53
FX	16.41	25.42	29.98	31.22	6.02	7.20	9.93	11.05
F_2NX	12.57	9.79	15.91	20.11	5.34	4.16	5.82	6.85
FOX	15.30	16.81	22.88	26.11	6.00	5.37	7.59	8.90
F_2NOX	a	a	a	39.20	10.23	6.30	13.53	15.24

[a] F_2NOX molecule breaks apart during optimization in complex

Table 4-3. Differences (Å) between the distance of the X^+ from the acid A and base B in the complex as compared to the isolated AX and BH^+ monomers

	NMe_3	H^+	Cl^+	Br^+	I^+	NCl_3	H^+	Cl^+	Br^+	I^+
F_3CX	$\Delta r_a(X\text{-}CF_3)$	0.003	-0.001	0.007	0.020	$\Delta r_a(X\text{-}CF_3)$	-0.001	-0.001	0.000	0.000
	Δr_b	1.162	1.057	0.800	0.552	Δr_b	1.382	1.166	0.992	0.832
	$\Delta r_a / \Delta r_b$	0.003	-0.001	0.009	0.036	$\Delta r_a / \Delta r_b$	-0.001	-0.001	0.000	0.000
FX	Δr_a (X-F)	0.059	0.153	0.113	0.083	Δr_a (X-F)	0.014	0.028	0.031	0.026
	Δr_b	0.543	0.281	0.246	0.222	Δr_b	0.785	0.635	0.490	0.416
	$\Delta r_a / \Delta r_b$	0.109	0.544	0.460	0.372	$\Delta r_a / \Delta r_b$	0.018	0.044	0.063	0.063
F_2NX	Δr_a (X-NF_2)	0.024	0.046	0.056	0.034	Δr_a (X-NF_2)	0.003	0.001	0.001	-0.003
	Δr_b	0.782	0.652	0.465	0.362	Δr_b	1.003	0.993	0.817	0.664
	$\Delta r_a / \Delta r_b$	0.031	0.070	0.120	0.093	$\Delta r_a / \Delta r_b$	0.003	0.001	0.002	-0.004
FOX	Δr_a (X-OF)	0.044	0.126	0.093	0.069	Δr_a (X-OF)	0.009	0.013	0.016	0.015
	Δr_b	0.636	0.408	0.337	0.279	Δr_b	0.867	0.837	0.653	0.524
	$\Delta r_a / \Delta r_b$	0.069	0.309	0.278	0.247	$\Delta r_a / \Delta r_b$	0.011	0.015	0.024	0.029
F_2NOX	$\Delta r_a(X\text{-}ONF_2)$	a	a	a	0.236	$\Delta r_a(X\text{-}ONF_2)$	0.027	0.024	0.076	0.074
	Δr_b	a	a	a	0.133	Δr_b	0.766	0.725	0.546	0.429
	$\Delta r_a / \Delta r_b$	a	a	a	1.781	$\Delta r_a / \Delta r_b$	0.035	0.033	0.138	0.173

[a] F_2NOX molecule breaks apart during optimization in complex

Table 4-4. Shifts of ν(A-X) stretching frequency (cm-1) upon formation of complex

	NMe_3				NCl_3			
	H^+	Cl^+	Br^+	I^+	H^+	Cl^+	Br^+	I^+
F_3CX	-56.1	9.5	14.7	23.5	10.7	1.6	3.8	6.8
FX	-1296.7	-249.1	-162.7	-105.0	-354.1	-79.3	-57.5	-41.0
F_2NX	-392.7	-61.1	-49.0	-21.9	-56.5	-4.0	-2.6	2.8
FOX	-882.7	-165.6	-95.1	-59.3	-203.4	-29.0	-20.8	-13.7
F_2NOX	a	a	a	-392.9	-521.0	-355.7	-274.6	-279.8

[a] F_2NOX molecule breaks apart during optimization in complex

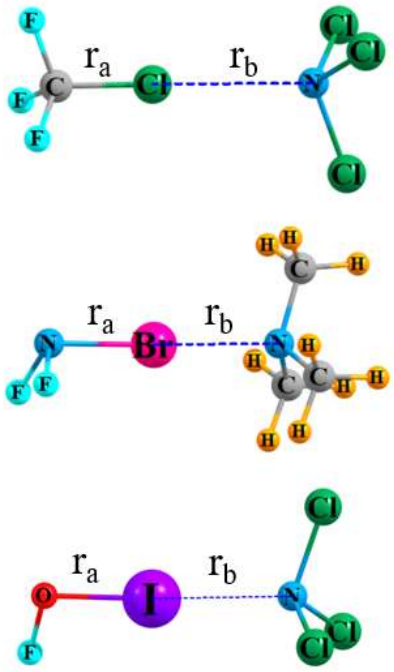

Figure 4-1. Geometries of several sample complexes, defining ra and rb distances. All geometries were fully optimized with no geometric or symmetry restrictions at the MP2/aug-cc-pVDZ level.

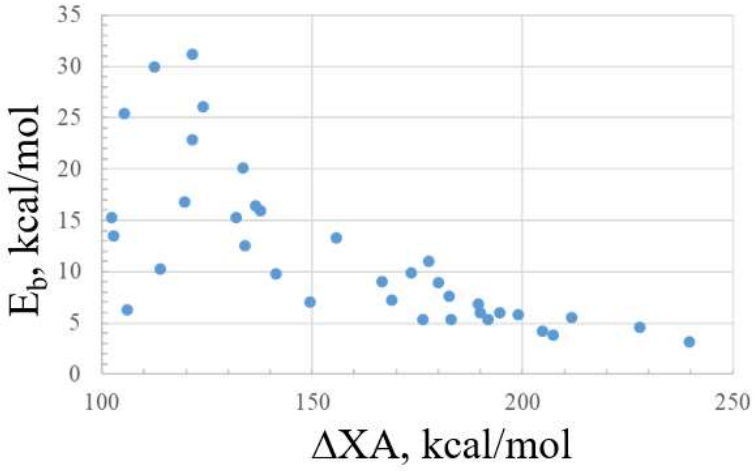

Figure 4-2. Comparison of the binding energy of various complexes with the difference in H^+/X^+ affinity ΔXA between the acid and base fragments.

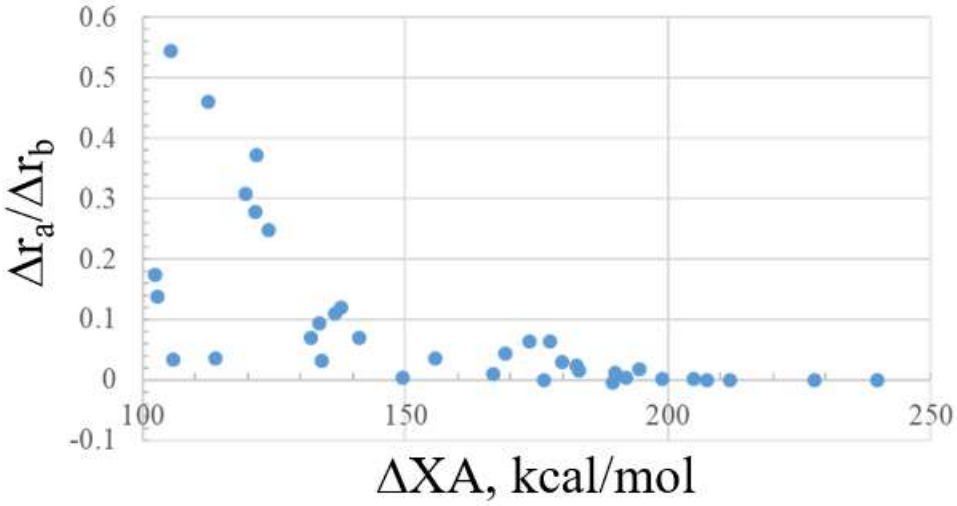

Figure 4-3. Comparison of the degree of transfer of the central ion with the difference in H^+/X^+ affinity ΔXA between the acid and base fragments.

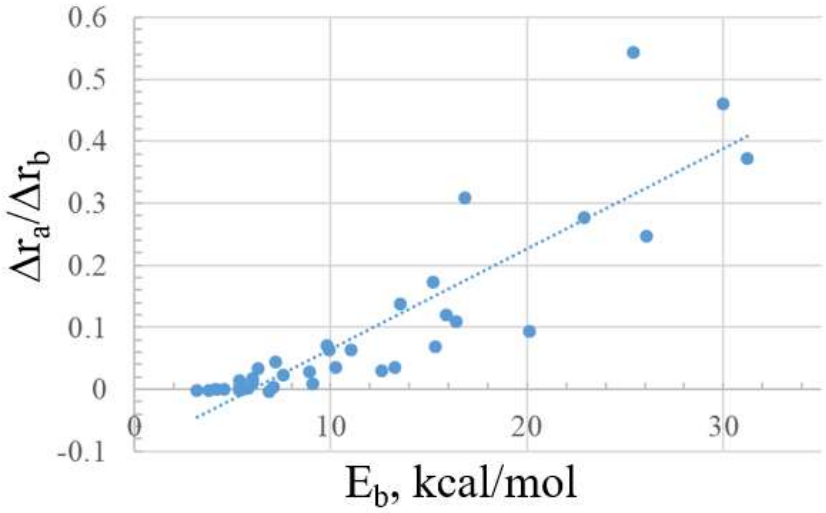

Figure 4-4. Correlation between the degree of transfer of the central ion with the binding energy of the individual complex.

CHAPTER 5 EFFECTS OF HALGEN, CHACOLGEN, PNICOGEN AND TETREL BONDS ON IR AND NMR SPECTRA[d]

5.1 Introduction

Recent years have witnessed a growing recognition of a range of newly rediscovered noncovalent bonds. Like their closely related H-bond cousin, this class of bonds[68, 143-166] are similarly derived from a primary electrostatic attraction, supplemented by substantial amounts of charge transfer, polarization, and dispersion ingredients. In addition to their occurrence in small model dimers, these sorts of interactions are a major factor in the structure and function of much larger supramolecular systems[167-176].

Rather than utilizing a H atom as a bridge between a pair of molecules, these related interactions incorporate a more electronegative atom, drawn from the right side of the periodic table. The primary difference from the H-bond is that this bridging atom does not have a partial positive charge which can draw in the negative region of an approaching nucleophile. Although the bridging atom may have an overall negative charge, its electrostatic potential is more complex, and quite anisotropic. Taking the R-X bond of halogen atom X as an example, the potential around X is characterized by a negative equator around the R-X bond, accompanied by a positive polar region lying along the extension of the R-X bond. This positive region, commonly referred to as a σ-hole, attracts the nucleophile in the same manner as the H atom within a H-bond.

Depending upon the family of elements from which this bridging atom is drawn,

[d] Coauthored by Jia Lu and Steve Scheiner. Reproduced from *Molecules 2019, 24, 2822* with permission. Copyright is retained by the authors.

the resulting noncovalent bond is typically dubbed a halogen, chalcogen, pnicogen, or tetrel bond. These interactions share a number of features. In the first place, they are typically of a strength comparable to a H-bond, sometimes stronger by a substantial amount. Each such bond is systematically strengthened by electron-withdrawing substituents which intensify the σ-hole. These bonds are usually strengthened as one moves down each column of the periodic table, e.g. Cl < Br < I. First-row atoms, i.e. F, O, N, and C, engage in only weak bonds of this type if at all, but can be coaxed into measurable interactions by appropriate substituents or adding a charge[177-183].

In the case of the H-bond, its spectroscopic consequences have been examined over a span of decades, and are well understood[97, 184-186]. Such spectra are one of the most often used tools in the toolbox of chemists and biochemists in deciphering the interactions that are present in a complex system. Indeed, the shifts in certain IR spectroscopic bands or NMR peaks are frequently interpreted as a quantitative measure of the strength of each such bond. Work has also unraveled the source of these shifts, in terms of the most fundamental physical characteristics of the molecules involved. The surprise finding that certain H-bonds can shift an IR stretching frequency to the blue, rather than to the red which is the normal situation, has been analyzed and provided new insights into the source of this discrepancy [100, 187-191].

Alas, while a good deal of information has accumulated in recent years concerning certain aspects of the related halogen etc. bonds, there is less available concerning their spectra. The data that has appeared[177, 192-201] has been informative to be sure, but does not consider these systems in a systematic manner. As such, there is not now available a thorough account of the manner in which each sort of interaction

modulates the spectra, nor a solid understanding of the contributing factors. Such information would be crucial in detecting their presence in a given chemical or biological system. It would also be especially useful if correlations could be established, as is already the case with H-bonds, between certain spectroscopic parameters and the strength or geometry of a given bond.

The present work represents an attempt to fill this gap. A number of small model systems are generated in which a halogen, chalcogen, pnicogen, or tetrel bond is present. Quantum calculations evaluate the strength of each interaction, as well as its geometric properties. The effects of each bond upon the IR and NMR spectra of the system are determined and compared with the binding strength, identity of the bond, and nature of the specific halogen etc atom. In this way, a systematic set of rules is generated that will assist in identification of these sorts of bonds in a complicated system, and to provide some measure of its strength.

5.2 Computational methods

In order to examine this question systematically, three different Lewis acids were considered for each sort of bond. The central atom is drawn from the second, third, and fourth row of the periodic table where these bonds are the strongest. An F atom was placed as a substituent on each such atom, as its electron-withdrawing power will facilitate the development of the noncovalent bond of interest. Thus, FCl, FBr, and FI were taken as prototype halogen bonding molecules. In a related manner, chalcogen bonds were considered via FSH, FSeH, and FTeH. The corresponding pnicogen and tetrel-bonding units are respectively (FPH_2, $FAsH_2$, $FSbH_2$) and ($FSiH_3$, $FGeH_3$, $FSnH_3$). NH_3 was taken as the common electron donor/nucleophile due first to its strength as a

base. As a second benefit, its small size facilitates analysis and avoids complicating secondary interactions.

Calculations were carried out with the M06-2X variant [202] of DFT within the framework of the Gaussian 09 [90] suite of programs. The aug-cc-pVDZ basis set [203, 204] was used for all atoms except fourth row I, Te, Sb and Sn for which relativistic effects sere incorporated via the aug-cc-pVDZ-PP pseudopotential [5, 205]. The reliability of such methods applied in similar systems is supported by numerous previous works [206-212]. Geometries were optimized and harmonic frequency analysis assured the presence of a minimum.

Interaction energies, E_{int}, were taken as a measure of strength of each interaction. This quantity refers to the difference in energy between the fully optimized complex and the energy sum of the two monomers, both in the geometry that pertains to the complex. This quantity was corrected for basis set superposition [213] by the counterpoise prescription [214] originally proposed by Boys and Bernardi. NMR chemical shielding was assessed via the GIAO procedure [215, 216] incorporated within Gaussian. The Natural Bond Orbital (NBO) method [217] was utilized to extract natural atomic charges using the NBO-3.1 program, included within the Gaussian-09 program.

5.3 Results and discussion

The optimized geometries of several sample complexes are pictured in Figure 5-1. The others are quite similar, and are contained in Figure 5-3. The NH_3 approaches the central A atom of each molecule opposite to the A-F bond (where A denotes the halogen, chalcogen, etc atom) although in the case of the chalcogen and pnicogen bonds, the θ(FA··N) angle is not quite 180° due to considerations of orientation of σ-hole and

secondary interactions [218-221]. It is the A-F bond of the Lewis acid molecule which ought to be most susceptible to modifications due to the interaction with the base, and where focus is placed below.

Energetics and IR Spectra

The first column of Table 5-1 displays the interaction energy of each complex. It may be noted first that these noncovalent bonds are all rather strong. To place this result in context, the water dimer as a H-bonding parallel has an interaction energy on the order of 5 kcal/mol [222, 223]. The quantities in Table 5-1 are all larger than this amount, going up to as high as four times larger.

As is typically the case, each sort of interaction strengthens as the bridging atom, whether halogen, chalcogen, or otherwise, grows larger (with one minor exception for Ge vs Si). In terms of class of bond, the halogen bonds are the strongest followed by chalcogen, tetrel, and pnicogen. A common measure of the charge transfer taking place in each noncovalent bond derives from the NBO second-order perturbation energy E(2). In each case, the donor is the N lone pair and the acceptor is the σ*(A-F) antibonding orbital. These quantities in the second column of Table 5-1 generally follow the interaction energy trends, albeit imperfectly. For example, it is the second-row tetrel atom Si which shows a larger value of E(2) than either third or fourth-row analogue. And third-row Br is associated with the largest E(2) of the three halogen atoms.

The transfer of electron density into the antibonding σ*(A-F) bond ought to weaken and lengthen this bond, which can be seen by the stretches Δr documented in the penultimate column of Table 5-1. As in the prior parameters, Δr follows the general pattern halogen > chalcogen > tetrel ~ pnicogen. This A-F bond weakening is also

manifested in a red shift of the stretching frequency Δν. Like the energetics, the halogen > chalcogen > tetrel > pnicogen order holds here as well. But there is also a very significant difference as well. Unlike the energetics, these red shifts are largest for the lightest of each class of A atom. Taking the halogens as an example, this shift of 175 cm^{-1} for Cl drops down to 107 for Br and then to 49 for I. But perhaps most importantly, these shifts are all large enough that they ought to be plainly evident in IR spectra of these systems, falling in the range of 42-175 cm^{-1}.

As is typical of H-bonds, the red shift is accompanied by an intensification of the stretching band. The magnification of this intensity is displayed in the last column of Table 5-1 as the ratio of intensities in the complex and the monomer. This intensification ratio varies from as small as 1.2 up to 7.7 for $FCl\cdot\cdot NH_3$. This quantity decreases smoothly as each A atom becomes larger, and also follows the general pattern halogen > chalcogen > tetrel > pnicogen, very much in line with the red shifts Δν.

NMR Shielding

The NMR chemical shielding of each of the salient atoms is reported in Table 5-2 as a change from the shielding within the uncomplexed monomer. While the shielding change in the central A atom is positive, its magnitude is highly variable. The halogen systems are a case in point. The shielding change on the I atom is 72 ppm, rises to 478 ppm for Cl and then ramps way up to 1675 ppm for Br. Indeed, there does appear to be a pattern that it is the third-row atom in each class that undergoes the largest change, and the fourth-row atom the smallest. The order observed here is fairly consistent with those in Table 5-1, with halogen the largest, followed by chalcogen. However, the pnicogen bonds clearly display larger NMR shifts than the tetrel atoms.

Unlike the increased shielding of the A atoms, the F substituents undergo a dramatic decrease, in the range between 55 and 422 ppm. But the order is the same: halogen > chalcogen > pnicogen > tetrel. The dependence upon the particular row of the periodic table is erratic however. $\Delta\sigma$ clearly rises in magnitude as the halogen atom grows in size, but is less sensitive for the three other sorts of bonds.

Since the H atoms on the Lewis acid are not directly involved in the noncovalent bond, one would not anticipate their shielding to change much upon complexation. Nevertheless, while certainly smaller, these changes ought to be detectable. The H shielding increases in all cases: it is largest for the chalcogen bonds in the 4-5 ppm range, drops to about 1 ppm for pnicogen, and then below 0.5 ppm for the tetrel bonds.

As the electron donor atom, it is not surprising that the chemical shielding of the N atom of NH_3 suffers a drop upon complexation. This decrease falls in the 7-27 ppm range so again, ought to be easily detectable. Unlike the other parameters discussed above, it is the tetrel bond that displays the largest perturbation for the N shielding change. The halogen bonds are somewhat less sensitive, followed by the two others. There is no clear pattern in terms of periodic table row. For example, while it is the lightest halogen atom that changes the N shielding the most, it is the heaviest of the pnicogen atoms that has this distinction.

Atomic Charges

One would expect that the shielding of each atom ought to have some relation with the total charge surrounding that atom. The changes in the atomic charge of each atom that accompany the complexation are thus displayed in Table 5-3. The negative values for the A atoms indicate an increased surrounding electron density, which is

consistent with the greater shielding indicated in Table 5-2. On the other hand, the magnitudes of the charge changes bear little resemblance to the shieldings. For example, the P, As, and Sb atoms all increase their negative charge by the same 0.035 e, yet there is a great variability in the shielding change, from 5 ppm for Sb to as high as 166 ppm for As. As an even greater disparity, the F atoms also accrue additional density during the complexation, comparable to that observed on A, but suffer a very substantial drop in their shielding, opposite to the increase on A.

The charges on the H atoms are small, 0.005 e or less, but vary in sign. While positive for the chalcogen and pnicogen bonds, they reverse sign for the tetrel bonds, even though the shielding change is positive for all systems. With respect to electron donor N, it suffers a loss of density, with its atomic charge growing more positive. But this change is not universal, and is even negative for a few cases. There is some parallel to $\Delta\sigma$ in that the most positive charge changes occur in the halogen bonds which also display the largest change in N shielding. Smaller in both quantities are the chalcogen bonds. However, the very small N charge changes in the tetrel bonds are in dissonance with their large shielding changes.

Electron Density Shifts

A more thorough examination of the electron density shifts can perhaps offer some deeper insights into the changes in both atomic charges and NMR chemical shielding perturbations. Figure 5-2 displays the shifts in density caused by the complexation of NH_3 with FBr as a sample. The purple regions represent gains of density and losses are shown in green. Two different levels are shown to provide a more complete picture. The $\Delta\rho$=0.001 au contour is displayed in Figure 5-2a while the larger

value of 0.005 au in Figure 5-2b focuses attention on regions of more concentrated charge gain and depletion.

Considering the central Br atom first, one can see in Figure 5-2a a purple region of density gain to its left and a green area of loss to its right. The former is larger than the latter which accounts for the more negative charge on the Br atom in Table 5-3. Consideration of only the 0.005 au contour in Figure 5-2b would offer a contrasting picture as the green area is much more extensive than the purple. The increased density around the Br atom is in part responsible for the higher NMR shielding indicated in Table 5-2. In the case of the N atom of NH_3, the green lobes of density loss appear to dominate at either contour value, which is consistent with the more positive charge of N in Table 5-3 and its reduced shielding in Table 5-2.

The F atom offers an interesting picture. One can see a green region of density loss close to the nucleus in Figure 5-2a, which is surrounded on both sides by two more extensive purple lobes of gain. These areas persist in the more concentrated density loss regions shown in Figure 5-2b. As indicated in Table 5-3, it is the purple areas of gain that are more influential, as the overall charge on the F atom becomes more negative. On the other hand, the shielding of this atom is reduced substantially. One way of viewing this apparent paradox is consideration of the placement of these lobes. The green region of density loss occurs directly around the F nucleus, where they may have more direct influence on the shielding than the more distant purple regions of gain.

The density shifts of the $FBr\cdots NH_3$ complex are not unique, but rather characteristic of all of the systems examined here. Comparable density shift diagrams are provided in Figure 5-4 where the similarities are evident.

5.4 Conclusion

Prior studies have provided confidence that NMR and IR data computed by DFT and ab inito approaches offer some reliability[179, 197, 224-227]. As a specific example, an early study [228] calculated nuclear shielding changes involved in the P···N pnicogen bond in the $FH_2P\cdots NH_3$ complex at the MP2/aug'-cc-pVTZ level. The P and N atoms changed their shielding by +77 and -10 ppm, respectively, very similar to the quantities described here.

There have been several studies which have attempted to relate spectroscopic data with noncovalent bond energies. Mokrai et al observed [229] through-space coupling constants within a pnicogen bond in solid-state NMR spectra. The NMR chemical shift of the C that is covalently attached to the halogen bonding I in a C-I bond increases markedly as the XB is enhanced by an anionic electron donor [230]. Within the framework of C-tetrel bonds, Southern and Bryce [179] observed a strong correlation between the C chemical shifts and the length of the C-tetrel bond, although this correlation deteriorated when compared to the actual strength of the bond. One should be cautious, however, in drawing parallels between observations in the broad context of noncovalent bonds in general and a limited set of tetrel bonds involving only the C atom, which tends to form very weak tetrel bonds. As another point of agreement, the N electron donor of an aromatic ring suffers a drop in its chemical shielding by a variable amount within a CX··N halogen bond [231], up to as much as 19 ppm,. As in the case of our NH_3 electron donor, halogen bonding causes deshielding of the F atom when it acts as electron donor in a halogen bond [232]. Also consonant with our own findings, a red shift of the F-X stretching frequency has been observed [233] in its halogen bonds to aromatic N electron

donors, in the range of about 140 cm^{-1}.

In summary the noncovalent bonds that fall into the categories of halogen, chalcogen, pnicogen, and tetrel bonds have a number of spectroscopic features in common. As the base takes a position opposite the F-A bond of the FH_nA molecule, the covalent A-F bond is weakened and stretched by some 0.025-0.060 Å. The stretching frequency of this bond is shifted to the red by at least 40 cm^{-1}, up to as much as 175 cm^{-1}. The amount of this red shift is largest for the A atoms of the second row of the periodic table: Cl, S, P, and Si. Halogen bonds cause the largest shift, followed by chalcogen, tetrel, and then pnicogen.

Each of the atoms involved in these bonds undergo a characteristic change in its NMR signal. The shielding of the A atom is increased while that of the F and electron donor N atom are lowered. The changes observed for the A and F atoms follow the order halogen > chalcogen > pnicogen > tetrel, but in the case of the N atom, the order changes to tetrel > halogen > chalcogen ~ pnicogen. Unlike the IR frequency shifts, it is the third row A atoms that undergo the largest change in NMR shielding and fourth-row the smallest. The latter small quantity stands in contrast to the greatest interaction energies of the noncovalent bonds involving these heavy atoms. In terms of magnitude, $\Delta\sigma$ for A is highly variable, ranging from negligible for $FSnH_3$ all the way up to 1675 ppm for FBr. F shielding changes are not quite as variable, covering the range from 55 to 422 ppm. Although smaller in magnitude, the changes in the N shielding are still easily detectable, between 7 and 27 ppm.

Table 5-1. Interaction energy, NBO charge transfer energy, bond length change, and bond stretch frequency change upon forming complex with NH3.

	$-E_{int}$, kcal/mol	E(2), kcal/mol	Δr(AF), Å	Δν(AF), cm^{-1}	I ratio
halogen					
FCl	12.01	39.3	0.060	-174.9	7.690
FBr	16.28	51.3	0.061	-107.1	4.967
FI	19.17	43.6	0.055	-48.6	2.874
chalcogen					
FSH	9.12	21.0	0.034	-85.8	2.983
FSeH	12.25	30.9	0.042	-70.3	2.598
FTeH	16.14	20.9[a]	0.042	-44.8	1.937
pnicogen					
FPH_2	7.39	13.9	0.022	-58.1	1.916
$FAsH_2$	8.98	16.3	0.029	-47.3	1.780
$FSbH_2$	11.75	17.2	0.034	-42.1	1.535
tetrel					
$FSiH_3$	9.01	18.1	0.027	-74.7	3.433
$FGeH_3$	8.50	12.7	0.025	-55.2	1.609
$FSnH_3$	12.18	13.3	0.030	-54.9	1.244

[a]σ(Te-N)→σ*(Te-F) - NBO treats complex as single unit

Table 5-2. Changes in chemical shielding (ppm) that accompany complexation with NH3.

	A	F	H[a]	N
halogen				
FCl	478.2	-272.7	-	-20.2
FBr	1674.9	-391.2	-	-17.6
FI	72.3	-421.7	-	-6.9
chalcogen				
FSH	264.0	-184.1	3.8	-11.5
FSeH[a]	847.5	-234.0	4.9	-12.5
FTeH	34.8	-233.4	5.0	-8.3
pnicogen				
FPH_2	68.2	-92.0	1.2	-10.6
$FAsH_2$	165.9	-88.6	1.1	-8.7
$FSbH_2$	5.0	-88.3	1.0	-12.4
tetrel				
$FSiH_3$	46.3	-70.0	0.4	-26.6
$FGeH_3$	70.7	-54.8	0.3	-16.3
$FSnH_3$	-0.3	-59.7	0.3	-21.3

[a]average of all H atoms on central atom

Table 5-3. Changes in natural atomic charge (e) that accompany complexation with NH_3.

	A	F	H[a]	N
halogen				
FCl	-0.076	-0.087	-	0.067
FBr	-0.084	-0.099	-	0.066
FI	-0.067	-0.086	-	0.031
chalcogen				
FSH	-0.044	-0.050	0.005	0.019
FSeH[a]	-0.058	-0.061	0.004	0.026
FTeH	-0.053	-0.056	0.001	0.007
pnicogen				
FPH_2	-0.035	-0.029	0.003	0.003
$FAsH_2$	-0.035	-0.034	0.002	0.001
$FSbH_2$	-0.036	-0.035	-0.001	-0.007
tetrel				
$FSiH_3$	-0.040	-0.028	-0.005	0.005
$FGeH_3$	-0.016	-0.027	-0.005	-0.004
$FSnH_3$	-0.012	-0.029	-0.010	-0.011

[a]average of all H atoms on central atom

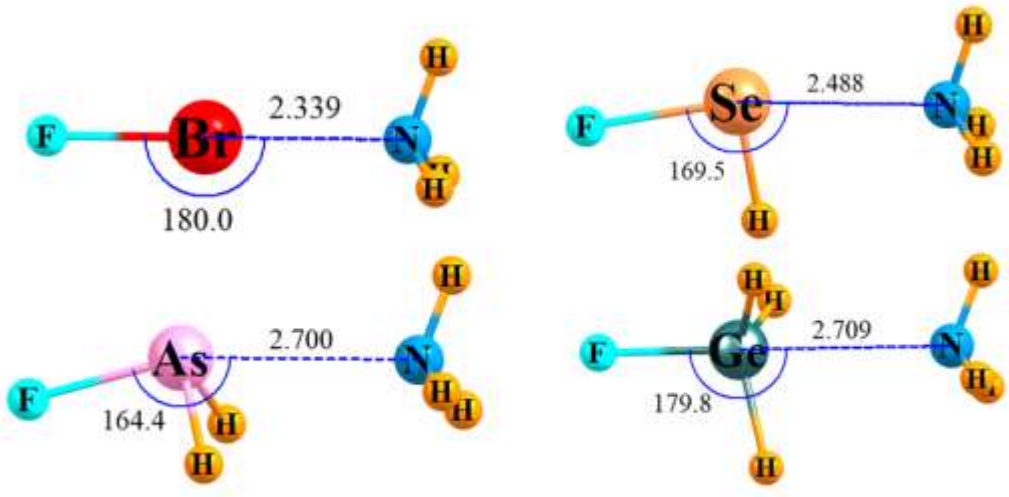

Figure 5-1. Optimized geometries of sample noncovalently bonded complexes. Distance

in Å and angles in degs.

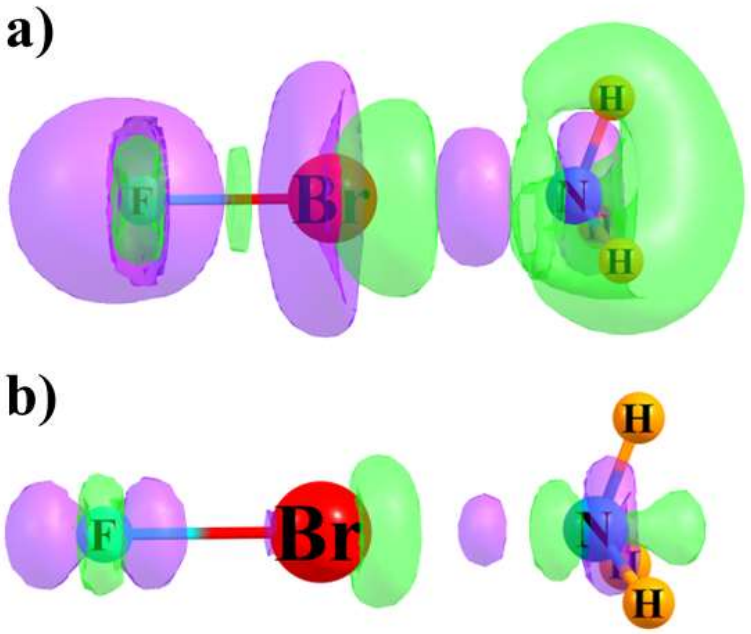

Figure 5-2. Electron density shifts caused by complexation between FBr and NH3. Purple areas indicate gains and losses are shown in green. Contours shown represent a) 0.001 au and b) 0.005 au.

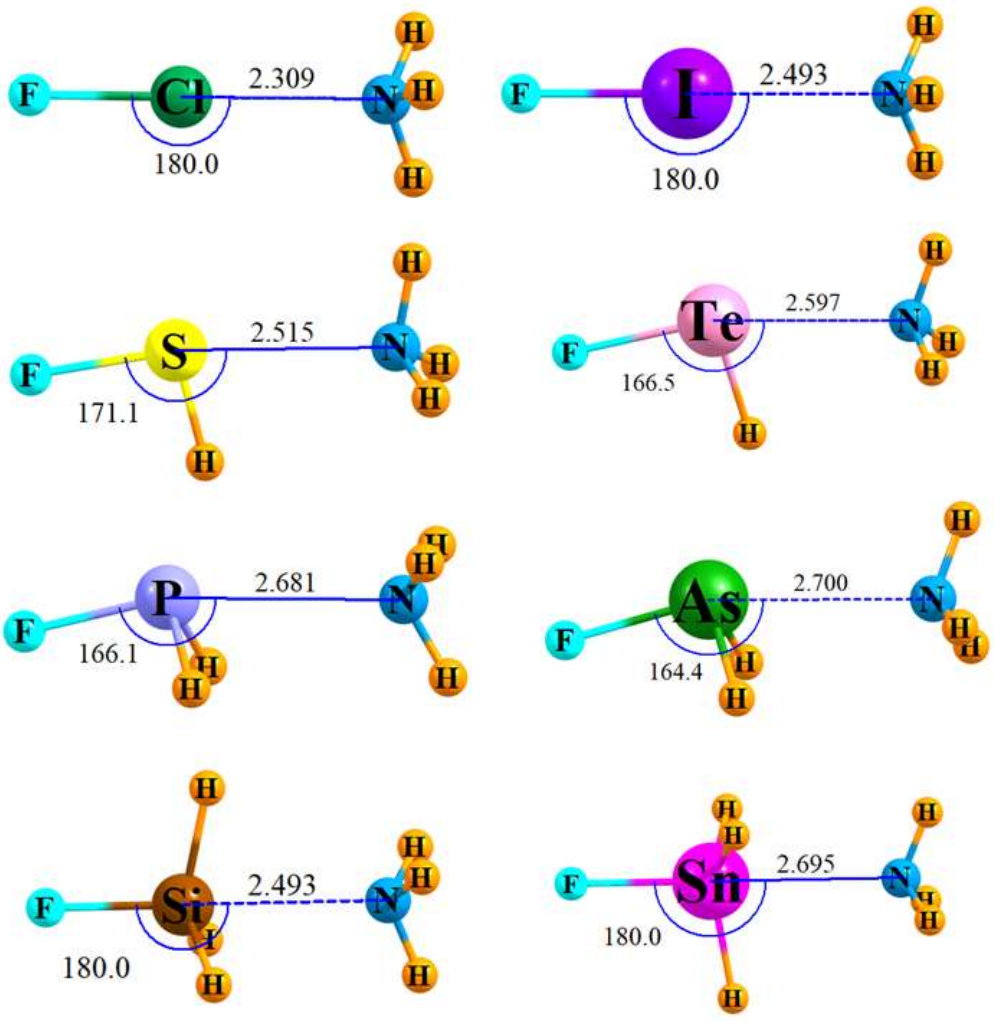

Figure 5-3. Optimized geometry of complexes with NH3. The geometries that include FSH and FSeH are not pure minima as they include one negative frequency.

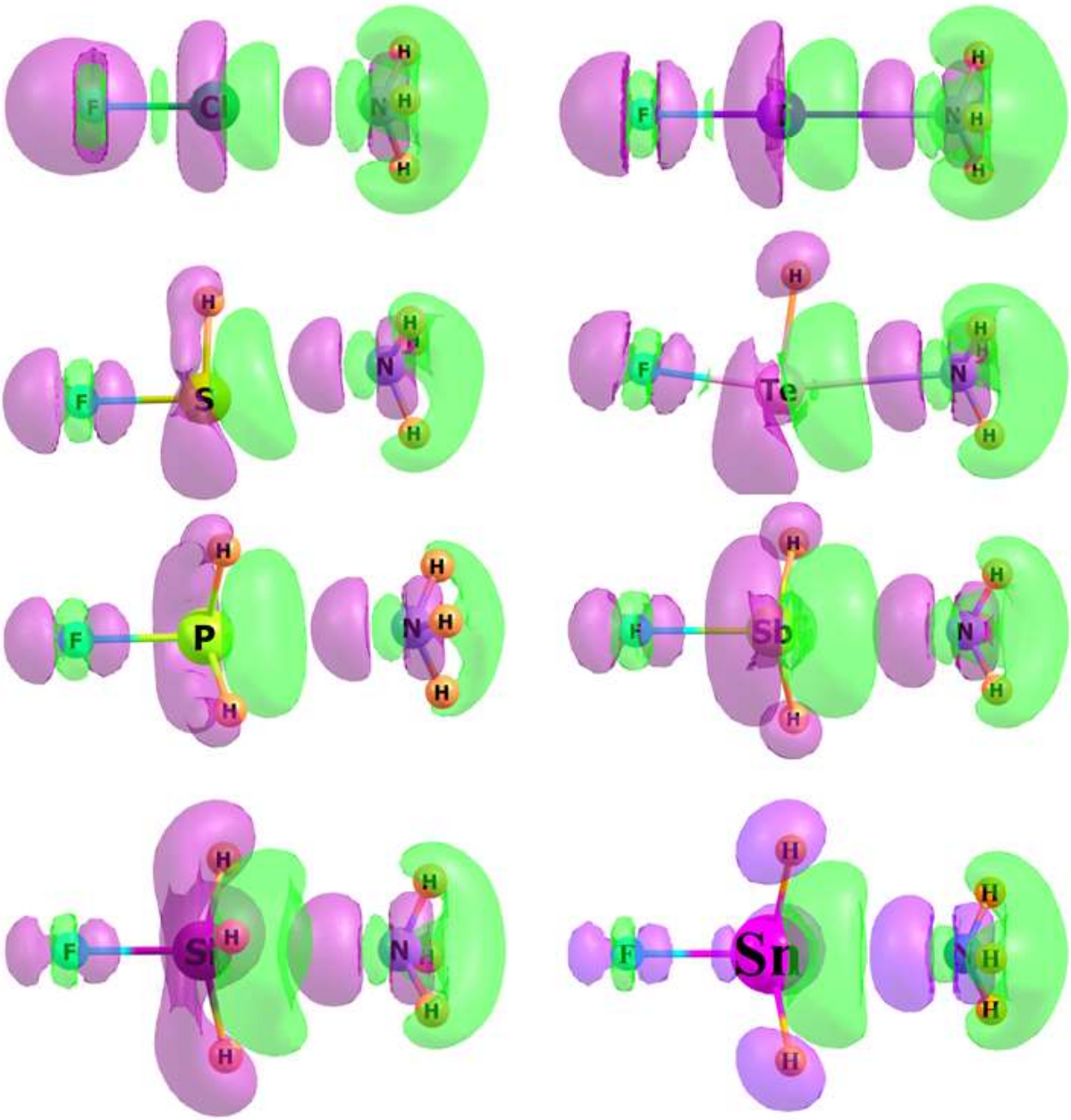

Figure 5-4. Electron density shifts caused by complexation between Lewis acid and NH3. Purple areas indicate gains and losses are shown in green. Contours shown represent 0.001 au.

CHAPTER 6 RELATIONSHIPS BETWEEN BOND STRENGTH AND SPECTROSCOPIC QUANTITIES IN H-BONDS AND RELATED HALOGEN, CHACOLGEN AND PNICOGEN BONDS[e]

6.1 Introduction

During the long history of study of the H-bond (HB) it was observed [96, 97, 184, 234, 235] that the formation of a AH···D bond of this type causes a red shift of the ν(AH) vibrational frequency relative to the monomer. A secondary effect is the intensification of this band. In respect to their contention [236] that these spectroscopic changes were related to the strength of the HB, this correlation has been commonly referred to as the Badger-Bauer rules. There has been a great deal of testing of these ideas over the years [237-243]. For example, Joesten and Drago [244] observed a linear relationship when phenol was paired with 33 different bases in CCl_4 solution. Shortly thereafter, Ghersetti and Lusa extended these ideas to include [245] both $\Delta H°$ and $\Delta G°(298)$, echoed by the correlation with ΔH observed by Drago and Epley [246]. A correlation coefficient of 0.92 was evaluated [247] for combinations of both n-propanol and 2,2,3,3-tetrafluoropropanol with various bases. There have been numerous evaluations of possible correlations over the years [248-251], including computational [252-256] as well as experimental [257] data, with mixed results. Correlations can be less than perfect [258-263] as for example when p-fluorophenol was paired with a total of 35 bases [264]. There is also the finding that the relationships between red shift and enthalpy can be different for different base atoms, e.g.

[e] Coauthered by Jia Lu and Steve Scheiner. Reproduced from *The Journal of Physical Chemistry A 2020, 124 (38), 7716-7725* with permission. Copyright © 2020, American Chemical Society

S vs O [265]. It should also be mentioned that recent years have presented an opposite scenario wherein certain sorts of HBs shift the band to higher rather than lower frequencies [188, 190, 266-268]. While there are a range of different H-bonds for which such blue-shifting occur, the most common are CH···O HBs [100-102, 269-271]. Another common feature of HBs is the downfield shift of the bridging proton's NMR signal, which is also thought to correlate with the strength of the interaction [272-274].

In recent years it has been recognized that the HB has a number of close cousins [133, 146, 149, 179, 275-287] in which the bridging proton is replaced by any of a variety of electronegative atoms. Depending upon the periodic table column from which these bridging atoms are derived, these bonds have been christened as halogen (XB), chalcogen (YB), and pnicogen (ZB) bonds. Their ability to attract a nucleophile rests on each atom's highly asymmetric charge distribution, which contains a depleted electron density and corresponding positive region of electrostatic potential that lies directly opposite any covalent bond in which these atoms participate. Despite the electronegativity of these atoms, the corresponding noncovalent bond with a nucleophile is comparable in strength, and frequently even stronger than the related HB. Concerted study of these noncovalent bonds has led to understanding of a number of trends and underlying phenomena that govern them. The diminishing electronegativity and rising polarizability that comes with moving down the relevant periodic table column also leads to an enhanced strength. For example, first-row atoms F, O, and N seldom participate in such bonds. Electron-withdrawing substituents strengthen the bond by pulling density away from the bridging atom, making it overall more positive.

But the many similarities with the HB lead to the obvious question: do these

related noncovalent bonds also obey the Badger-Bauer rules? Does the frequency of the R-A stretching mode (where A=X, Y, or Z) also shift to the red, and is this shift a linear function of bond strength? It is also intriguing to consider the possible intensification of this band. A second question concerns the NMR chemical shift; is there a relationship with the strength of these noncovalent bonds analogous to that observed for HBs? The answers to these questions will have profound implications as these newly recognized noncovalent bonds undergo examination by spectroscopic means, just as has been the case over the years for HBs.

The present communication represents an effort to answer these questions. A large database of XB, YB, and ZB systems are considered with a highly diverse set of Lewis acids and bases. Their spectroscopic parameters are evaluated by high-level computations, and possible correlations with interaction energies are probed. An advantage of a theoretical approach such as this is the ability to target a wide range of different systems, and without the complications that might occur as a result of solvation effects or of alternate sites of interactions that might arise with larger systems. The geometries clearly delineate the particular noncovalent bond involved in each spectroscopic shift.

6.2 Computational methods

The systems considered paired all combinations of a Lewis acid and base drawn from the list in Table 6-1. Listing of Lewis acids and bases considered in dimers. Each Lewis acid contained a F atom bonded to a generic A atom so as to draw electron density toward the highly electron-withdrawing F and generate a σ-hole on A. H-bonded systems with FH as proton donor were taken as a point of reference. Halogen bonds (XBs) were

generated with A=Cl, Br, or I in the FCl, FBr and FI molecules. S, Se, and Te participated in a chalcogen bond (YB), and pnicogen bonds (ZBs) involved P, As, and Sb. A wide assortment of bases was considered so as to make the analysis as generally applicable as possible. The N atom was embedded in several substituted amines, NCH and its NC^- anion, as well as integral to a ring in imidazole. Numerous bonding schemes for the O atom were also considered, ranging from substituted HOH, the amide group in N-methylamide, phenol, and the formate anion. SH_2 and SMe_2 were used to examine S, and the chloride anion incorporated Cl. Since the π-systems of several sorts of aromatic rings can also donate electrons to these sorts of bonds, benzene, phenol, and both the 5- and 6-membered rings of indole were examined. Altogether, the entire data set comprised 190 different dimers. A few sample dimers are illustrated in Figure 6-1; all coordinates are contained in the Supplementary Information section.

The Gaussian-09 [90] program was employed for all calculations which were carried out with the M06-2X DFT functional using the aug-cc-pVDZ basis set. This level of theory has demonstrated its accuracy and effectiveness in numerous previous studies [207-211, 288-291] of related systems. The aug-cc-pVDZ-PP pseudopotential basis sets [5, 205] were applied to 4th-row atoms I, Te, and Sb so as to capture relativistic effects. However, due to the importance of inner-shell electrons for NMR calculations [292], these same atoms were considered within the context of the all-electron Sapporo-DKH3-DZP-2012-diffuse basis set [293, 294] when computing NMR data.

All geometries were fully optimized with no geometrical restrictions. The interaction energy, E_{int}, was defined as the difference between the energy of the complex and the sum of the energies of monomers in the geometries they adopt within the

complex. Basis set superposition error was eliminated via the counterpoise [214] protocol. Zero-point vibrational energies were not added so as to focus on the pure interactions themselves. But these corrections are included in the values reported below for ΔG, which was evaluated using standard physical chemistry formulas. NMR chemical shielding was evaluated by the GIAO prescription [215]. Due to the importance of inner-shell electrons for NMR calculations [292], the shielding of 4th row atoms I, Te, and Sb was evaluated in the context of the all-electron Sapporo-DKH3-DZP-2012-diffuse basis set [294].

6.3 Results and discussion

Vibrational Spectra

It is widely recognized that the formation of a RH···B H-bond results in the stretching of the RH bond, along with a red shift and intensification of the ν(RH) stretching band. (Of course, there are a number of systems which have been studied in recent years where the frequency can shift to the blue [295-298] but these still remain the exception to the rule.) Figure 6-2a illustrates the fairly tight correlation between the HB energy and the red shift of the ν(RH) frequency for the set of systems considered here in which FH serves as the proton donor. This energy spans a wide range from 5 to 33 kcal/mol, so the set of systems considered cover a similarly broad range from moderate to strong HBs. There is a similarly broad set of red shifts, in the range between 120 and 1800 cm^{-1}. Despite this wide range, the energy and red shift are linearly related with a correlation coefficient R^2 of 0.93, as indicated by the first entry in Table 6-2. The best-fit relation is illustrated by the broken line in Figure 6-2a. The slope of this line, presented in Table 3, is 0.017 which translates to an increase in the interaction energy by this

amount for each additional cm^{-1} of red shift. In other words, one can anticipate an increased H-bond energy of 1.7 kcal/mol for each 100 cm^{-1} shift increment.

The corresponding correlations for the other noncovalent interactions are presented in Figure 6-2b, Figure 6-2c, and Figure 6-2d for the halogen, chalcogen, and pnicogen bonds, respectively, which also undergo red shifts of various magnitude. In each case, the 2nd row atom is represented by the green points and line, while red indicates 3rd row, and 4th row is presented in purple. As in the HB cases, there is again a linear relationship between energetics and frequency shift. Comparison of the various values in the first column of Table 6-2 indicates that the correlations are comparable in quality to those of the HB systems. Due to the much larger mass of these atoms as compared to H, the relevant ν(FA) vibrational frequencies are much smaller, as are their shifts upon complexation. These smaller shifts correspond to greater sensitivity of the interaction energy, as witness the larger slopes in the first column of Table 6-3, as compared to that for H. This slope rises sharply along with the size of the interacting atoms, e.g. S < Se < Te, which translates to larger increases in interaction energy upon a given shift in frequency. To place these quantities in perspective, a slope of 0.20, typical of those evaluated here, corresponds to an increase of interaction energy by 2.0 kcal/mol for each additional 10 cm^{-1} of red shift. Of course, this is not an exact relationship, just as the correlation coefficient is not unity. So one might presume a 10 cm^{-1} shift might be associated with a rise in bond strength of perhaps 1.8 - 2.2 kcal/mol.

Another feature of the ν(RH) stretching band in H-bonded systems is its intensification caused by complexation. This quantity is assessed here as I/Io, the ratio between the intensity in the complex and that in the isolated monomer. Fig 3a indicates a

fair linear relationship between this intensity enhancement and the HB energy. The corresponding correlation coefficient for this relation is 0.89, as indicated in Table 6-2. However, this linearity deteriorates for the other sorts of noncovalent bonds. The pertinent correlation coefficients are all somewhat lower, between 0.35 and 0.72. It might be noted that the correlation deteriorates as the bridging atom, whether halogen, chalcogen, or pnicogen, grows larger. The scattering is evident in Figure 6-3b-d. So whereas the frequency shit in the ν(FA) band can be used as an accurate measure of the interaction energy, its intensification is more loosely correlated.

As another factor, whereas the HB intensification is quite substantial, representing a magnification of as much as 3000, the enlargement for the other systems is much smaller, reaching only up to a factor of about 16. This distinction makes for much steeper slopes of the I/Io ratios in the second column of Table 6-3. As was the case for the frequency shifts, the sensitivity of the interaction energy to intensity magnification grows along with bridging atom size. There is also growth in the order XB < YB < ZB in this slope, indicating progressively greater sensitivity of the energy to the particular type of bond.

There is of course some arbitrariness in the particular choice of basis set. The aug-cc-pVDZ (PP) basis set applied to the above spectroscopic and energetic quantities is of polarized double-ζ quality. It is worthwhile to compare these results with a different set. The 6-311++G(2d,2p) basis is of polarized triple-ζ quality and was originally derived under a different set of criteria. This set was used to reoptimize geometries of a select set of complexes, after which energetics and IR data were recomputed. So as to consider a diverse set of systems for this test, two bases were considered, NMe_3 and

OC(Me)NHMe, encompassing both O and N bases. The Lewis acids in this sample included halogen bonding (FCl and FBr), chalcogen bonding FHS and FHSe, and pnicogen-bonding FH_2P and FH_2As. The data differed very little from the original values described above. Energetics remained within 2% of the earlier data, changes in vibrational frequency $\Delta\nu$(FA) were stable to some 10%, and even the intensity ratio I/Io displayed little variation, also within the 10% range for the most part.

NMR Spectra

Another spectroscopic parameter that is commonly taken as a measure of HB strength is the downfield NMR chemical shift of the bridging proton. This shift is computed here as the difference in chemical shielding of this proton between the complex and the optimized monomer. This negative quantity, indicating a drop in shielding, is depicted in Figure 6-4a along with the HB interaction energy. There would appear to be only a fair linear relationship, as measured by the correlation coefficient of 0.66 reported in the first row of Table 6-2. Figure 6-4b, 4c, and 4d display the corresponding linear relationships for the XB, YB, and ZB complexes, respectively. With the exceptions of Cl, Te, and Sb, these correlations are improved versus HB, as witness the data in Table 6-2. A glance at Figure 6-4 indicates that the poor correlations for these three atoms can be attributed to the anions for which the chemical shift is less than proportional to the binding energetics, so removal of anionic bases from consideration would markedly improve the correlations for these atoms as well. Note that all bridging atoms with the exception of H, undergo a rise in shielding upon complexation.

One feature which all types of noncovalent bonds share regards the row from which the bridging atom is drawn. The green curves are the steepest in Figure 6-4, red

less so, and purple the least of all. That is, the interaction energy is most sensitive to chemical shift of 2nd row atoms Cl, S, and P, and least sensitive for their 4th row analogues, I, Te, and Sb. This diminishing sensitivity is also plainly evident in the slope data in the third column of Table 6-3, which also documents greater sensitivity in the order XB < YB < ZB. The negative slope listed for A=H in the first row refers to the fact that the bridging H atom suffers a loss of chemical shielding upon complexation, opposite to the shielding increases incurred by the other bridging atoms. Its much larger absolute value indicates a higher interaction energy is associated with even minute changes in the proton's shielding.

In addition to the shielding change that engulfs the bridging atom, one can also consider a similar effect upon the atom which is directly bonded to the central one. In these cases, it is a F atom that is covalently attached to each bridging atom. The shielding around this atom is diminished by the formation of each of the various noncovalent bonds. The relationship between this shielding drop and the interaction energy is illustrated in Figure 6-5, which displays a bit more scatter than some of the other plots. The correlation coefficients for this relation are contained in the last column of Table 6-2, and suggest moderate correlation. R^2 is highest, exceeding 0.8 for A=I and P, and considerably lower for the other complexes. But importantly, all of the correlations for the various noncovalent bonds are superior to that for the HB systems for which R^2 is only 0.52.

The slopes of the linear relationships reported in the last column of Table 6-3 are all negative, indicative of the reduced shielding of the F nucleus resulting from noncovalent bond formation. As in the case of the bridging atom, the slope is

numerically much larger for FH than for the F atoms bound to the other bridging atoms. This larger slope conveys the idea that small changes in chemical shielding are associated with larger increases in the H-bond energy. It is the 3rd row atoms Br, Se, and As that have the largest slopes. As in the cases above, the slopes for the pnicogen bonds are larger than for the chalcogen bonds, which are in turn larger than for halogen bonds; i.e. the slopes decrease in the order HB > ZB > YB > XB.

The change in shielding of the Lewis acid atoms can be attributed to two different factors. The first is the presence of the base whose electron density exerts a direct effect upon the shielding. The second is less direct in that the base causes a geometrical distortion of the acid, including a stretch of the F-A bond. One can separately evaluate the first of these two factors independent of the second, by measuring the change in the shielding with the acid molecule in the same (dimer) geometry in both monomer and dimer.

The correlations of these modified chemical shieldings with the interaction energy are displayed in Figure 6-6 and Figure 6-7 for the A and F atoms, respectively. In general, these patterns are similar to those of the full NMR shifts in Figure 6-4 and Figure 6-5 but with some interesting differences. In the first place, the fixed-geometry shieldings of the bridging A atoms are larger, suggesting that the adjustment of the molecular geometry within the dimer attenuates the pure electronic effects of the base to some degree. This reduction can be sizable, amounting to several hundred cm^{-1} in many cases, averaging some 30% of the total shift. With respect to correlations with the interaction energy, considering first the A atoms, as noted in Table 6-5, the correlation of the H shift deteriorates without the geometry changes whereas those concerning the other

noncovalent bonds improve. Thus consideration of only the direct influence of the base correlates much better with interaction energy for the XB, YB, and ZB systems than do the H-bonds. It makes sense that the elimination of the complicating effects of internal geometry changes from the pure effects of the proximity of the base's electron density improves the correlation with the interaction energy. With regard to the slopes of these curves listed in Table 6-6, there are moderate modifications induced by ignoring internal deformation, suggesting the latter distortions reduce the chemical shift by between 20% and 50%. There is little effect of geometry change upon the F atom correlations with one notable exception. The H-bond systems have very little correlation between F shift and bond strength unless the F-H bond stretch is included as a second factor.

It would be logical to presume that the poor quality of some of these fits to NMR data arise from the diversity of the bases that were considered. For example, an approaching N atom might be expected to alter the electron density around a H, X or other bridging atom in a fundamentally different way than would O. In fact, the correlation seems worst for the HB systems, which is consistent with the diversity of H-bonds noted earlier, for example by a delocalization index analysis [299]. Separate evaluations of NMR data for the N and O base atoms did show some improvement in the correlations, but only by a little and not consistently. It is concluded then that there remains an intrinsic scatter to the NMR chemical shifts that prevents as tight a correlation with the bond strength as is observed in the red shift of the FA stretching frequency.

Another notion might be to consider the effect of the noncovalent bond upon the chemical shift of the base atom. In other words, for any given base, say NH_3, the change in chemical shielding of the N atom was correlated with the interaction energy for the

various Lewis acids, including the entire set of XB, YB, and ZB types. However, the correlations were found to be quite poor. This finding is perhaps unsurprising given the variety of the approaching Lewis acid atoms, each of which can be expected to perturb the electron cloud surrounding the base atom in a different way.

It might be added finally that the data computed here by a DFT approach are consistent with IR and NMR spectroscopic changes that were derived earlier [291, 292, 300] by MP2 treatment of electron correlation. A very recent work [301] has verified that calculations are capable of nicely reproducing experimental spectroscopic shifts of Se when involved in chalcogen bonds.

As it is generally more common for experimental measurements to provide free energies than electronic interaction energies, it is of practical interest to consider the relation between the various spectroscopic parameters and ΔG. The correlation coefficients displayed in Table 6-4 are generally quite similar to those in Table 6-2 for $E_{int,}$ suggesting that the spectroscopic quantities can be used to estimate either energetic measure with equal success. The plots of ΔG versus the various spectroscopic data, analogous to those in Figure 6-2 to Figure 6-5, are contained in Figure 6-8 to Figure 6-11.

6.4 Conclusions

Many of the same relationships that relate the strength of H-bonding to spectroscopic parameters apply as well to the related noncovalent bonds. The linear correlation between the interaction energy and the red shift of the F-A stretching frequency is a tight one, so this shift has excellent potential as a gauge of bond strength. This strong correlation is important as several prior experimental studies have suggested these correlations can deteriorate if monomers are of different structure or if the nature of

the electron donor is varied, or even the hybridization of the particular atom involved, or if different solvents are used, or even if different experimental techniques test the relationship. The intensification of this band occurs in all systems, but is less strongly correlated to bond strength in the XB, YB, or ZB systems than it is for HBs. The very widely used linear relation between NMR chemical shifts and H-bond strength is even better for most of the other noncovalent bonds, displaying a tighter correlation with the energetics. The internal geometry changes induced by complexation play a significant role in the chemical shifts.

What is perhaps most notable about the correlations discussed above is the diversity of systems to which they apply. For any given Lewis acid molecule, the bases with which it was paired covered a wide range, encompassing N, O, Cl, and S electron-donor atoms as well as π-systems of aromatic rings, also including anions as well as neutral molecules. There is also extensive coverage of interaction energies, that varied from as little as 4 kcal/mol up to a maximum of 52 kcal/mol. This diversity speaks to the idea that these correlations between energetic and spectroscopic aspects of these noncovalent bonds are a common feature that can be exploited in experimental studies of a wide range of systems.

It is certainly possible that the environment in which a given bonding interaction finds itself, whether immersion in any of various solvents, or placement within a macromolecule, would influence the properties discussed here. The data provided above describe these interactions in a pure sense, prior to these environmental effects taking hold. Future studies will consider the tenacity of these relationships within the context of differing environments.

Table 6-1. Listing of Lewis acids and bases considered in dimers

acid	base
FH	NH_3
FCl	NCl_3
FBr	NMe_3
FI	NC^-
FHS	NCH
FHSe	imidazole-N
FHTe	OH_2
FH_2P	MeOH
FH_2As	OMe_2
FH_2Sb	OC(Me)NHMe
	phenol-O
	$HCOO^-$
	Cl^-
	SH_2
	SMe_2
	aromatic rings
	benzene
	phenol
	indole(5)
	indole(6)

Table 6-2. Correlation coefficient R2 for linear fit of interaction energy to indicated parameter.

	Δν(FA)	I/Io	$\Delta\sigma_A$ (opt)	$\Delta\sigma_F$ (opt)
H	0.93	0.89	0.66	0.52
Cl	0.91	0.72	0.36	0.68
Br	0.94	0.46	0.67	0.69
I	0.90	0.41	0.69	0.84
S	0.95	0.67	0.75	0.77
Se	0.96	0.43	0.71	0.74
Te	0.98	0.35	0.42	0.58
P	0.98	0.69	0.85	0.82
As	0.99	0.64	0.79	0.79
Sb	0.98	0.53	0.48	0.71

Table 6-3. Slope of ΔE vs indicated quantities in the best-fit linear relationship.

	Δν(FA) $kcal \cdot mol^{-1}/cm^{-1}$	I/Io	$\Delta\sigma_A$(opt) $kcal \cdot mol^{-1}$/ppm	$\Delta\sigma_F$(opt) $kcal \cdot mol^{-1}$/ppm
H	0.017	0.0098	-1.669	-0.422
Cl	0.102	2.26	0.030	-0.075
Br	0.175	4.07	0.020	-0.087
I	0.261	9.87	0.008	-0.076
S	0.097	5.59	0.062	-0.093
Se	0.160	9.52	0.032	-0.117
Te	0.229	16.24	0.009	-0.102
P	0.105	9.54	0.146	-0.148
As	0.161	19.62	0.093	-0.206
Sb	0.244	36.46	0.021	-0.197

Table 6-4. Correlation coefficient R2 for linear fit of ΔG(298 K) to indicated parameter.

	Δν(FA)	I/Io	$\Delta\sigma_A$	$\Delta\sigma_F$
H	0.85	0.83	0.58	0.54
Cl	0.90	0.70	0.35	0.67
Br	0.93	0.44	0.65	0.67
I	0.90	0.41	0.67	0.81
S	0.93	0.64	0.72	0.73
Se	0.95	0.43	0.70	0.72
Te	0.98	0.32	0.40	0.57
P	0.97	0.69	0.88	0.82
As	0.98	0.64	0.81	0.78
Sb	0.98	0.52	0.52	0.71

Table 6-5. Correlation coefficient R^2 for linear fit of interaction energy to changes in NMR chemical shielding caused by complexation with monomer in geometry of complex

	$\Delta\sigma_A$	$\Delta\sigma_F$
H	0.55	0.05
Cl	0.87	0.60
Br	0.91	0.72
I	0.85	0.83
S	0.91	0.78
Se	0.86	0.75
Te	0.67	0.59
P	0.90	0.81
As	0.87	0.75
Sb	0.67	0.71

Table 6-6. Slope of ΔE vs NMR chemical shielding caused by complexation with monomer in geometry of complex

	$\Delta\sigma_A$ kcal·mol^{-1}/ppm	$\Delta\sigma_F$ kcal·mol^{-1}/ppm
H	-1.831	+0.162
Cl	0.018	-0.086
Br	0.010	-0.085
I	0.006	-0.078
S	0.030	-0.090
Se	0.018	-0.117
Te	0.007	-0.097
P	0.114	-0.149
As	0.073	-0.216
Sb	0.017	-0.187

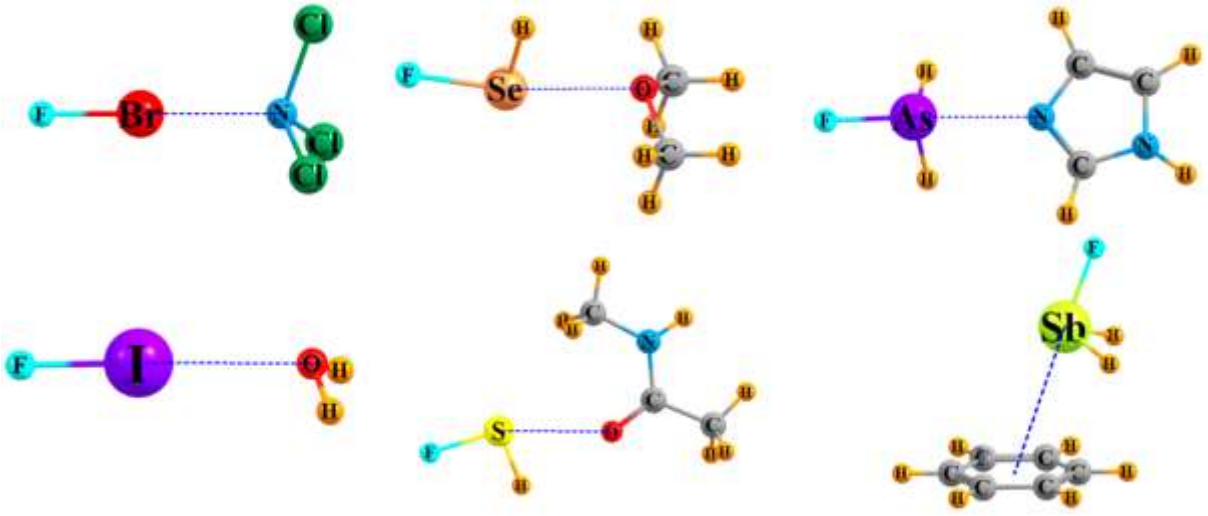

Figure 6-1. Optimized geometries of sample dimers.

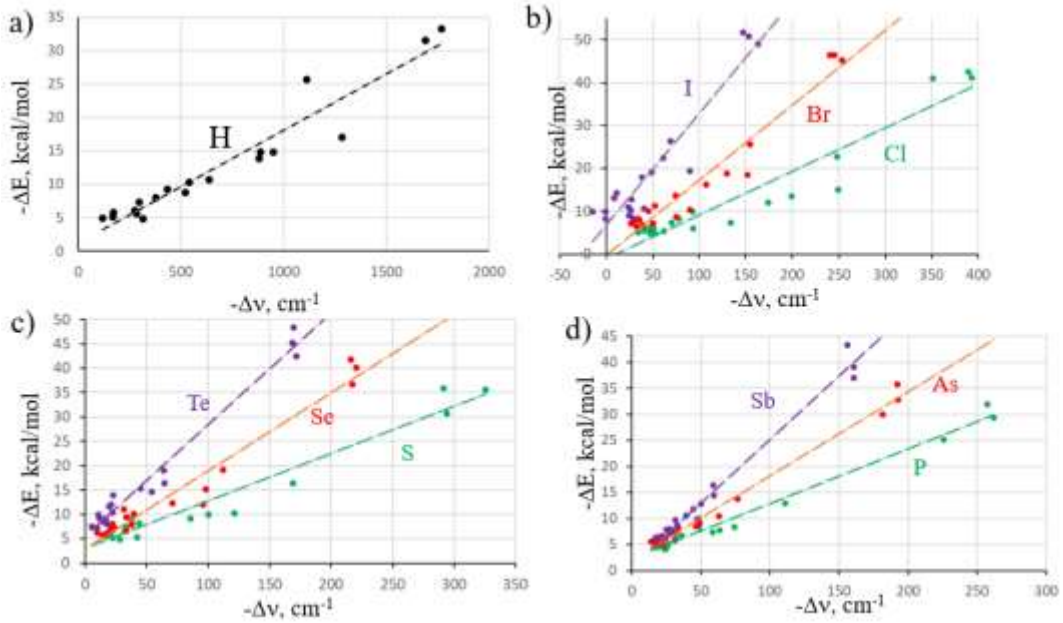

Figure 6-2. Correlation between interaction energy and red shift of the ν(F-A) stretching frequency for a) HB, b) XB, c) YB, and d) ZB complexes. Second, third, and fourth-row A atom data in green, red, and purple, respectively.

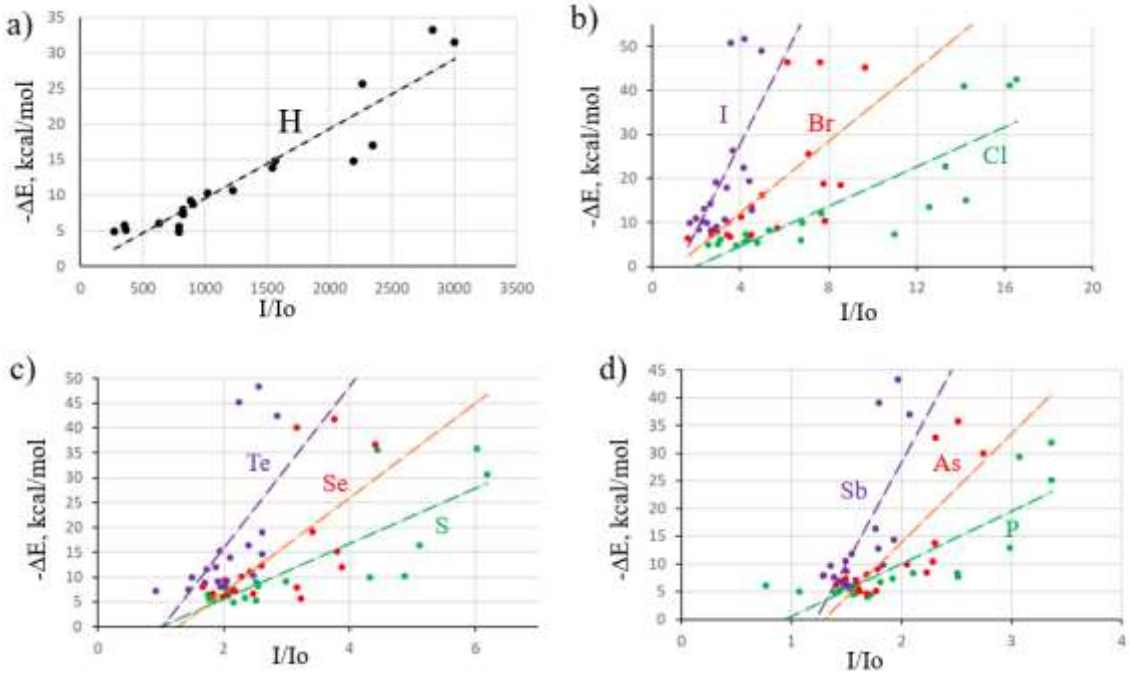

Figure 6-3. Correlation between interaction energy and intensification of the ν(F-A) stretching frequency for a) HB, b) XB, c) YB, and d) ZB complexes.

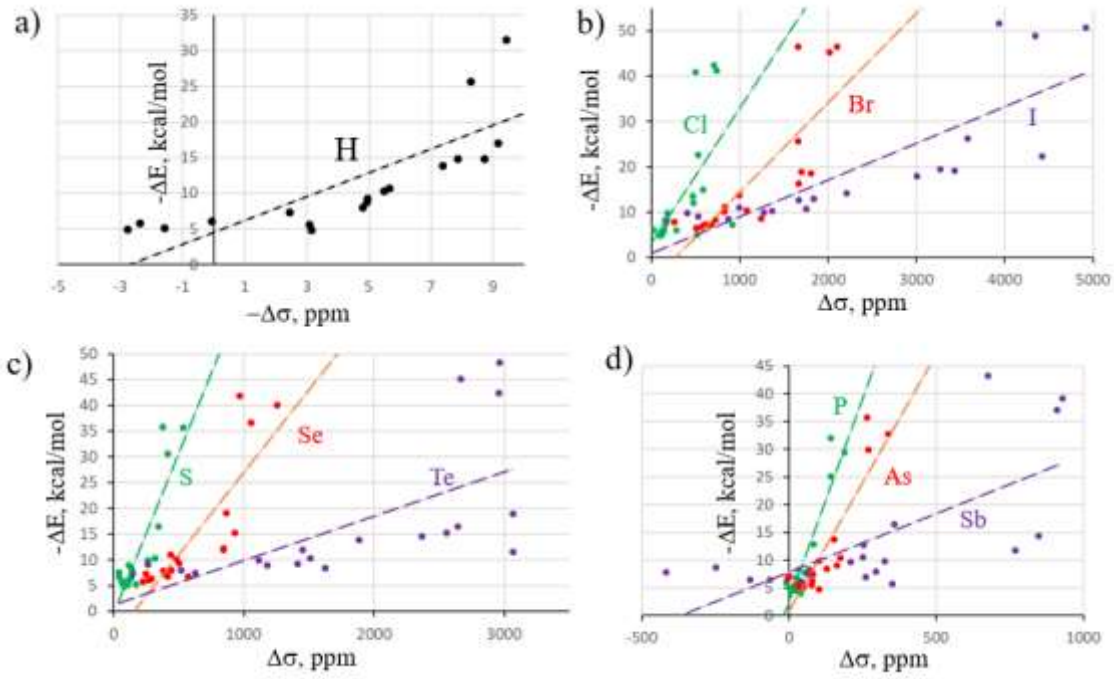

Figure 6-4. Correlation between interaction energy and NMR chemical shielding change of A atom caused by complexation for a) HB, b) XB, c) YB, and d) ZB complexes. (Note negative sign of Δσ in a.)

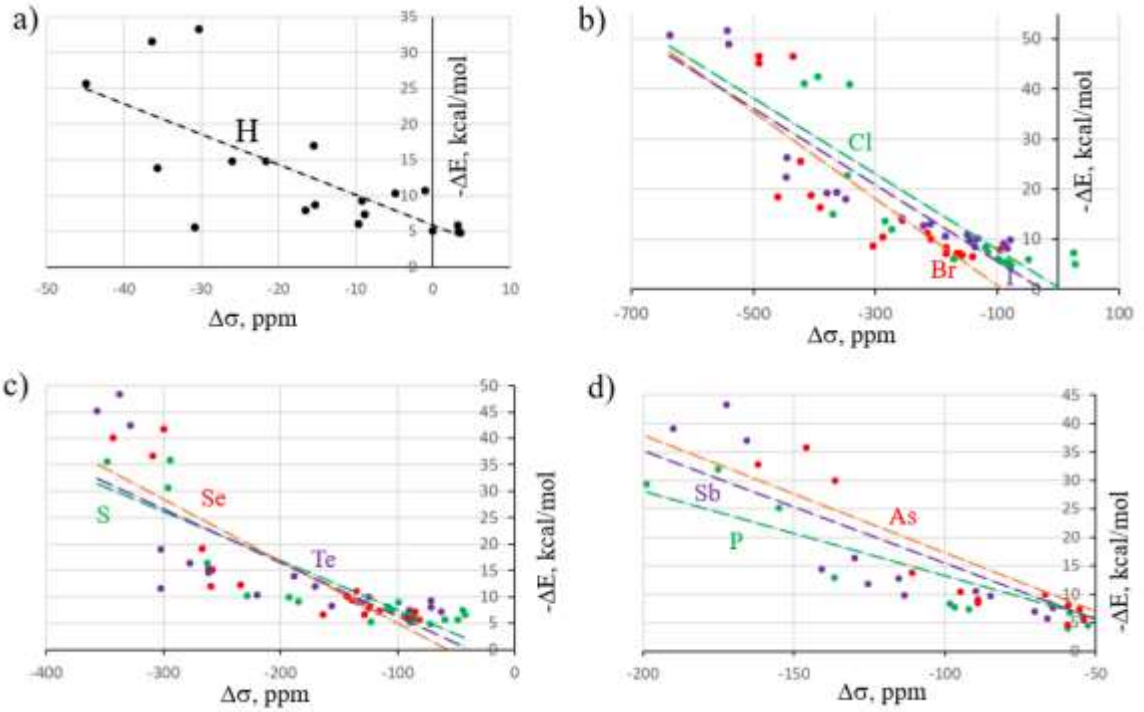

Figure 6-5. Correlation between interaction energy and NMR chemical shielding change of F atom caused by complexation for a) HB, b) XB, c) YB, and d) ZB complexes.

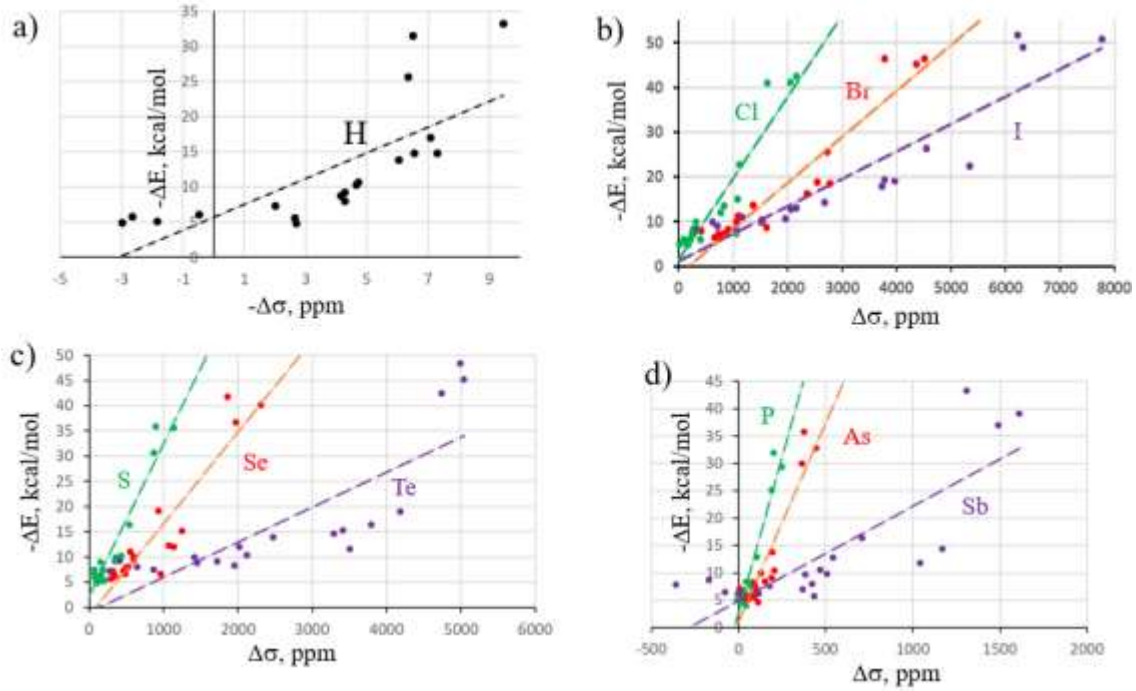

Figure 6-6. Correlation between interaction energy and NMR chemical shielding change of A atom caused by complexation, with no change in Lewis acid geometry, for a) HB, b) XB, c) YB, and d) ZB complexes. (Note negative sign of Δσ in a.)

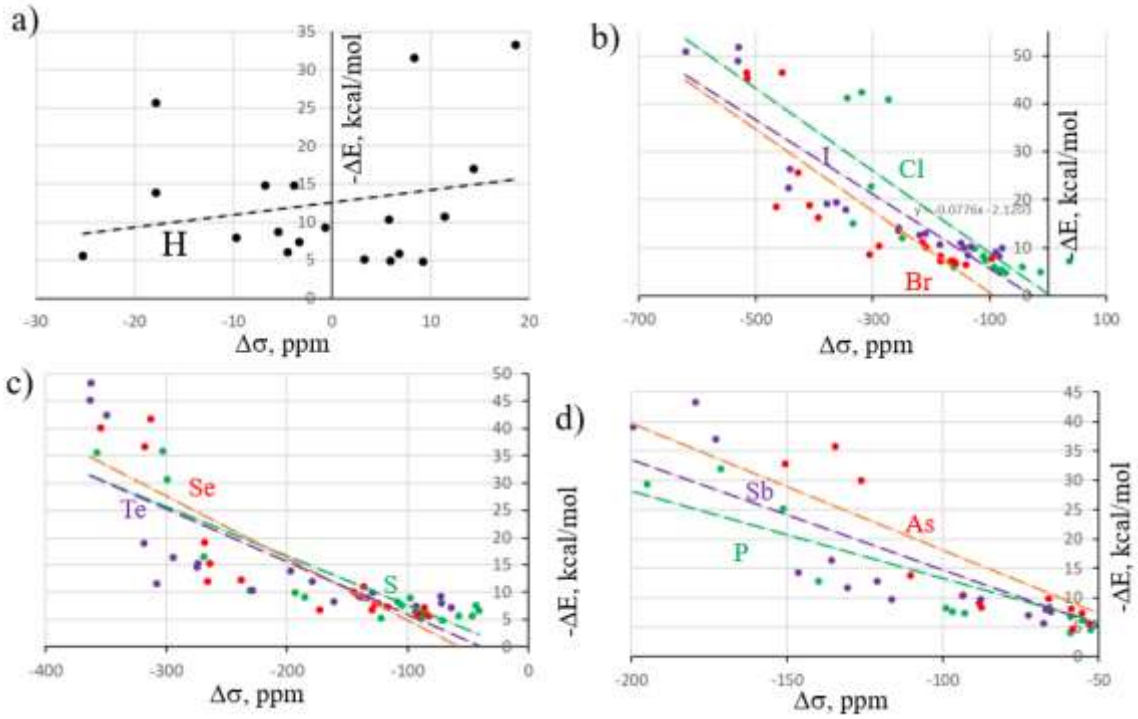

Figure 6-7. Correlation between interaction energy and NMR chemical shielding change of F atom caused by complexation, with no change in Lewis acid geometry, for a) HB, b) XB, c) YB, and d) ZB complexes. (Note negative sign of Δσ in a.)

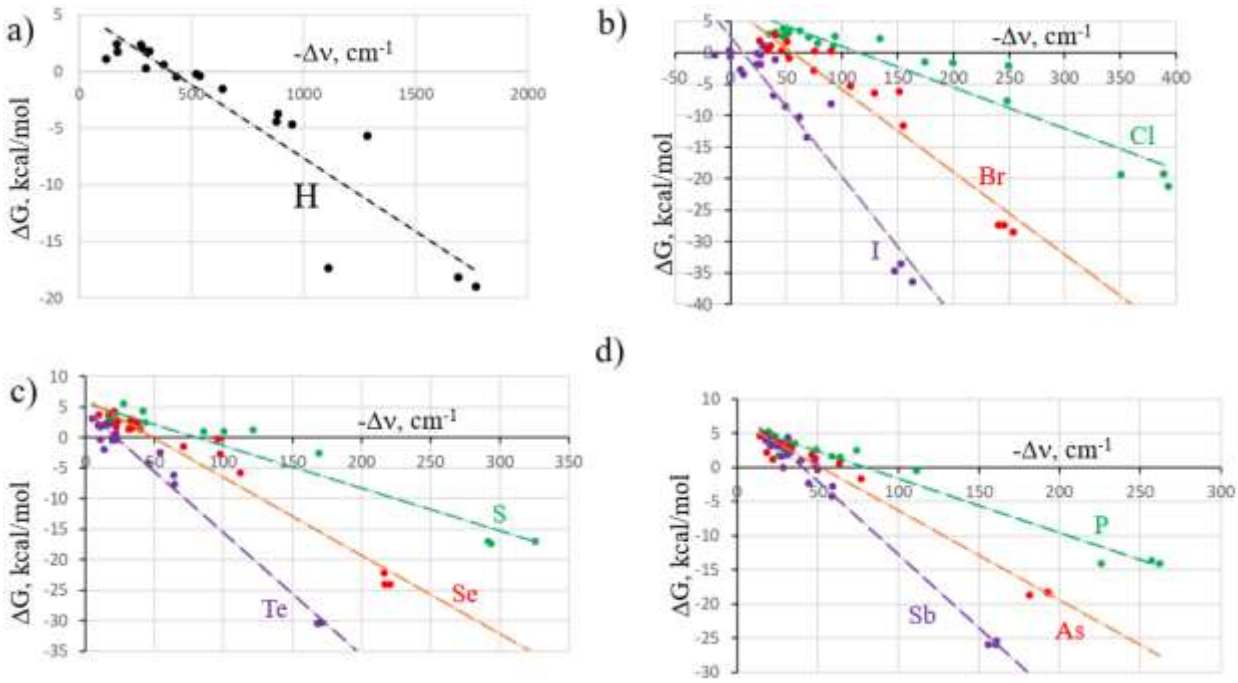

Figure 6-8. Correlation between ΔG(298) and red shift of the ν(F-A) stretching frequency for a) HB, b) XB, c) YB, and d) ZB complexes. Second, third, and fourth-row A atom data in green, red, and purple, respectively.

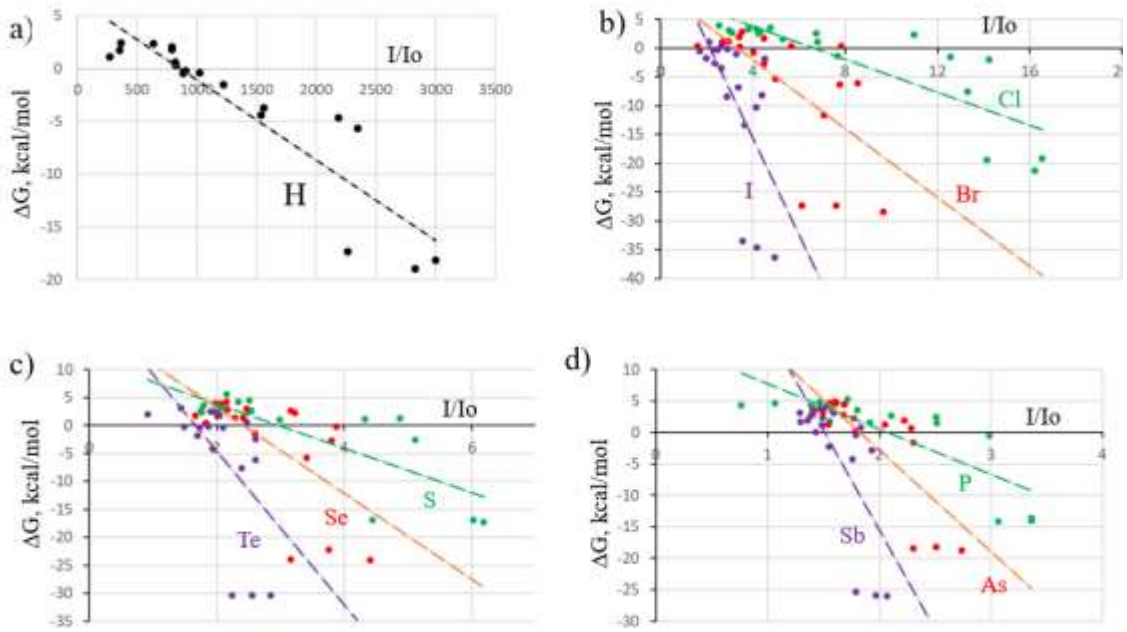

Figure 6-9. Correlation between ΔG(298) and intensification of the ν(F-A) stretching frequency for a) HB, b) XB, c) YB, and d) ZB complexes.

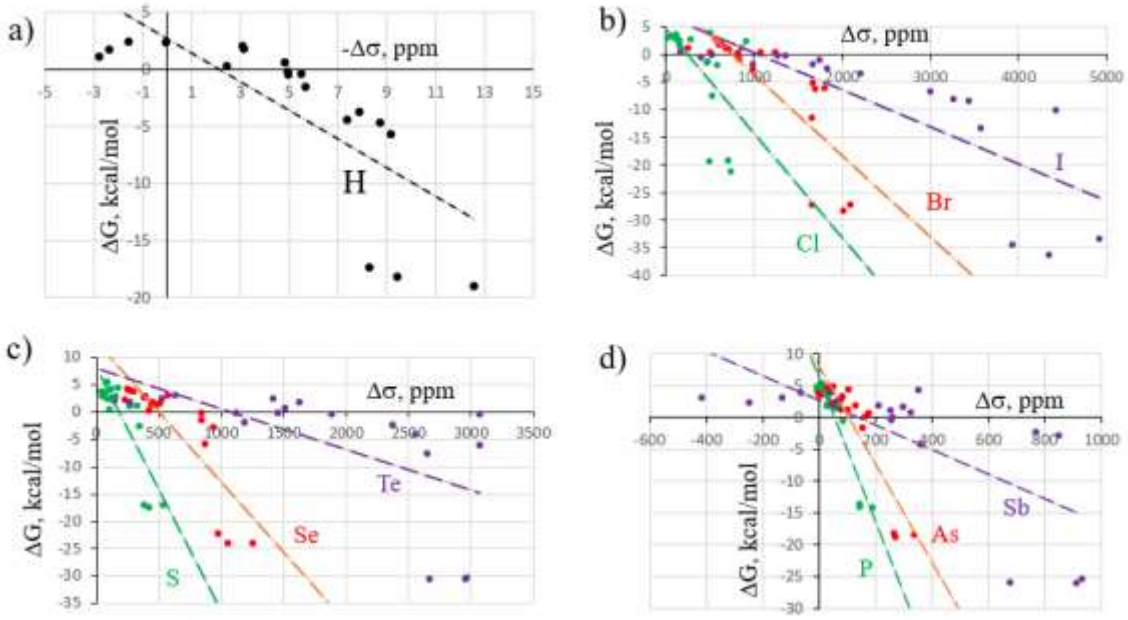

Figure 6-10. Correlation between ΔG(298) and NMR chemical shielding change of A atom caused by complexation for a) HB, b) XB, c) YB, and d) ZB complexes. (Note negative sign of Δσ in a.)

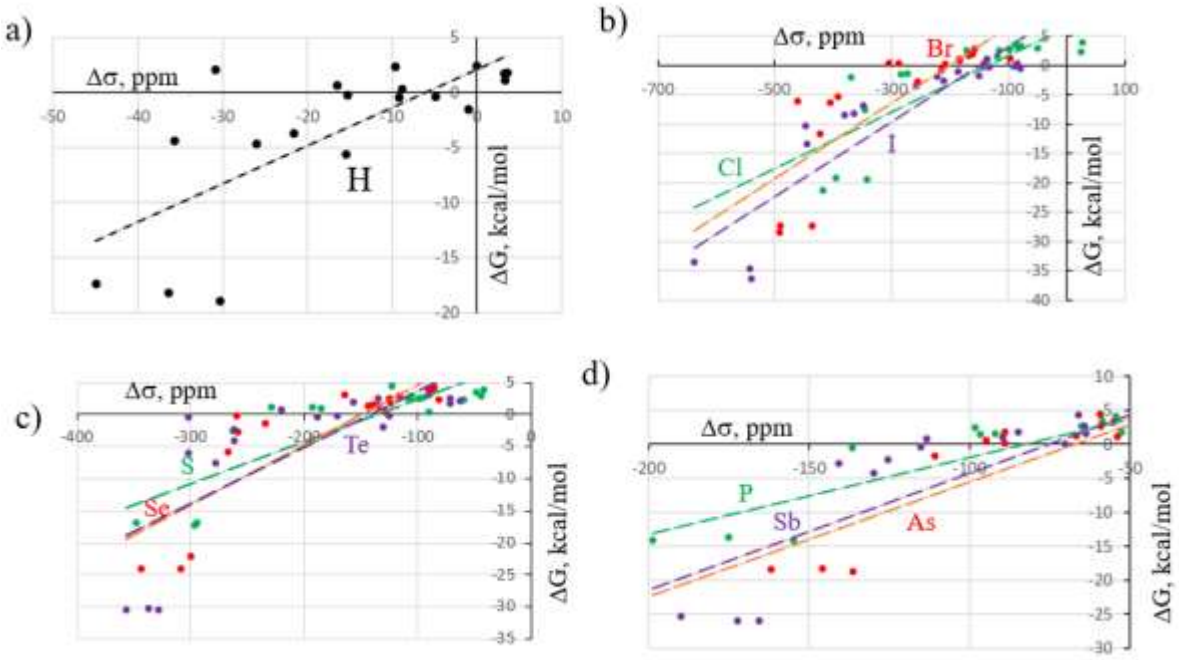

Figure 6-11. Correlation between ΔG(298) and NMR chemical shielding change of F atom caused by complexation for a) HB, b) XB, c) YB, and d) ZB complexes.

CHAPTER 7 SUMMARY

With the development of computational tools of quantum chemistry, computational chemistry has been an essential and powerful tool to calculate the quantitative geometric, structural and bonding features of chemistry systems to inspire, predict and improve the understanding of the part which can't be readily achieved by experiments.

Due to the well-understanding on hydrogen bonds and similarities between hydrogen bonds and halogen bonds, this thesis studied the detailed features quantitatively of halogen, chalcogen and pnicogen bonds systematically in various projects. In Chapter 1, the bond definition, related terms and computational methods used in this thesis were clarified. Chapter 2 introduced the first project in my program. The additional substituents arising from hypervalency present a number of complicating issues for the formation of noncovalent bonds. The XF_5 molecule (X=Cl, Br, I) was allowed to form a halogen bond with NH_3 as base. Hypervalent chalcogen bonding is examined by way of YF_4 and YF_6 (Y=S, Se, Te), and ZF_5 (Z=P, As, Sb) is used to model pnicogen bonding. Pnicogen bonds are particularly strong, with interaction energies approaching 50 kcal/mol, and also involve wholesale rearrangement from trigonal bipyramidal in the monomer to square pyramidal in the complex, subject to a large deformation energy. YF_4 chalcogen bonding is also strong, and like pnicogen bonding, is enhanced by a heavier central atom. XF_5 halogen bond energies are roughly 9 kcal/mol, and display a unique sensitivity to the identity of the X atom. The crowded octahedral structure of YF_6 permits only very weak interactions. As the F atoms of SeF_6 are replaced progressively

by H, a chalcogen bond appears in combination with SeH··N and NH··F H-bonds. The strongest such chalcogen bond appears in SeF_3H_3··NH_3, with a binding energy of 7 kcal/mol, wherein the base is located in the H_3 face of the Lewis acid. Results are discussed in the context of the way in which the positions and intensities of σ-holes are influenced by the locations of substituents and lone electron pairs.

Chapter 3 introduced the transfer of the halogen atom X within $(A{\cdot\cdot}X{\cdot\cdot}A)^+$ systems was calculated for A = NH_3, OH_2, and CH_3, and where X=Cl, Br, and I. These potentials are similar to those computed for equivalent proton transfers. Each contains a single symmetric well for short R(A··A) distances. As R is stretched a second minimum appears, separated from the first by a transfer barrier $E^{\dagger}$ which climbs quickly as R is elongated. The central X prefers association with the N in asymmetric systems $(H_3NX{\cdot\cdot}OH_2)^+$, but a second $(H_3N{\cdot\cdot}XOH_2)^+$ minimum, albeit less stable than the first, can appear if R(N··O) is stretched. Chapter 4 followed the Chapter 3's topic to further studied whether a complete ion pair can form in the halogen, chalcogen and pnicogen transfer. Ab initio calculations assess the displacement of the bridging atom within halogen-bonded complexes and comparison is made with proton transfers within H-bonds. Lewis acid units considered include C-X, N-X, and O-X bonds within the context of F_3CX, FX, F_2NX, FOX, and F_2NOX where X = Cl, Br, and I, and H in the corresponding H-bonded complexes. NMe_3 and NCl_3. were both taken as bases due to their widely differing nucleophilicity. The degree of transfer is small even when a strong acid is combined with a strong base. This reluctance to transfer is due in part to the fact that such a transfer would lead to a high-energy ion pair. Cl shifts its position the most within most of these complexes, followed by Br and then I; the proton is more resistant to transfer. The results

showed though a complete ion pair can't be achieved, there was partial transfer of the bridging atom in some systems.

Chapter 5 studied the Complexes that were formed pairing FX, FHY, FH_2Z, and FH_3T (X=Cl,Br,I; Y=S,Se,Te; Z=P,As,Sb; T=Si,Ge,Sn) with NH_3 so as to form a A···N noncovalent bond, where A refers to the central atom. Geometries, energetics, atomic charges, and spectroscopic characteristics of these complexes were evaluated via DFT calculations. In all cases, the A-F bond, which lies opposite the base and is responsible for the σ-hole on the A atom, elongates and its stretching frequency undergoes a shift to the red. This shift varies from 42 to 175 cm^{-1}, and is largest for the halogen bonds, followed by chalcogen, tetrel, and then pnicogen. The shift also decreases as the central A atom is enlarged. The NMR chemical shielding of the A atom is increased while that of the F and electron donor N atom are lowered. Unlike the IR frequency shifts, it is the third row A atoms that undergo the largest change in NMR shielding. The shielding change of A is highly variable, ranging from negligible for $FSnH_3$ all the way up to 1675 ppm for FBr, while those of the F atom lie in the 55-422 ppm range. Although smaller in magnitude, the changes in the N shielding are still easily detectable, between 7 and 27 ppm. Chapter 6 extended the Badger-Bauer rules that shows the linear correlation between red shift and bond strength to halogen, chalcogen and pnicogen bonds. Also there were similar linear relationship between NMR chemical shift and bond strength.

REFERENCES

1 . Lewis, G. N. The atom and the molecule. *Journal of the American Chemical Society* **1916**, *38* (4), 762-785.

2 . Simandiras, E. D.; Amos, R. D.; Handy, N. C. The analytic evaluation of second-order møller-plesset (MP2) dipole moment derivatives. *Chemical Physics* **1987**, *114* (1), 9-20. DOI: https://doi.org/10.1016/0301-0104(87)80015-0.

3 . Zhao, Y.; Truhlar, D. G. The M06 suite of density functionals for main group thermochemistry, thermochemical kinetics, noncovalent interactions, excited states, and transition elements: two new functionals and systematic testing of four M06-class functionals and 12 other functionals. *Theoretical Chemistry Accounts* **2008**, *120* (1-3), 215-241.

4 . Gaussian09, R. A. 1, MJ Frisch, GW Trucks, HB Schlegel, GE Scuseria, MA Robb, JR Cheeseman, G. Scalmani, V. Barone, B. Mennucci, GA Petersson et al., Gaussian. *Inc., Wallingford CT* **2009**, *121*, 150-166.

5 . Feller, D. The role of databases in support of computational chemistry calculations. *Journal of computational chemistry* **1996**, *17* (13), 1571-1586.

6 . Schuchardt, K. L.; Didier, B. T.; Elsethagen, T.; Sun, L.; Gurumoorthi, V.; Chase, J.; Li, J.; Windus, T. L. Basis set exchange: a community database for computational sciences. *Journal of chemical information and modeling* **2007**, *47* (3), 1045-1052.

7 . Bende, A.; Tosa, V. AB INITIO DENSITY FUNCTIONAL THEORY STUDY OF CF2HCL AND ITS ISOTOPIC SPECIES.

8 . Mohan, N.; Suresh, C. H. Accurate binding energies of hydrogen, halogen, and dihydrogen bonded complexes and cation enhanced binding strengths. *International Journal of Quantum Chemistry* **2014**, *114* (13), 885-894. DOI: https://doi.org/10.1002/qua.24688.

9 . Wang, Y.-H.; Zou, J.-W.; Lu, Y.-X.; Yu, Q.-S.; Xu, H.-Y. Single-electron halogen bond: Ab initio study. *International Journal of Quantum Chemistry* **2007**, *107* (2), 501-506. DOI: https://doi.org/10.1002/qua.21097.

10 . Lu, Y.-X.; Zou, J.-W.; Wang, Y.-H.; Jiang, Y.-J.; Yu, Q.-S. Ab initio investigation of the complexes between bromobenzene and several electron donors: some insights into the magnitude and nature of halogen bonding interactions. *The Journal of Physical Chemistry A* **2007**, *111* (42), 10781-10788.

11 . El-Sheshtawy, H. S.; Bassil, B. S.; Assaf, K. I.; Kortz, U.; Nau, W. M. Halogen bonding inside a molecular container. *Journal of the American Chemical Society* **2012**, *134* (48), 19935-19941.

12 . Riley, K. E.; Hobza, P. Strength and character of halogen bonds in protein–ligand complexes. *Crystal growth & design* **2011**, *11* (10), 4272-4278.

13 . Zhou, P.-P.; Qiu, W.-Y.; Liu, S.; Jin, N.-Z. Halogen as halogen-bonding donor and hydrogen-bonding acceptor simultaneously in ring-shaped H 3 N ·X (Y) ·HF (X= Cl, Br and Y= F, Cl, Br) Complexes. *Physical Chemistry Chemical Physics* **2011**, *13* (16), 7408-7418.

14 . Li, Q.-Z.; Li, R.; Guo, P.; Li, H.; Li, W.-Z.; Cheng, J.-B. Competition of chalcogen bond, halogen bond, and hydrogen bond in SCSHOX and SeCSeHOX (X= Cl and Br) complexes. *Computational and Theoretical Chemistry* **2012**, *980*, 56-61.

15 . Li, Q. Z.; Li, R.; Liu, X. F.; Li, W. Z.; Cheng, J. B. Concerted Interaction between Pnicogen and Halogen Bonds in XCl FH2P NH3 (X= F, OH, CN, NC, and FCC). *ChemPhysChem* **2012**, *13* (5), 1205-1212.

16 . Scheiner, S.; Nziko, V. d. P. Comparison of π-hole tetrel bonding with σ-hole halogen bonds in complexes of XCN (X= F, Cl, Br, I) and NH3. *Physical Chemistry Chemical Physics* **2016**, *18* (5), 3581.

17 . Latajka, Z.; Scheiner, S.; Ratajczak, H. The proton position in hydrogen halide-amine complexes. BrH-NH3 and BrH-NH2CH3. *Chemical physics letters* **1987**, *135* (4-5), 367-372.

18 . Boys, S. F.; Bernardi, F. The calculation of small molecular interactions by the differences of separate total energies. Some procedures with reduced errors. *Molecular Physics* **1970**, *19* (4), 553-566. DOI: 10.1080/00268977000101561.

19 . Gutowski, M.; Van Duijneveldt, F.; Chałasiński, G.; Piela, L. Does the Boys and Bernardi function counterpoise method actually overcorrect the basis set superposition error? *Chemical physics letters* **1986**, *129* (3), 325-328.

20 . Lu, T.; Chen, F. Multiwfn: a multifunctional wavefunction analyzer. *Journal of computational chemistry* **2012**, *33* (5), 580-592.

21 . Foster, a. J.; Weinhold, F. Natural hybrid orbitals. *Journal of the American Chemical Society* **1980**, *102* (24), 7211-7218.

22 . Reed, A. E.; Curtiss, L. A.; Weinhold, F. Intermolecular interactions from a natural bond orbital, donor-acceptor viewpoint. *Chemical Reviews* **1988**, *88* (6), 899-926.

23 . Keith, T. A. AIMAll (Version 13.05. 06). *TK Gristmill Software: Overland Park,*

KS, USA **2013**.

24 . Bader, R. F. W.; Carroll, M. T.; Cheeseman, J. R.; Chang, C. Properties of atoms in molecules: atomic volumes. *Journal of the American Chemical Society* **1987**, *109* (26), 7968-7979. DOI: 10.1021/ja00260a006.

25 . Bader, R. A quantum theory. *Clarendon: Oxford, UK* **1990**.

26 . Pimentel, G.; McClellan, A. The Hydrogen Bond WH Freeman and Co. San Francisco and London. Reinhold Publishing Corporation: New York, USA: 1960.

27 . Hadzi, D. Vibrational spectroscopy of the hydrogen bond. *The Hydrogen Bond-Recent Developments in Theory and Experiments* **1976**, 565-611.

28 . Grabowski, S. J. *Hydrogen bonding: new insights*; Springer, 2006.

29 . Badger, R. M.; Bauer, S. H. Spectroscopic studies of the hydrogen bond. II. The shift of the O–H vibrational frequency in the formation of the hydrogen bond. *The Journal of Chemical Physics* **1937**, *5* (11), 839-851.

30 . Pimentel, G. C.; McClellan, A. Hydrogen bonding. *Annual Review of Physical Chemistry* **1971**, *22* (1), 347-385.

31 . Scheiner, S. *Hydrogen bonding: a theoretical perspective*; Oxford University Press on Demand, 1997.

32 . Desiraju, G.; Steiner, T. The Weak Hydrogen Bond in Structural Chemistry and Biology New York: Oxford University Press Inc. **1999**.

33 . Gilli, G.; Gilli, P. *The nature of the hydrogen bond: outline of a comprehensive hydrogen bond theory*; Oxford university press, 2009.

34 . Politzer, P.; Lane, P.; Concha, M. C.; Ma, Y.; Murray, J. S. An overview of halogen

bonding. *Journal of molecular modeling* **2007**, *13*, 305-311.

35 . Politzer, P.; Murray, J. S. Halogen Bonding: An Interim Discussion. *ChemPhysChem* **2013**, *14* (2), 278-294. DOI: https://doi.org/10.1002/cphc.201200799.

36 . Kozuch, S.; Martin, J. M. Halogen bonds: Benchmarks and theoretical analysis. *Journal of chemical theory and computation* **2013**, *9* (4), 1918-1931.

37 . Desiraju, G. R.; Ho, P. S.; Kloo, L.; Legon, A. C.; Marquardt, R.; Metrangolo, P.; Politzer, P.; Resnati, G.; Rissanen, K. Definition of the halogen bond (IUPAC Recommendations 2013). *Pure and applied chemistry* **2013**, *85* (8), 1711-1713.

38 . Cavallo, G.; Metrangolo, P.; Milani, R.; Pilati, T.; Priimagi, A.; Resnati, G.; Terraneo, G. The halogen bond. *Chemical reviews* **2016**, *116* (4), 2478-2601.

39 . Brinck, T.; Murray, J. S.; Politzer, P. Surface electrostatic potentials of halogenated methanes as indicators of directional intermolecular interactions. *International Journal of Quantum Chemistry* **1992**, *44* (S19), 57-64. DOI: https://doi.org/10.1002/qua.560440709.

40 . Kolář, M. H.; Hobza, P. Computer Modeling of Halogen Bonds and Other σ-Hole Interactions. *Chemical Reviews* **2016**, *116* (9), 5155-5187. DOI: 10.1021/acs.chemrev.5b00560.

41 . Clark, T.; Hennemann, M.; Murray, J. S.; Politzer, P. Halogen bonding: the σ-hole. *Journal of Molecular Modeling* **2007**, *13* (2), 291-296. DOI: 10.1007/s00894-006-0130-2.

42 . Politzer, P.; Murray, J. S.; Clark, T. Halogen bonding and other σ-hole interactions: A perspective. *Physical Chemistry Chemical Physics* **2013**, *15* (27), 11178-11189.

43 . Glendening, E. D.; Landis, C. R.; Weinhold, F. NBO 6.0: natural bond orbital

analysis program. *Journal of computational chemistry* **2013**, *34* (16), 1429-1437.

44 . Szalewicz, K. J., B. Symmetry-adapted perturbation theory of intermolecular interactions. In Molecular Interactions. From Van der Waals to Strongly Bound Complexes; Scheiner, S., Ed. Wiley: New York; pp 3– 43. **1997**.

45 . Moszynski, R.; Wormer, P. E.; Jeziorski, B.; van der Avoird, A. Symmetry-adapted perturbation theory of nonadditive three-body interactions in van der Waals molecules. I. General theory. *The Journal of chemical physics* **1995**, *103* (18), 8058-8074.

46 . H.-J. Werner, P. J. Knowles, G. Knizia, F. R. Manby, M. Schütz, P. Celani, T. Korona, R. Lindh, A. Mitrushenkov, G. Rauhut, K. R. Shamasundar, T. B. Adler, R. D. Amos, A. Bernhardsson, A. Berning, D. L. Cooper, M. J. O. Deegan, A. J. Dobbyn, F. Eckert, E. Goll, C. Hampel, A. Hesselmann, G. Hetzer, T. Hrenar, G. Jansen, C. Köppl, Y. Liu, A. W. Lloyd, R. A. Mata, A. J. May, S. J. McNicholas, W. Meyer, M. E. Mura, A. Nicklass, D. P. O'Neill, P. Palmieri, K. Pflüger, R. Pitzer, M. Reiher, T. Shiozaki, H. Stoll, A. J. Stone, R. Tarron, T. Thorsteinsson, M. Wang, A. Wolf in MOLPRO, version 2010.1, a package of ab initio programs.

47 . Caldin, E.; Gold, V. Proton-Transfer Reactions. Halsted Press: New York, 1975; p 448.

48 . Dodd, J. A.; Baer, S.; Moylan, C. R.; Brauman, J. I. Gas-phase proton-transfer reactions between alkoxide anions. *J. Am. Chem. Soc.* **1991**, *113*, 5942-5949.

49 . Kresge, A. J. What makes proton transfer fast? *Acc. Chem. Res.* **1975**, *8*, 354-360.

50 . Scheiner, S.; Wang, L. Hydrogen bonding and proton transfers of the amide group. *J. Am. Chem. Soc.* **1993**, *115*, 1958-1963.

51 . Scheiner, S.; Hillenbrand, E. A. Modification of pK Values Caused by Change in H-

Bond Geometry. *Proc. Nat. Acad. Sci., USA* **1985**, *82*, 2741-2745.

52 . Scheiner, S. Theoretical studies of proton transfers. *Acc. Chem. Res.* **1985**, *18*, 174-180.

53 . Hillenbrand, E. A.; Scheiner, S. Effects of molecular charge and methyl substitution on proton transfers between oxygen atoms. *J. Am. Chem. Soc.* **1984**, *106*, 6266-6273.

54 . Scheiner, S.; Duan, X. Effect of intermolecular orientation upon proton transfer within a polarizable medium. *Phys. Chem. Chem. Phys.* **1991**, *60*, 874-883.

55 . Scheiner, S. Comparison of proton transfers in cationic heterodimers and homodimers of NH_3 and OH_2. *J. Chem. Phys.* **1982**, *77*, 4039-4050.

56 . Kohen, A.; Jonsson, T.; Klinman, J. P. Effects of protein glycosylation on catalysis: Changes in hydrogen tunneling and enthalpy of activation in the glucose oxidase reaction. *Biochem.* **1997**, *36*, 2603-2611.

57 . Isaacson, A. D.; Wang, L.; Scheiner, S. Variational transition state theory calculation of proton transfer dynamics in $(H_3CH\cdots CH_3)^-$. *J. Phys. Chem.* **1993**, *97*, 1765-1769.

58 . Scheiner, S.; Latajka, Z. Kinetics of proton transfer in $(H_3CH\cdots CH_3)^-$. *J. Phys. Chem.* **1987**, *91*, 724-730.

59 . Hassel, O. Structural aspects of interatomic charge-transfer bonding. *Science* **1970**, *170*, 497-502.

60 . Allen, F. H.; Lommerse, J. P. M.; Hoy, V. J.; Howard, J. A. K.; Desiraju, G. R. Halogen$\cdots$O(nitro) supramolecular synthon in crystal engineering: A combined crystallographic database and ab initio molecular orbital study. *Acta Cryst.* **1997**, *B53*,

1006-1016.

61 . Ikuta, S. Anisotropy of electron-density distribution around atoms in molecules: N, P, O and S atoms. *J. Mol. Struct. (Theochem)* **1990**, *205*, 191-201.

62 . Sedlak, R.; Kolář, M. H.; Hobza, P. Polar Flattening and the Strength of Halogen Bonding. *J. Chem. Theory Comput.* **2015**, *11* (10), 4727-4732. DOI: 10.1021/acs.jctc.5b00687.

63 . Clark, T.; Hennemann, M.; Murray, J. S.; Politzer, P. Halogen bonding: the σ-hole. *J. Mol. Model.* **2007**, *13*, 291-296.

64 . Thirman, J.; Engelage, E.; Huber, S. M.; Head-Gordon, M. Characterizing the interplay of Pauli repulsion, electrostatics, dispersion and charge transfer in halogen bonding with energy decomposition analysis. *Phys. Chem. Chem. Phys.* **2018**, *20* (2), 905-915, 10.1039/C7CP06959F. DOI: 10.1039/C7CP06959F.

65 . Ibrahim, M. A. A.; Hasb, A. A. M. Polarization plays the key role in halogen bonding: a point-of-charge-based quantum mechanical study. *Theor. Chem. Acc.* **2018**, *138* (1), 2, journal article. DOI: 10.1007/s00214-018-2388-8.

66 . Adhikari, U.; Scheiner, S. Substituent effects on Cl ··N, S ··N, and P ··N noncovalent bonds. *J. Phys. Chem. A* **2012**, *116*, 3487-3497.

67 . Bauzá, A.; Ramis, R.; Frontera, A. A Combined Theoretical and Cambridge Structural Database Study of π-Hole Pnicogen Bonding Complexes between Electron Rich Molecules and Both Nitro Compounds and Inorganic Bromides (YO_2Br, Y = N, P, and As). *J. Phys. Chem. A* **2014**, *118*, 2827-2834.

68 . Riley, K. E.; Tran, K.-A. Strength, character, and directionality of halogen bonds

involving cationic halogen bond donors. *Faraday Disc.* **2017**, *203* (0), 47-60, 10.1039/C7FD00106A. DOI: 10.1039/C7FD00106A.

69 . Esrafili, M. D.; Mousavian, P. Unusual cooperativity effects between halogen bond and donor-acceptor interactions: The role of orbital interaction. *Chem. Phys. Lett.* **2017**, *678*, 275-282. DOI: https://doi.org/10.1016/j.cplett.2017.04.052.

70 . Fanfrlík, J.; Holub, J.; Růžičková, Z.; Řezáč, J.; Lane, P. D.; Wann, D. A.; Hnyk, D.; Růžička, A.; Hobza, P. Competition between Halogen, Hydrogen and Dihydrogen Bonding in Brominated Carboranes. *ChemPhysChem.* **2016**, *17* (21), 3373-3376. DOI: 10.1002/cphc.201600848.

71 . Zierkiewicz, W.; Bieńko, D. C.; Michalska, D.; Zeegers-Huyskens, T. Theoretical investigation of the halogen bonded complexes between carbonyl bases and molecular chlorine. *J. Comput. Chem.* **2015**, *36* (11), 821-832. DOI: 10.1002/jcc.23860.

72 . Alkorta, I.; Legon, A. Strengths of non-covalent interactions in hydrogen-bonded complexes B[three dots, centered]HX and halogen-bonded complexes B[three dots, centered]XY (X, Y = F, Cl): an ab initio investigation. *New J. Chem.* **2018**, *42* (13), 10548-10554, 10.1039/C8NJ00470F. DOI: 10.1039/C8NJ00470F.

73 . Grinblat, J.; Ben-Zion, M.; Hoz, S. Halophilic Reactions: Anomalies in Bromine Transfer Reactions. *Journal of the American Chemical Society* **2001**, *123* (43), 10738-10739. DOI: 10.1021/ja011014n.

74 . Makhotkina, O.; Lieffrig, J.; Jeannin, O.; Fourmigué, M.; Aubert, E.; Espinosa, E. Cocrystal or Salt: Solid State-Controlled Iodine Shift in Crystalline Halogen-Bonded Systems. *Crystal Growth & Design* **2015**, *15* (7), 3464-3473. DOI: 10.1021/acs.cgd.5b00535.

75 . Del Bene, J. E.; Alkorta, I.; Elguero, J. Spin−Spin Coupling across Intermolecular F−Cl···N Halogen Bonds. *The Journal of Physical Chemistry A* **2008**, *112* (34), 7925-7929. DOI: 10.1021/jp804119r.

76 . Del Bene, J. E.; Alkorta, I.; Elguero, J. Do traditional, chlorine-shared, and ion-pair halogen bonds exist? an ab initio investigation of FCl:CNX complexes. *J. Phys. Chem. A* **2010**, *114*, 12958-12962.

77 . Del Bene, J. E.; Alkorta, I.; Elguero, J. Influence of Substituent Effects on the Formation of P ··Cl Pnicogen Bonds or Halogen Bonds. *J. Phys. Chem. A* **2014**, *118*, 2360-2366.

78 . Alkorta, I.; Elguero, J.; Del Bene, J. E. Characterizing Traditional and Chlorine-Shared Halogen Bonds in Complexes of Phosphine Derivatives with ClF and Cl2. *The Journal of Physical Chemistry A* **2014**, *118* (23), 4222-4231. DOI: 10.1021/jp503436f.

79 . Alkorta, I.; Elguero, J.; Del Bene, J. E. Boron as an Electron-Pair Donor for B···Cl Halogen Bonds. *ChemPhysChem.* **2016**, *17* (19), 3112-3119. DOI: 10.1002/cphc.201600435.

80 . Chalanchi, S. M.; Alkorta, I.; Elguero, J.; Quiñonero, D. Hydrogen Bond versus Halogen Bond in Cation–Cation Complexes: Effect of the Solvent. *ChemPhysChem* **2017**, *18* (23), 3462-3468.

81 . Carlsson, A.-C. C.; Gräfenstein, J.; Laurila, J. L.; Bergquist, J.; Erdélyi, M. Symmetry of [N–X–N]+halogen bonds in solution. *Chem. Commun.* **2012**, *48* (10), 1458-1460, 10.1039/C1CC15839B. DOI: 10.1039/C1CC15839B.

82 . Carlsson, A.-C. C.; Gräfenstein, J.; Budnjo, A.; Laurila, J. L.; Bergquist, J.; Karim,

A.; Kleinmaier, R.; Brath, U.; Erdélyi, M. Symmetric Halogen Bonding Is Preferred in Solution. *J. Am. Chem. Soc.* **2012**, *134* (12), 5706-5715. DOI: 10.1021/ja301341h.

83 . Georgiou, D. C.; Butler, P.; Browne, E. C.; Wilson, D. J. D.; Dutton, J. L. On the Bonding in Bis-pyridine Iodonium Cations. *Austr. J. Chem.* **2013**, *66* (10), 1179-1188. DOI: https://doi.org/10.1071/CH13202.

84 . Carlsson, A.-C. C.; Mehmeti, K.; Uhrbom, M.; Karim, A.; Bedin, M.; Puttreddy, R.; Kleinmaier, R.; Neverov, A. A.; Nekoueishahraki, B.; Gräfenstein, J.; et al. Substituent Effects on the $[N–I–N]^+$ Halogen Bond. *J. Am. Chem. Soc.* **2016**, *138* (31), 9853-9863. DOI: 10.1021/jacs.6b03842.

85 . Karim, A.; Reitti, M.; Carlsson, A.-C. C.; Gräfenstein, J.; Erdélyi, M. The nature of [N–Cl–N]+ and [N–F–N]+ halogen bonds in solution. *Chem. Sci.* **2014**, *5* (8), 3226-3233, 10.1039/C4SC01175A. DOI: 10.1039/C4SC01175A.

86 . Struble, M. D.; Holl, M. G.; Scerba, M. T.; Siegler, M. A.; Lectka, T. Search for a Symmetrical C–F–C Fluoronium Ion in Solution: Kinetic Isotope Effects, Synthetic Labeling, and Computational, Solvent, and Rate Studies. *J. Am. Chem. Soc.* **2015**, *137* (35), 11476-11490. DOI: 10.1021/jacs.5b07066.

87 . Pitts, C. R.; Holl, M. G.; Lectka, T. Spectroscopic Characterization of a $[C{-}F{-}C]^+$ Fluoronium Ion in Solution. *Angew. Chem. Int. Ed.* **2018**, *57* (7), 1924-1927. DOI: 10.1002/anie.201712021.

88 . Lindblad, S.; Mehmeti, K.; Veiga, A. X.; Nekoueishahraki, B.; Gräfenstein, J.; Erdélyi, M. Halogen Bond Asymmetry in Solution. *J. Am. Chem. Soc.* **2018**, *140* (41), 13503-13513. DOI: 10.1021/jacs.8b09467.

89 . Crugeiras, J.; Ríos, A. Halogen transfer through halogen bonds in halogen-bound

ammonia homodimers. *Physical Chemistry Chemical Physics* **2016**, *18* (45), 30961-30971.

90 . *Gaussian 09*; Wallingford, CT, 2009. (accessed.

91 . Wang, Y.; Zeng, Y.; Li, X.; Meng, L.; Zhang, X. The mutual influence between π-hole pnicogen bonds and σ-hole halogen bonds in complexes of PO_2Cl and XCN/C_6H_6 (X = F, Cl, Br). *Struct. Chem.* **2016**, *27* (5), 1427-1437, journal article. DOI: 10.1007/s11224-016-0762-5.

92 . Spada, L.; Gou, Q.; Geboes, Y.; Herrebout, W. A.; Melandri, S.; Caminati, W. Rotational Study of Dimethyl Ether–Chlorotrifluoroethylene: Lone Pair···π Interaction Links the Two Subunits. *J. Phys. Chem. A* **2016**, *120* (27), 4939-4943. DOI: 10.1021/acs.jpca.5b12571.

93 . Tang, Q.; Li, Q. Non-additivity of F substituent in enhancing the halogen bond in C_6H_5I···NCH. *Comput. Theor. Chem.* **2015**, *1070*, 21-26. DOI: http://dx.doi.org/10.1016/j.comptc.2015.07.024.

94 . Li, W.; Zeng, Y.; Li, X.; Sun, Z.; Meng, L. The competition of Y···O and X···N halogen bonds to enhance the group V σ-hole interaction in the NCY···O=PH_3···NCX and O=PH_3···NCX···NCY (X, Y=F, Cl, and Br) complexes. *J. Comput. Chem.* **2015**, *36* (18), 1349-1358. DOI: 10.1002/jcc.23922.

95 . Geboes, Y.; Proft, F. D.; Herrebout, W. A. Expanding Lone Pair···π Interactions to Nonaromatic Systems and Nitrogen Bases: Complexes of C_2F_3X (X = F, Cl, Br, I) and TMA-d9. *J. Phys. Chem. A* **2015**, *119* (22), 5597-5606. DOI: 10.1021/acs.jpca.5b02283.

96 . Pimentel, G. C.; McClellan, A. L. *The Hydrogen Bond*; Freeman, 1960.

97 . Schuster, P.; Zundel, G.; Sandorfy, C. The Hydrogen Bond. Recent Developments in

Theory and Experiments. North-Holland Publishing Co.: Amsterdam, 1976.

98 . Desiraju, G. R.; Steiner, T. *The Weak Hydrogen Bond in Structural Chemistry and Biology*; Oxford, 1999.

99 . Scheiner, S. Fundamental Features of Hydrogen Bonds. In *Pauling's Legacy - Modern Modelling of the Chemical Bond*, Maksic, Z. B., Orville-Thomas, W. J. Eds.; Theoretical and Computational Chemistry, Vol. 6; Elsevier, 1997; pp 571-591.

100 . Hobza, P.; Havlas, Z. Blue-shifting hydrogen bonds. *Chem. Rev.* **2000**, *100*, 4253-4264.

101 . Hermansson, K. Blue-shifting hydrogen bonds. *J. Phys. Chem. A* **2002**, *106*, 4695-4702.

102 . Li, X.; Liu, L.; Schlegel, H. B. On the physical origin of blue-shifted hydrogen bonds. *J. Am. Chem. Soc.* **2002**, *124*, 9639-9647.

103 . Karpfen, A.; Kryachko, E. S. Blue-shifted hydrogen-bonded complexes. II. $CH_3F\cdots(HF)_{1\leq n\leq 3}$ and $CH_2F_2\cdots(HF)_{1\leq n\leq 3}$. *Chem. Phys.* **2005**, *310*, 77-84.

104 . Scheiner, S.; Kar, T. Red versus blue-shifting hydrogen bonds: Are there fundamental distinctions? *J. Phys. Chem. A* **2002**, *106*, 1784-1789.

105 . Frey, P. A. Characterization of a low barrier hydrogen bond in the active site of chymotrypsin. *J. Mol. Struct.* **2002**, *615*, 153-161.

106 . Steiner, T.; Wilson, C. C.; Majerz, I. Neutron diffraction study of a very short O-H...N hydrogen bond: Crystalline adduct of 2-methylpyridine and pentachlorophenol. *Chem. Commun.* **2000**, 1231-1232.

107 . Cleland, W. W.; Frey, P. A.; Gerlt, J. A. The low barrier hydrogen bond in

enzymatic catalysis. *J. Biol. Chem.* **1998**, *273*, 25529-25532.

108 . Scheiner, S.; Kar, T. The nonexistence of specially stabilized hydrogen bonds in enzymes. *J. Am. Chem. Soc.* **1995**, *117*, 6970-6975.

109 . Chatterjee, P.; Ghosh, A. K.; Samanta, M.; Chakraborty, T. Barrierless Proton Transfer in the Weak C–H ··O Hydrogen Bonded Methacrolein Dimer upon Nonresonant Multiphoton Ionization in the Gas Phase. *J. Phys. Chem. A* **2018**, *122* (25), 5563-5573. DOI: 10.1021/acs.jpca.8b02597.

110 . Cybulski, S. M.; Scheiner, S. Hydrogen bonding and proton transfers involving the carboxylate group. *J. Am. Chem. Soc.* **1989**, *111*, 23-31.

111 . Cybulski, S.; Scheiner, S. Hydrogen bonding and proton transfers involving triply bonded atoms. HC≡N and HC≡CH. *J. Am. Chem. Soc.* **1987**, *109*, 4199-4206.

112 . Legon, A. C.; Rego, C. A. The extent of proton transfer from X to N in the gas-phase dimers $(CH_3)_{3-n}H_nN\cdots HX$. Evidence from rotational spectroscopy. *Chem. Phys. Lett.* **1989**, *162*, 369-375.

113 . Bountis, T. Proton Transfer in Hydrogen-Bonded Systems. In *NATO ASI*, Plenum Press: New York, 1992; Vol. Series B: Physics Vol. 291, p 361.

114 . Scheiner, S. Bent hydrogen bonds and proton transfer. *Acc. Chem. Res.* **1994**, *27*, 402-408.

115 . Shida, N.; Almlöf, J.; Barbara, P. F. Tunneling paths in intramolecular proton transfer. *J. Phys. Chem.* **1991**, *95*, 10457-10464.

116 . Rucker, J.; Klinman, J. P. Computational study of tunneling and coupled motion in alcohol dehydrogenase-catalyzed reactions: Implication for measured hydrogen and

carbon isotope effects. *J. Am. Chem. Soc.* **1999**, *121*, 1997-2006.

117 . Riley, K. E.; Merz, K. M. Insights into the strength and origin of halogen bonding: The halobenzene-formaldehyde dimer. *J. Phys. Chem. A* **2007**, *111*, 1688-1694.

118 . Metrangolo, P.; Resnati, G. *Halogen Bonding. Fundamentals and Applications*; Springer, 2008.

119 . Alkorta, I.; Sanchez-Sanz, G.; Elguero, J. Linear free energy relationships in halogen bonds. *CrystEngComm* **2013**, *15*, 3178-3186.

120 . Duarte, D. J. R.; Sosa, G. L.; Peruchena, N. M.; Alkorta, I. Halogen bonding. The role of the polarizability of the electron-pair donor. *Phys. Chem. Chem. Phys.* **2016**, *18* (10), 7300-7309, 10.1039/C5CP07941A. DOI: 10.1039/C5CP07941A.

121 . Grabowski, S. J. Hydrogen and halogen bonds are ruled by the same mechanisms. *Phys. Chem. Chem. Phys.* **2013**, *15*, 7249-7259.

122 . Grabowski, S. J. Halogen bond and its counterparts: Bent's rule explains the formation of nonbonding interactions. *J. Phys. Chem. A* **2011**, *115*, 12340-12347.

123 . Bauzá, A.; Quiñonero, D.; Frontera, A.; Deyà, P. M. Substituent effects in halogen bonding complexes between aromatic donors and acceptors: a comprehensive ab initio study. *Phys. Chem. Chem. Phys.* **2011**, *13*, 20371-20379.

124 . Turunen, L.; Hansen, J. H.; Erdélyi, M. Halogen Bonding: An Odd Chemistry? *The Chemical Record* **2021**, *21* (5), 1252-1257. DOI: https://doi.org/10.1002/tcr.202100060.

125 . Lapp, J.; Scheiner, S. Proximity Effects of Substituents on Halogen Bond Strength. *J. Phys. Chem. A* **2021**, *125* (23), 5069-5077. DOI: 10.1021/acs.jpca.1c03817.

126 . de Azevedo Santos, L.; van der Lubbe, S. C. C.; Hamlin, T. A.; Ramalho, T. C.;

Matthias Bickelhaupt, F. A Quantitative Molecular Orbital Perspective of the Chalcogen Bond. *ChemistryOpen* **2021**, *10* (4), 391-401. DOI: https://doi.org/10.1002/open.202000323.

127 . Auffinger, P.; Hays, F. A.; Westhof, E.; Ho, P. S. Halogen bonds in biological molecules. *Proc. Nat. Acad. Sci., USA* **2004**, *101*, 16789-16794.

128 . Del Bene, J. E.; Alkorta, I.; Montero-Campillo, M. M.; Elguero, J. Using protonation to change a Cl···N halogen bond in N-Base:ClOH complexes to a Cl···O halogen bond. *Chem. Phys. Lett.* **2018**, *710*, 123-128. DOI: https://doi.org/10.1016/j.cplett.2018.08.027.

129 . Del Bene, J. E.; Alkorta, I.; Elguero, J. Using one halogen bond to change the nature of a second bond in ternary complexes with P···Cl and F···Cl halogen bonds. *Faraday Disc.* **2017**, *203* (0), 29-45, 10.1039/C7FD00048K. DOI: 10.1039/C7FD00048K.

130 . Del Bene, J. E.; Alkorta, I.; Elguero, J. Hydrogen bonds and halogen bonds in complexes of carbones L→C←L as electron donors to HF and ClF, for L = CO, N_2, HNC, PH_3, and SH_2. *Phys. Chem. Chem. Phys.* **2020**, *22* (28), 15966-15975, 10.1039/D0CP02009E. DOI: 10.1039/D0CP02009E.

131 . Del Bene, J. E.; Alkorta, I.; Elguero, J. Do nitrogen bases form chlorine-shared and ion-pair halogen bonds? *Chem. Phys. Lett.* **2011**, *508*, 6-9.

132 . Scheiner, S.; Michalczyk, M.; Wysokiński, R.; Zierkiewicz, W. Structures and energetics of clusters surrounding diatomic anions stabilized by hydrogen, halogen, and other noncovalent bonds. *Chem. Phys.* **2020**, *530*, 110590. DOI: https://doi.org/10.1016/j.chemphys.2019.110590.

133 . Scheiner, S.; Michalczyk, M.; Zierkiewicz, W. Coordination of anions by noncovalently bonded σ-hole ligands. *Coord. Chem. Rev.* **2020**, *405*, 213136. DOI: https://doi.org/10.1016/j.ccr.2019.213136.

134 . Scheiner, S.; Michalczyk, M.; Zierkiewicz, W. Structures of clusters surrounding ions stabilized by hydrogen, halogen, chalcogen, and pnicogen bonds. *Chem. Phys.* **2019**, *524*, 55-62. DOI: https://doi.org/10.1016/j.chemphys.2019.05.005.

135 . Lu, J.; Scheiner, S. Comparison of halogen with proton transfer. Symmetric and asymmetric systems. *Chemical Physics Letters* **2019**, *731*, 136593. DOI: https://doi.org/10.1016/j.cplett.2019.136593.

136 . *Gaussian 09*; Wallingford, CT, 2009. (accessed.

137 . Wang, R.; Lu, Y.; Xu, Z.; Liu, H. Triangular Interchalcogen Interactions: A Joint Crystallographic Data Analysis and Theoretical Study. *J. Phys. Chem. A* **2021**, *125* (19), 4173-4183. DOI: 10.1021/acs.jpca.1c03244.

138 . Devore, D. P.; Ellington, T. L.; Shuford, K. L. Interrogating the Interplay between Hydrogen and Halogen Bonding in Graphitic Carbon Nitride Building Blocks. *J. Phys. Chem. A* **2020**, *124* (51), 10817-10825. DOI: 10.1021/acs.jpca.0c09154.

139 . Sanchez-Sanz, G.; Trujillo, C.; Alkorta, I.; Elguero, J. Intramolecular pnicogen interactions in phosphorus and arsenic analogues of proton sponges. *Phys. Chem. Chem. Phys.* **2014**, *16* (Physical Chemistry Chemical Physics30), 15900-15909, 10.1039/C4CP01072H. DOI: 10.1039/C4CP01072H.

140 . Scheiner, S.; Grabowski, S. J.; Kar, T. Influence of hybridization and substitution upon the properties of the CH ·O hydrogen bond. *J. Phys. Chem. A* **2001**, *105*, 10607-

10612.

141 . Hou, M.; Li, Q.; Scheiner, S. The ability of a tetrel bond to transition a neutral amino acid into a zwitterion. *Chem. Phys. Lett.* **2019**, *731,* 136584. DOI: https://doi.org/10.1016/j.cplett.2019.07.012.

142 . Wei, Y.; Li, Q.; Scheiner, S. The π-Tetrel Bond and its Influence on Hydrogen Bonding and Proton Transfer. *ChemPhysChem.* **2018**, *19* (6), 736-743. DOI: doi:10.1002/cphc.201701136.

143 . Del Bene, J. E.; Alkorta, I.; Elguero, J. Exploring N…C tetrel and O…S chalcogen bonds in HN(CH)SX:OCS systems, for X = F, NC, Cl, CN, CCH, and H. *Chem. Phys. Lett.* **2019**, *730*, 466-471. DOI: https://doi.org/10.1016/j.cplett.2019.05.044.

144 . Gougoula, E.; Medcraft, C.; Alkorta, I.; Walker, N. R.; Legon, A. C. A chalcogen-bonded complex $H_3N\cdots S{=}C{=}S$ formed by ammonia and carbon disulfide characterised by chirped-pulse, broadband microwave spectroscopy. *J. Chem. Phys.* **2019**, *150* (8), 084307. DOI: 10.1063/1.5085281.

145 . Alkorta, I.; Legon, A. An Ab Initio Investigation of the Geometries and Binding Strengths of Tetrel-, Pnictogen-, and Chalcogen-Bonded Complexes of CO_2, N_2O, and CS_2 with Simple Lewis Bases: Some Generalizations. *Molecules* **2018**, *23* (9), 2250.

146 . Grabowski, S. J. Pnicogen and tetrel bonds—tetrahedral Lewis acid centres. *Struct. Chem.* **2019**, *30* (4), 1141-1152, journal article. DOI: 10.1007/s11224-019-01358-1.

147 . Grabowski, S. Tetrel Bonds with π-Electrons Acting as Lewis Bases—Theoretical Results and Experimental Evidences. *Molecules* **2018**, *23* (5), 1183.

148 . Alkorta, I.; Elguero, J.; Grabowski, S. J. Pnicogen and hydrogen bonds: complexes

between PH_3X^+ and PH_2X systems. *Phys. Chem. Chem. Phys.* **2015**, *17* (5), 3261-3272, 10.1039/C4CP04840G. DOI: 10.1039/C4CP04840G.

149 . Franconetti, A.; Quiñonero, D.; Frontera, A.; Resnati, G. Unexpected chalcogen bonds in tetravalent sulfur compounds. *Phys. Chem. Chem. Phys.* **2019**, *21* (21), 11313-11319, 10.1039/C9CP01033E. DOI: 10.1039/C9CP01033E.

150 . Franconetti, A.; Frontera, A. Theoretical and Crystallographic Study of Lead(IV) Tetrel Bonding Interactions. *Chem. Eur. J.* **2019**, *25* (23), 6007-6013. DOI: 10.1002/chem.201900447.

151 . Frontera, A.; Bauzá, A. S···Sn Tetrel Bonds in the Activation of Peroxisome Proliferator-Activated Receptors (PPARs) by Organotin Molecules. *Chem. Eur. J.* **2018**, *24* (62), 16582-16587. DOI: doi:10.1002/chem.201804676.

152 . Murray, J. S.; Politzer, P. σ-Holes and Si ··N intramolecular interactions. *J. Mol. Model.* **2019**, *25* (4), 101, journal article. DOI: 10.1007/s00894-019-3962-2.

153 . Clark, T.; Murray, J. S.; Politzer, P. A perspective on quantum mechanics and chemical concepts in describing noncovalent interactions. *Phys. Chem. Chem. Phys.* **2018**, *20* (48), 30076-30082, 10.1039/C8CP06786D. DOI: 10.1039/C8CP06786D.

154 . Riley, K. E.; Vazquez, M.; Umemura, C.; Miller, C.; Tran, K.-A. Exploring the (Very Flat) Potential Energy Landscape of R−Br···π Interactions with Accurate CCSD(T) and SAPT Techniques. *Chem. Eur. J.* **2016**, *22* (49), 17690-17695. DOI: 10.1002/chem.201603674.

155 . Scheiner, S. The pnicogen bond: Its relation to hydrogen, halogen, and other noncovalent bonds. *Acc. Chem. Res.* **2013**, *46*, 280-288.

156 . Zierkiewicz, W.; Michalczyk, M.; Wysokiński, R.; Scheiner, S. On the ability of pnicogen atoms to engage in both σ and π-hole complexes. Heterodimers of $ZF_2C_6H_5$ (Z = P, As, Sb, Bi) and NH_3. *J. Mol. Model.* **2019**, *25* (6), 152, journal article. DOI: 10.1007/s00894-019-4031-6.

157 . Zierkiewicz, W.; Michalczyk, M.; Wysokiński, R.; Scheiner, S. Dual Geometry Schemes in Tetrel Bonds: Complexes between TF_4 (T = Si, Ge, Sn) and Pyridine Derivatives. *Molecules* **2019**, *24* (2), 376.

158 . Zierkiewicz, W.; Fanfrl ĸ, J.; Michalczyk, M.; Michalska, D.; Hobza, P. S···N chalcogen bonded complexes of carbon disulfide with diazines. Theoretical study. *Chem. Phys.* **2018**, *500*, 37-44. DOI: https://doi.org/10.1016/j.chemphys.2017.11.014.

159 . Dong, W.; Niu, B.; Liu, S.; Cheng, J.; Liu, S.; Li, Q. Comparison of σ-/π-Hole Tetrel Bonds between TH_3F/F_2TO and H_2CX (X=O, S, Se). *ChemPhysChem.* **2019**, *20* (4), 627-635. DOI: doi:10.1002/cphc.201800990.

160 . Dong, W.; Wang, Y.; Cheng, J.; Yang, X.; Li, Q. Competition between σ-hole pnicogen bond and π-hole tetrel bond in complexes of $CF_2{=}CFZH_2$ (Z = P, As, and Sb). *Mol. Phys.* **2019**, *117* (3), 251-259. DOI: 10.1080/00268976.2018.1508782.

161 . Dong, W.; Li, Q.; Scheiner, S. Comparative Strengths of Tetrel, Pnicogen, Chalcogen, and Halogen Bonds and Contributing Factors. *Molecules* **2018**, *23* (7), 1681.

162 . Stasyuk, O. A.; Sedlak, R.; Guerra, C. F.; Hobza, P. Comparison of the DFT-SAPT and Canonical EDA Schemes for the Energy Decomposition of Various Types of Noncovalent Interactions. *J. Chem. Theory Comput.* **2018**, *14* (7), 3440-3450. DOI: 10.1021/acs.jctc.8b00034.

163 . Sedlak, R.; Eyrilmez, S. M.; Hobza, P.; Nachtigallova, D. The role of the σ-holes

in stability of non-bonded chalcogenide···benzene interactions: the ground and excited states. *Phys. Chem. Chem. Phys.* **2018**, *20* (1), 299-306, 10.1039/C7CP05537D. DOI: 10.1039/C7CP05537D.

164 . Esrafili, M.; Mousavian, P. Strong Tetrel Bonds: Theoretical Aspects and Experimental Evidence. *Molecules* **2018**, *23* (10), 2642.

165 . Scheiner, S.; Adhikari, U. Abilities of different electron donors (D) to engage in a P···D noncovalent interaction. *J. Phys. Chem. A* **2011**, *115*, 11101-11110.

166 . Esrafili, M. D.; Mousavian, P.; Mohammadian-Sabet, F. Tuning of pnicogen and chalcogen bonds by an aerogen-bonding interaction: a comparative ab initio study. *Mol. Phys.* **2019**, *117* (1), 58-66. DOI: 10.1080/00268976.2018.1492746.

167 . Scilabra, P.; Terraneo, G.; Resnati, G. The Chalcogen Bond in Crystalline Solids: A World Parallel to Halogen Bond. *Acc. Chem. Res.* **2019**, *52* (5), 1313-1324. DOI: 10.1021/acs.accounts.9b00037.

168 . Kuwano, S.; Suzuki, T.; Yamanaka, M.; Tsutsumi, R.; Arai, T. Catalysis Based on C−I · · · π Halogen Bonds: Electrophilic Activation of 2-Alkenylindoles by Cationic Halogen-Bond Donors for [4+2] Cycloadditions. *Angew. Chem. Int. Ed.* **2019**, *58* (30), 10220-10224. DOI: 10.1002/anie.201904689.

169 . Scheiner, S. Comparison of halide receptors based on H, halogen, chalcogen, pnicogen, and tetrel bonds. *Faraday Disc.* **2017**, *203* (0), 213-226, 10.1039/C7FD00043J. DOI: 10.1039/C7FD00043J.

170 . Dreger, A.; Wonner, P.; Engelage, E.; Walter, S. M.; Stoll, R.; Huber, S. M. A halogen-bonding-catalysed Nazarov cyclisation reaction. *Chem. Commun.* **2019**, *55* (57),

8262-8265, 10.1039/C9CC02816A. DOI: 10.1039/C9CC02816A.

171 . Trievel, R. C.; Scheiner, S. Crystallographic and Computational Characterization of Methyl Tetrel Bonding in S-Adenosylmethionine-Dependent Methyltransferases. *Molecules* **2018**, *23* (11), 2965-2981.

172 . Vanderkooy, A.; Gupta, A. K.; Földes, T.; Lindblad, S.; Orthaber, A.; Pápai, I.; Erdélyi, M. Halogen Bonding Helicates Encompassing Iodonium Cations. *Angew. Chem. Int. Ed.* **2019**, *58* (27), 9012-9016. DOI: 10.1002/anie.201904817.

173 . Pan, F.; Chen, Y.; Li, S.; Jiang, M.; Rissanen, K. Iodine Clathrated: A Solid-State Analogue of the Iodine–Starch Complex. *Chem. Eur. J.* **2019**, *25* (31), 7485-7488. DOI: 10.1002/chem.201901734.

174 . Perera, M. D.; Aakeröy, C. B. Organocatalysis by a multidentate halogen-bond donor: an alternative to hydrogen-bond based catalysis. *New J. Chem.* **2019**, *43* (21), 8311-8314, 10.1039/C9NJ01404G. DOI: 10.1039/C9NJ01404G.

175 . Scheiner, S. Differential Binding of Tetrel-Bonding Bipodal Receptors to Monatomic and Polyatomic Anions. *Molecules* **2019**, *24* (2), 227.

176 . Scheiner, S. Assembly of Effective Halide Receptors from Components. Comparing Hydrogen, Halogen, and Tetrel Bonds. *J. Phys. Chem. A* **2017**, *121* (18), 3606-3615. DOI: 10.1021/acs.jpca.7b02305.

177 . Del Bene, J. E.; Alkorta, I.; Elguero, J. Anionic complexes of F^- and Cl^- with substituted methanes: Hydrogen, halogen, and tetrel bonds. *Chem. Phys. Lett.* **2016**, *655–656*, 115-119. DOI: http://dx.doi.org/10.1016/j.cplett.2016.05.030.

178 . Scheiner, S. Can two trivalent N atoms engage in a direct N···N noncovalent

interaction? *Chem. Phys. Lett.* **2011**, *514*, 32-35.

179 . Southern, S. A.; Bryce, D. L. NMR Investigations of Noncovalent Carbon Tetrel Bonds. Computational Assessment and Initial Experimental Observation. *J. Phys. Chem. A* **2015**, *119* (49), 11891-11899. DOI: 10.1021/acs.jpca.5b10848.

180 . Scheiner, S. Comparison of CH ··O, SH ··O, Chalcogen, and Tetrel Bonds Formed by Neutral and Cationic Sulfur-Containing Compounds. *The Journal of Physical Chemistry A* **2015**, *119* (34), 9189-9199. DOI: 10.1021/acs.jpca.5b06831.

181 . Nziko, V. d. P. N.; Scheiner, S. Comparison of π-hole tetrel bonding with σ-hole halogen bonds in complexes of XCN (X = F, Cl, Br, I) and NH_3. *Phys. Chem. Chem. Phys.* **2016**, *18* (5), 3581-3590, 10.1039/C5CP07545A. DOI: 10.1039/C5CP07545A.

182 . Liu, M.; Li, Q.; Scheiner, S. Comparison of tetrel bonds in neutral and protonated complexes of pyridineTF_3 and furanTF_3 (T = C, Si, and Ge) with NH_3. *Phys. Chem. Chem. Phys.* **2017**, *19* (7), 5550-5559, 10.1039/C6CP07531B. DOI: 10.1039/C6CP07531B.

183 . Scheiner, S. Systematic Elucidation of Factors That Influence the Strength of Tetrel Bonds. *J. Phys. Chem. A* **2017**, *121* (29), 5561-5568. DOI: 10.1021/acs.jpca.7b05300.

184 . Hadzi, D.; Bratos, S. Vibrational Spectroscopy of the hydrogen bond. In *The Hydrogen Bond. Recent Developments in Theory and Experiments*, Schuster, P., Zundel, G., Sandorfy, C. Eds.; Vol. 2; North-Holland Publishing Co., 1976; pp 565-611.

185 . Gilli, G.; Gilli, P. *The Nature of the Hydrogen Bond*; Oxford University Press, 2009.

186 . Scheiner, S. *Hydrogen Bonding: A Theoretical Perspective*; Oxford University

Press, 1997.

187 . Masunov, A.; Dannenberg, J. J.; Contreras, R. H. C-H bond-shortening upon hydrogen bond formation: Influence of an electric field. *J. Phys. Chem. A* **2001**, *105*, 4737-4740.

188 . Gu, Y.; Kar, T.; Scheiner, S. Fundamental properties of the CH···O interaction: Is it a true hydrogen bond? *J. Am. Chem. Soc.* **1999**, *121*, 9411-9422.

189 . Qian, W.; Krimm, S. C-H···O and O-H···O hydrogen bonding in formic acid dimer structures: A QM/MM study confirms the common origin of their different spectroscopic behavior. *J. Phys. Chem. A* **2002**, *106*, 11663-11671.

190 . Jabłoński, M. Red and blue shifted hydridic bonds. *J. Comput. Chem.* **2014**, *35* (24), 1739-1747. DOI: 10.1002/jcc.23678.

191 . Gu, Y.; Kar, T.; Scheiner, S. Comparison of the CH···N and CH···O interactions involving substituted alkanes. *J. Mol. Struct.* **2000**, *552*, 17-31.

192 . Bene, J. E. D.; Alkorta, I.; Elguero, J. Properties of cationic pnicogen-bonded complexes $F_{4-n}H_nP^+$:N-base with H–P ··N linear and n = 1–4. *Mol. Phys.* **2016**, *114* (1), 102-117. DOI: 10.1080/00268976.2015.1086835.

193 . Ellington, T. L.; Reves, P. L.; Simms, B. L.; Wilson, J. L.; Watkins, D. L.; Tschumper, G. S.; Hammer, N. I. Quantifying the Effects of Halogen Bonding by Haloaromatic Donors on the Acceptor Pyrimidine. *ChemPhysChem.* **2017**, *18* (10), 1267-1273. DOI: 10.1002/cphc.201700114.

194 . Esrafili, M. D.; Vakili, M. The effect of hydrogen-bonding cooperativity on the strength and properties of σ-hole interactions: an ab initio study. *Mol. Phys.* **2017**, *115*

(8), 913-924. DOI: 10.1080/00268976.2017.1292013.

195 . Gholipour, A.; Farhadi, S.; Neyband, R. S. Theoretical investigation of the nature and strength of simultaneous interactions of π–π stacking and halogen bond including NMR, SAPT, AIM and NBO analysis. *Struct. Chem.* **2016**, *27* (5), 1543-1551, journal article. DOI: 10.1007/s11224-016-0784-z.

196 . Cormanich, R. A.; Rittner, R.; O'Hagan, D.; Bühl, M. Inter- and intramolecular CF ··C=O interactions on aliphatic and cyclohexane carbonyl derivatives. *J. Comput. Chem.* **2016**, *37* (1), 25-33. DOI: 10.1002/jcc.23918.

197 . Viger-Gravel, J.; Leclerc, S.; Korobkov, I.; Bryce, D. L. Correlation between ^{13}C chemical shifts and the halogen bonding environment in a series of solid para-diiodotetrafluorobenzene complexes. *CrystEngComm* **2013**, *15*, 3168-3177.

198 . Alkorta, I.; Sánchez-Sanz, G.; Elguero, J.; Del Bene, J. E. Influence of hydrogen bonds on the P ··P pnicogen bond. *J. Chem. Theory Comput.* **2012**, *8*, 2320-2327.

199 . Ma, N.; Zhang, Y.; Ji, B.; Tian, A.; Wang, W. Structural competition between halogen bonds and lone-pair..π interactions in solution. *ChemPhysChem.* **2012**, (13), 1411-1414.

200 . Ghafari Nikoo Jooneghani, S.; Gholipour, A. Mutual cooperation of π-π stacking and pnicogen bond interactions of substituted monomeric Lawesson's reagent and pyridine rings: Theoretical insight into Pyr||X-PhPS2⊥pyr complexes. *Chem. Phys. Lett.* **2019**, *721*, 91-98. DOI: https://doi.org/10.1016/j.cplett.2019.02.027.

201 . Watson, B.; Grounds, O.; Borley, W.; Rosokha, S. V. Resolving the halogen vs. hydrogen bonding dichotomy in solutions: intermolecular complexes of trihalomethanes with halide and pseudohalide anions. *Phys. Chem. Chem. Phys.* **2018**, *20* (34), 21999-

22007, 10.1039/C8CP03505A. DOI: 10.1039/C8CP03505A.

202 . Zhao, Y.; Truhlar, D. G. The M06 suite of density functionals for main group thermochemistry, thermochemical kinetics, noncovalent interactions, excited states, and transition elements: two new functionals and systematic testing of four M06-class functionals and 12 other functionals. *Theor. Chem. Acc.* **2008**, *120*, 215-241.

203 . Dunning, T. H. J. Gaussian basis sets for use in correlated molecular calculations. I. The atoms boron through neon and hydrogen. *J. Chem. Phys.* **1989**, *90*, 1007-1023.

204 . Woon, D. E.; Jr., T. H. D. Gaussian basis sets for use in correlated molecular calculations. V. Core-valence basis sets for boron through neon. *J. Chem. Phys.* **1995**, *103* (11), 4572-4585. DOI: 10.1063/1.470645.

205 . Schuchardt, K. L.; Didier, B. T.; Elsethagen, T.; Sun, L.; Gurumoorthi, V.; Chase, J.; Li, J.; Windus, T. L. Basis Set Exchange: A Community Database for Computational Sciences. *J. Chem. Infor. Model.* **2007**, *47* (3), 1045-1052. DOI: 10.1021/ci600510j.

206 . Ang, S. J.; Ser, C. T.; Wong, M. W. Modeling halogen bonding with planewave density functional theory: Accuracy and challenges. *J. Comput. Chem.* **2019**, *40* (20), 1829-1835. DOI: 10.1002/jcc.25835.

207 . Orlova, A. P.; Jasien, P. G. Halogen bonding in self-assembling systems: A comparison of intra- and interchain binding energies. *Comput. Theor. Chem.* **2018**, *1139*, 63-69. DOI: https://doi.org/10.1016/j.comptc.2018.07.004.

208 . Forni, A.; Pieraccini, S.; Franchini, D.; Sironi, M. Assessment of DFT Functionals for QTAIM Topological Analysis of Halogen Bonds with Benzene. *J. Phys. Chem. A* **2016**, *120* (45), 9071-9080. DOI: 10.1021/acs.jpca.6b07578.

209 . Bauzá, A.; García-Llinás, X.; Frontera, A. Charge-assisted triel bonding

interactions in solid state chemistry: A combined computational and crystallographic study. *Chem. Phys. Lett.* **2016**, *666*, 73-78. DOI: http://dx.doi.org/10.1016/j.cplett.2016.11.010.

210 . Esrafili, M. D.; Vessally, E. A theoretical evidence for cooperative enhancement in aerogen-bonding interactions: Open-chain clusters of $KrOF_2$ and $XeOF_2$. *Chem. Phys. Lett.* **2016**, *662*, 80-85. DOI: http://dx.doi.org/10.1016/j.cplett.2016.09.037.

211 . Mardirossian, N.; Head-Gordon, M. How Accurate Are the Minnesota Density Functionals for Noncovalent Interactions, Isomerization Energies, Thermochemistry, and Barrier Heights Involving Molecules Composed of Main-Group Elements? *J. Chem. Theory Comput.* **2016**, *12* (9), 4303-4325. DOI: 10.1021/acs.jctc.6b00637.

212 . Liao, M. S.; Lu, Y.; Scheiner, S. Performance assessment of density-functional methods for study of charge-transfer complexes. *J. Comput. Chem.* **2003**, *24* (5), 623-631. DOI: doi:10.1002/jcc.10226.

213 . Latajka, Z.; Scheiner, S. Primary and secondary basis set superposition error at the SCF and MP2 levels: H_3N--Li^+ and H_2O--Li^+. *J. Chem. Phys.* **1987**, *87*, 1194-1204.

214 . Boys, S. F.; Bernardi, F. The calculation of small molecular interactions by the differences of separate total energies. Some procedures with reduced errors. *Mol. Phys.* **1970**, *19*, 553-566.

215 . Ditchfield, R. GIAO studies of magnetic shielding in FHF^- and HF. *Chem. Phys. Lett.* **1976**, *40*, 53-56.

216 . Alkorta, I.; Elguero, J. Ab initio hybrid DFT-GIAO calculations of the shielding produced by carbon-carbon bonds and aromatic rings in ^1H NMR spectroscopy. *New J. Chem.* **1998**, 381-385.

217 . Reed, A. E.; Curtiss, L. A.; Weinhold, F. Intermolecular interactions from a natural bond orbital, donor-acceptor viewpoint. *Chem. Rev.* **1988**, *88*, 899-926.

218 . Murray, J. S.; Resnati, G.; Politzer, P. Close contacts and noncovalent interactions in crystals. *Faraday Disc.* **2017**, *203* (0), 113-130, 10.1039/C7FD00062F. DOI: 10.1039/C7FD00062F.

219 . Adhikari, U.; Scheiner, S. The S···N noncovalent interaction: Comparison with hydrogen and halogen bonds. *Chem. Phys. Lett.* **2011**, *514*, 36-39.

220 . Adhikari, U.; Scheiner, S. Sensitivity of pnicogen, chalcogen, halogen and H-bonds to angular distortions. *Chem. Phys. Lett.* **2012**, *532*, 31-35.

221 . Scheiner, S. Detailed comparison of the pnicogen bond with chalcogen, halogen and hydrogen bonds. *Int. J. Quantum Chem.* **2013**, *113*, 1609-1620.

222 . Horn, P. R.; Mao, Y.; Head-Gordon, M. Probing non-covalent interactions with a second generation energy decomposition analysis using absolutely localized molecular orbitals. *Phys. Chem. Chem. Phys.* **2016**, *18* (33), 23067-23079, 10.1039/C6CP03784D. DOI: 10.1039/C6CP03784D.

223 . Schütz, M.; Brdarski, S.; Widmark, P.-O.; Lindh, R.; Karlström, G. The water dimer interaction energy: Convergence to the basis set limit at the correlated level. *J. Chem. Phys.* **1997**, *107*, 4597-4605.

224 . Alcívar León, C. D.; Echeverría, G. A.; Piro, O. E.; Ulic, S. E.; Jios, J. L.; Burgos Paci, M.; Argüello, G. A. The role of halogen C–X1···X2–C contact on the preferred conformation of 2-perhalomethylchromones in solid state. *Chem. Phys.* **2016**, *472*, 142-155. DOI: http://dx.doi.org/10.1016/j.chemphys.2016.03.017.

225 . Chaudhary, P.; Goettel, J. T.; Mercier, H. P. A.; Sowlati-Hashjin, S.; Hazendonk, P.; Gerken, M. Lewis Acid Behavior of SF_4: Synthesis, Characterization, and Computational Study of Adducts of SF_4 with Pyridine and Pyridine Derivatives. *Chem. Eur. J.* **2015**, *21* (16), 6247-6256. DOI: 10.1002/chem.201406359.

226 . Hauchecorne, D.; van der Veken, B. J.; Herrebout, W. A.; Hansen, P. E. A ^{19}F NMR study of C–I···π halogen bonding. *Chem. Phys.* **2011**, *381*, 5-10.

227 . Pinheiro, P. d. S. M.; Rodrigues, D. A.; Alves, M. A.; Tinoco, L. W.; Ferreira, G. B.; de Sant'Anna, C. M. R.; Fraga, C. A. M. Theoretical and experimental characterization of 1,4-N···S σ-hole intramolecular interactions in bioactive N-acylhydrazone derivatives. *New J. Chem.* **2018**, *42* (1), 497-505, 10.1039/C7NJ03543H. DOI: 10.1039/C7NJ03543H.

228 . Del Bene, J. E.; Alkorta, I.; Sanchez-Sanz, G.; Elguero, J. Structures, energies, bonding, and NMR properties of pnicogen complexes $H_2XP{:}NXH_2$ (X = H, CH_3, NH_2, OH, F, Cl). *J. Phys. Chem. A* **2011**, *115*, 13724-13731.

229 . Mokrai, R.; Barrett, J.; Apperley, D. C.; Batsanov, A. S.; Benkő, Z.; Heift, D. Weak Pnictogen Bond with Bismuth: Experimental Evidence Based on Bi−P Through-Space Coupling. *Chem. Eur. J.* **2019**, *25* (16), 4017-4024. DOI: 10.1002/chem.201900266.

230 . Szell, P. M. J.; Cavallo, G.; Terraneo, G.; Metrangolo, P.; Gabidullin, B.; Bryce, D. L. Comparing the Halogen Bond to the Hydrogen Bond by Solid-State NMR Spectroscopy: Anion Coordinated Dimers from 2- and 3-Iodoethynylpyridine Salts. *Chem. Eur. J.* **2018**, *24* (44), 11364-11376. DOI: doi:10.1002/chem.201801279.

231 . Cerreia Vioglio, P.; Catalano, L.; Vasylyeva, V.; Nervi, C.; Chierotti, M. R.;

Resnati, G.; Gobetto, R.; Metrangolo, P. Natural Abundance ^{15}N and ^{13}C Solid-State NMR Chemical Shifts: High Sensitivity Probes of the Halogen Bond Geometry. *Chem. Eur. J.* **2016**, *22* (47), 16819-16828. DOI: 10.1002/chem.201603392.

232 . Thangavadivale, V.; Aguiar, P. M.; Jasim, N. A.; Pike, S. J.; Smith, D. A.; Whitwood, A. C.; Brammer, L.; Perutz, R. N. Self-complementary nickel halides enable multifaceted comparisons of intermolecular halogen bonds: fluoride ligands vs. other halides. *Chem. Sci.* **2018**, *9* (15), 3767-3781, 10.1039/C8SC00890F. DOI: 10.1039/C8SC00890F.

233 . Masoodi, H. R.; Bagheri, S.; Ranjbar, M. Theoretical study of cooperativity between hydrogen bond–hydrogen bond, halogen bond–halogen bond and hydrogen bond–halogen bond in ternary FX…diazine…XF (X = H and Cl) complexes. *Mol. Phys.* **2016**, *114* (23), 3464-3474. DOI: 10.1080/00268976.2016.1236992.

234 . Joesten, M. D.; Schaad, L. J. *Hydrogen Bonding*; Marcel Dekker, 1974.

235 . Grabowski, S. J. Hydrogen Bonding - New Insights. In *Challenges and Advances in Computational Chemistry and Physics*, Leszczynski, J., Ed.; Springer: Dordrecht, Netherlands, 2006.

236 . Badger, R. M.; Bauer, S. H. Spectroscopic studies of the hydrogen bond. II. The shifts of the O-H vibrational frequency in the formation of the hydrogen bond. *J. Chem. Phys.* **1939**, *5*, 839-851.

237 . Joesten, M. D.; Drago, R. S. The validity of frequency shift-enthalpy correlations. I. Adducts of phenol with nitrogen and oxygen donors. *J. Am. Chem. Soc.* **1962**, *84*, 3817-3821.

238 . Osawa, E.; Yoshida, Z. The effects of solvents on the hydrogen bonded OH

stretching frequency. *Spectrochim. Acta* **1967**, *23A*, 2029-2036.

239 . Drago, R. S.; Epley, T. D. Enthalpies of hydrogen bonding and changes in $\Delta\nu_{OH}$ for a series of adducts with substituted phenols. *J. Am. Chem. Soc.* **1969**, *91*, 2883-2890.

240 . Gramstad, T.; Sandström, J. Thioamides and nitriles as proton acceptors in hydrogen bond formation and a discussion of solvent shifts in electronic spectra. *Spectrochim. Acta* **1969**, *25A*, 31-38.

241 . Kasende, O.; Zeegers-Huyskens, T. Infrared study of hydrogen-bonded complexes involving phenol derivatives and polyfunctional bases. 2. 3-methyl-4-pyrimidone, 1-methyl-2-pyrimidone, 1,4,4-trimethylcytosine, and 1,3-dimethyluracil. *J. Phys. Chem.* **1984**, *88*, 2636-2641.

242 . Bangal, P. R.; Chakravorti, S. Excited state proton transfer in indole-s-carboxylic acid and indole-5-carboxylic acid. *J. Phys. Chem. A* **1999**, *103*, 8585-8594.

243 . Rozenberg, M.; Loewenschuss, A.; Marcus, Y. An empirical correlation between stretching vibration redshift and hydrogen bond length. *Physical Chemistry and Chemical Physics* **2000**, *2*, 2699-2702.

244 . Joesten, M. D.; Drago, R. S. The Validity of Frequency Shift-Enthalpy Correlations. I. Adducts of Phenol with Nitrogen and Oxygen Donors. *J. Am. Chem. Soc.* **1962**, *84* (20), 3817-3821. DOI: 10.1021/ja00879a006.

245 . Ghersetti, S.; Lusa, A. Infrared study of hydrogen bonding between various phenols and diphenyl—sulphoxide: Thermodynamic properties. *Spectrochim. Acta* **1965**, *21* (6), 1067-1071. DOI: https://doi.org/10.1016/0371-1951(65)80185-0.

246 . Drago, R. S.; Epley, T. D. Enthalpies of hydrogen bonding and changes in hydroxy

frequency shifts for a series of adducts with substituted phenols. *J. Am. Chem. Soc.* **1969**, *91* (11), 2883-2890. DOI: 10.1021/ja01039a010.

247 . Singh, S.; Murthy, A. S. N.; Rao, C. N. R. Spectroscopic studies of hydrogen bonding in donor-acceptor systems. *Trans. Faraday Soc.* **1966**, *62* (0), 1056-1066, 10.1039/TF9666201056. DOI: 10.1039/TF9666201056.

248 . Rao, C. N. R.; Dwivedi, P. C.; Ratajczak, H.; Orville-Thomas, W. J. Relation between O-H stretching frequency and hydrogen bond energy: Re-examination of the Badger-Bauer rule. *Journal of the Chemical Society. Faraday Transactions.* **1975**, *71*, 955-966.

249 . Rao, C. N. R.; Dwivedi, P. C.; Ratajczak, H.; Orville-Thomas, W. J. Relation between O—H stretching frequency and hydrogen bond energy: re-examination of the Badger–Bauer rule. *Journal of the Chemical Society, Faraday Transactions 2: Molecular and Chemical Physics* **1975**, *71* (0), 955-966, 10.1039/F29757100955. DOI: 10.1039/F29757100955.

250 . Rivera-Rivera, L. A.; McElmurry, B. A.; Scott, K. W.; Lucchese, R. R.; Bevan, J. W. The Badger–Bauer Rule Revisited: Correlation of Proper Blue Frequency Shifts in the OC Hydrogen Acceptor with Morphed Hydrogen Bond Dissociation Energies in OC–HX (X = F, Cl, Br, I, CN, CCH). *J. Phys. Chem. A* **2013**, *117*, 8477-8483.

251 . Spaargaren, K.; Kruk, C.; Molenaar-Langeveld, T. A.; Korver, P. K.; van der Haak, P. J.; de Boer, T. J. Spectroscopic studies on N,N-dimethylamides. II. Substituent effects on infrared carbonyl strething vibrations and hydroxyl frequency shifts of *para*- and *meta*-substituted N,N-dimethylbenzamides and cinnamides. *Spectrochim. Acta* **1972**, *28A*, 965-975.

252 . Purcell, K. F.; Drago, R. S. Theoretical aspects of the linear enthalpy wavenumber shift relation for hydrogen-bonded phenols. *J. Am. Chem. Soc.* **1967**, *89*, 2874-2879.

253 . Zeegers-Huyskens, T. Correlation between the vibrational properties and the energy of the hydrogen bonds - OH...N and OH...O=C systems. *Bull. Soc. Chim. Belg.* **1977**, *86*, 823-832.

254 . McDowell, S. A. C.; Buckingham, A. D. On the Correlation between Bond-Length Change and Vibrational Frequency Shift in Hydrogen-Bonded Complexes: A Computational Study of Y ··HCl Dimers (Y = N2, CO, BF). *J. Am. Chem. Soc.* **2005**, *127* (44), 15515-15520. DOI: 10.1021/ja0543651.

255 . Klein, R. A. Hydrogen bonding in diols and binary diol-water systems investigated using DFT methods. II. Calculated infrared OH-stretch frequencies, force constants, and NMR chemical shifts correlate with hydrogen bond geometry and electron density topology. A reevaluation of geometrical criteria for hydrogen bonding. *J. Comput. Chem.* **2003**, *24*, 1120-1131.

256 . Montero, M. D. A.; Mart ńez, F. A.; Aucar, G. A. Magnetic descriptors of hydrogen bonds in malonaldehyde and its derivatives. *Phys. Chem. Chem. Phys.* **2019**, *21* (36), 19742-19754, 10.1039/C9CP02995H. DOI: 10.1039/C9CP02995H.

257 . Gould, I. R.; Hillier, I. H. The relation between hydrogen-bond strengths and vibrational frequency shifts: a theoretical study of complexes of oxygen and nitrogen proton acceptors and water. *J. Mol. Struct. Theochem* **1994**, *314* (1), 1-8. DOI: https://doi.org/10.1016/0166-1280(94)03796-N.

258 . West, R.; Powell, D. L.; Whatley, L. S.; Lee, M. K. T.; Schleyer, P. v. R. The relative strengths of alkyl halides as proton acceptor groups in hydrogen bonding. *J. Am.*

Chem. Soc. **1962**, *84*, 3221-3222.

259 . Gramstad, T. Studies of hydrogen bonding. Part VII. Hydrogen-bond association of phenol and pentachlorophenol with carbonyl compounds and ethers. *Spectrochim. Acta* **1963**, *19*, 497-508.

260 . West, R.; Powell, D. L.; Lee, M. K. T.; Whatley, L. S. Hydrogen bonding studies. IX. The thermodynamics of hydrogen bonding of phenol to ethers and related compounds. *J. Am. Chem. Soc.* **1964**, *86*, 3227-3229.

261 . Yoshida, Z.; Osawa, E. Intermolecular hydrogen bond inolviing a π-base as the proton acceptor. II. Interaction between phenol and various π-bases. Preliminary infrared study. *J. Am. Chem. Soc.* **1965**, *87*, 1467-1469.

262 . Arnett, E. M.; Joris, L.; Mitchell, E.; Murty, T. S. S. R.; Gorrie, T. M.; Schleyer, P. v. R. Studies of hydrogen-bonded complex formation. III. Thermodynamics of complexing by infrared spectroscopy and calorimetry. *J. Am. Chem. Soc.* **1970**, *92*, 2365-2377.

263 . Abraham, M. H.; Prior, D. V.; Schulz, R. A.; Morris, J. J.; Taylor, P. J. Hydrogen bonding Part 44 Thermodynamics of complexation of 3,5-dichlorophenol with ketones and ethers in cyclohexane: the Badger-Bauer relationship. In *Journal of the Chemical Society, Faraday Transactions*, 1998; Vol. 94, pp 879-885.

264 . Arnett, E. M.; Joris, L.; Mitchell, E.; Murty, T. S. S. R.; Gorrie, T. M.; Schleyer, P. v. R. Hydrogen-bonded complex formation. III. Thermodynamics of complexing by infrared spectroscopy and calorimetry. *J. Am. Chem. Soc.* **1970**, *92* (8), 2365-2377. DOI: 10.1021/ja00711a029.

265 . Sherry, A. D.; Purcell, K. F. Hydrogen bond interactions with sulfur donors. *J. Am.*

Chem. Soc. **1972**, *94* (6), 1848-1853. DOI: 10.1021/ja00761a010.

266 . Chandra, A. K.; Zeegers-Huyskens, T. Theoretical study of the cooperativity in substituted dimethyl ethers complexed with two water molecules. Red or blue shifts of the ν(CH) vibrations? *Chem. Phys.* **2013**, *410*, 66-70.

267 . Karpfen, A.; Kryachko, E. S. On the intramolecular origin of the blue shift of A-H stretching frequencies: Triatomic hydrides HAX. *J. Phys. Chem. A* **2009**, *113*, 5217-5223.

268 . Katsumoto, Y.; Komatsu, H.; Ohno, K. Origin of the blue shift of the CH stretching band for 2-butoxyethanol in water. *J. Am. Chem. Soc.* **2006**, *128*, 9278-9279.

269 . Jabłoński, M.; Sadlej, A. J. Blue-Shifting Intramolecular C−H···O Interactions. *J. Phys. Chem. A* **2007**, *111* (17), 3423-3431. DOI: 10.1021/jp068799+.

270 . Jablonski, M. Blue-shifting intramolecular C-H···O(S) contacts in sterically strained systems. *J. Mol. Struct. (Theochem)* **2007**, *820*, 118-127.

271 . Joseph, J.; Jemmis, E. D. Red-, blue-, or no-shift hydrogen bonds: A unified explanation. *J. Am. Chem. Soc.* **2007**, *129*, 4620-4632.

272 . Purcell, K. F.; Stikeleather, J. A.; Brunk, S. D. Linear enthalpy-spectral shift correlations for 1,1,1,3,3,3-hexafluoro-2-propanol. *J. Am. Chem. Soc.* **1969**, *91*, 4019-4027.

273 . Harris, R. K.; Jackson, P.; Merwin, L. H.; Say, B. J.; Haegele, G. Perspectives in high-resolution solid-state nuclear magnetic resonance, with emphasis on combined rotation and multiple-pulse spectroscopy. *J. Chem. Soc., Faraday Trans. 1* **1988**, *84* (11), 3649-3672.

274 . Dohnal, V.; Tkadlecova, M. A simple relation between ^{1}H NMR data and mixing enthalpy for systems with complex formation by hydrogen bonding. *J. Phys. Chem. B* **2002**, *106*, 12307-12310.

275 . Trujillo, C.; Rozas, I.; Elguero, J.; Alkorta, I.; Sánchez-Sanz, G. Modulating intramolecular chalcogen bonds in aromatic (thio)(seleno)phene-based derivatives. *Phys. Chem. Chem. Phys.* **2019**, *21* (42), 23645-23650, 10.1039/C9CP03694F. DOI: 10.1039/C9CP03694F.

276 . Del Bene, J. E.; Alkorta, I.; Elguero, J. Potential Energy Surfaces of $HN(CH)SX:CO_2$ for X = F, Cl, NC, CN, CCH, and H: N ··C Tetrel Bonds and O ··S Chalcogen Bonds. *J. Phys. Chem. A* **2019**, *123* (33), 7270-7277. DOI: 10.1021/acs.jpca.9b04144.

277 . Esrafili, M. D.; Vakili, M.; Javaheri, M.; Sobhi, H. R. Tuning of tetrel bonds interactions by substitution and cooperative effects in XH_3Si ··NCH ··HM (X = H, F, Cl, Br; M = Li, Na, BeH and MgH) complexes. *Mol. Phys.* **2016**, *114* (12), 1974-1982. DOI: 10.1080/00268976.2016.1174786.

278 . Bauzá, A.; Seth, S. K.; Frontera, A. Tetrel bonding interactions at work: Impact on tin and lead coordination compounds. *Coord. Chem. Rev.* **2019**, *384*, 107-125. DOI: https://doi.org/10.1016/j.ccr.2019.01.003.

279 . Politzer, P.; Murray, J. S. A look at bonds and bonding. *Struct. Chem.* **2019**, *30* (4), 1153-1157, journal article. DOI: 10.1007/s11224-019-01364-3.

280 . Zierkiewicz, W.; Wysokiński, R.; Michalczyk, M.; Scheiner, S. Chalcogen bonding of two ligands to hypervalent YF_4 (Y = S, Se, Te, Po). *Phys. Chem. Chem. Phys.* **2019**, *21* (37), 20829-20839, 10.1039/C9CP04006D. DOI: 10.1039/C9CP04006D.

281 . Legon, A. C. Tetrel, pnictogen and chalcogen bonds identified in the gas phase before they had names: a systematic look at non-covalent interactions. *Phys. Chem. Chem. Phys.* **2017**, *19* (23), 14884-14896, 10.1039/C7CP02518A. DOI: 10.1039/C7CP02518A.

282 . Mukherjee, A.; Tothadi, S.; Desiraju, G. R. Halogen Bonds in Crystal Engineering: Like Hydrogen Bonds yet Different. *Acc. Chem. Res.* **2014**, *47* (8), 2514-2524. DOI: 10.1021/ar5001555 (acccessed 2014/08/19).

283 . McDowell, S. A. C.; Joseph, J. A. Destabilization of the halogen bond in complexes of protonated NCX (X = F, Cl, Br) molecules. *Chem. Phys. Lett.* **2014**, *603*, 37-40.

284 . Zhuo, H.; Li, Q. Novel pnicogen bonding interactions with silylene as an electron donor: covalency, unusual substituent effects and new mechanisms. *Phys. Chem. Chem. Phys.* **2015**, *17* (14), 9153-9160, 10.1039/C5CP00187K. DOI: 10.1039/C5CP00187K.

285 . Mundlapati, V. R.; Sahoo, D. K.; Bhaumik, S.; Jena, S.; Chandrakar, A.; Biswal, H. S. Noncovalent Carbon-Bonding Interactions in Proteins. *Angew. Chem. Int. Ed.* **2018**, *57* (50), 16496-16500. DOI: doi:10.1002/anie.201811171.

286 . Metrangolo, P.; Resnati, G. Halogen Bonding: A Paradigm in Supramolecular Chemistry. *Chem. Eur. J.* **2001**, *7* (12), 2511-2519. DOI: 10.1002/1521-3765(20010618)7:12<2511::AID-CHEM25110>3.0.CO;2-T.

287 . Chi, Z.; Yan, T.; Li, Q.; Scheiner, S. Violation of Electrostatic Rules: Shifting the Balance between Pnicogen Bonds and Lone Pair−π Interactions Tuned by Substituents. *J. Phys. Chem. A* **2019**, *123* (33), 7288-7295. DOI: 10.1021/acs.jpca.9b06864.

288 . Forni, A.; Pieraccini, S.; Rendine, S.; Sironi, M. Halogen bonds with benzene: An

assessment of DFT functionals. *J. Comput. Chem.* **2014**, *35*, 386-394.

289 . Bauzá, A.; Alkorta, I.; Frontera, A.; Elguero, J. On the Reliability of Pure and Hybrid DFT Methods for the Evaluation of Halogen, Chalcogen, and Pnicogen Bonds Involving Anionic and Neutral Electron Donors. *J. Chem. Theory Comput.* **2013**, *9*, 5201-5210.

290 . Georg, H. C.; Fileti, E. E.; Malaspina, T. Ab initio study of weakly bound halogen complexes: RX···PH_3. *J. Mol. Model.* **2013**, *19*, 329-336.

291 . Lu, J.; Scheiner, S. Effects of Halogen, Chalcogen, Pnicogen, and Tetrel Bonds on IR and NMR Spectra. *Molecules* **2019**, *24* (15), 2822.

292 . Michalczyk, M.; Zierkiewicz, W.; Wysokiński, R.; Scheiner, S. Theoretical Studies of IR and NMR Spectral Changes Induced by Sigma-Hole Hydrogen, Halogen, Chalcogen, Pnicogen, and Tetrel Bonds in a Model Protein Environment. *Molecules* **2019**, *24* (18), 3329.

293 . Noro, T.; Sekiya, M.; Koga, T. Sapporo-(DKH3)-nZP (n = D, T, Q) sets for the sixth period s-, d-, and p-block atoms. *Theor. Chem. Acc.* **2013**, *132*. DOI: 10.1007/s00214-013-1363-7.

294 . Noro, T.; Sekiya, M.; Koga, T. Segmented contracted basis sets for atoms H through Xe: Sapporo-(DK)-nZP sets (n = D, T, Q). *Theor. Chem. Acc.* **2012**, *131* (2), 1124, journal article. DOI: 10.1007/s00214-012-1124-z.

295 . Karpfen, A. On the interaction of propynal with HNO, HF, HCl, H2O, CH3OH, and NH3: Red- and blue-shifting hydrogen bonds and tetrel bonds. *Comput. Theor. Chem.* **2019**, *1160*, 1-13. DOI: https://doi.org/10.1016/j.comptc.2019.05.010.

296 . Oliveira, B. G. Theoretical estimation of pnicogen bonds and hydrogen bonds in

small heterocyclic complexes: Red-shifts and blue-shifts ruled by polarization effects. *Chem. Phys.* **2014**, *443* (0), 67-75. DOI: http://dx.doi.org/10.1016/j.chemphys.2014.09.001.

297 . Zierkiewicz, W.; Czarnik-Matusewicz, B.; Michalska, D. Blue shifts and unusual intensity changes in the infrared spectra of the enflurane ··acetone complexes: Spectroscopic and theoretical studies. *J. Phys. Chem. A* **2011**, *115*, 11362-11368.

298 . Shirhatti, P. R.; Wategaonkar, S. Blue shifted hydrogen bond in 3-methylindole·CHX_3 complexes (X = Cl, F). *Phys. Chem. Chem. Phys.* **2010**, *12*, 6650-6659.

299 . Poater, J.; Fradera, X.; Solà, M.; Duran, M.; Simon, S. On the electron-pair nature of the hydrogen bond in the framework of the atoms in molecules theory. *Chem. Phys. Lett.* **2003**, *369* (1), 248-255. DOI: https://doi.org/10.1016/S0009-2614(02)01928-0.

300 . Scheiner, S. Ability of IR and NMR Spectral Data to Distinguish between a Tetrel Bond and a Hydrogen Bond. *J. Phys. Chem. A* **2018**, *122* (39), 7852-7862. DOI: 10.1021/acs.jpca.8b07631.

301 . Kumar, V.; Xu, Y.; Leroy, C.; Bryce, D. L. Direct investigation of chalcogen bonds by multinuclear solid-state magnetic resonance and vibrational spectroscopy. *Phys. Chem. Chem. Phys.* **2020**, *22* (7), 3817-3824, 10.1039/C9CP06267J. DOI: 10.1039/C9CP06267J.

APPENDICES

Appendix A. Permission Letters for Journal Copyright Release

JOHN WILEY AND SONS LICENSE
TERMS AND CONDITIONS
Aug 21, 2023

This Agreement between Ms. JIA LU ("You") and John Wiley and Sons ("John Wiley and Sons") consists of your license details and the terms and conditions provided by John Wiley and Sons and Copyright Clearance Center.

License Number	5613451157717
License date	Aug 21, 2023
Licensed Content Publisher	John Wiley and Sons
Licensed Content Publication	Chemistry - A European Journal
Licensed Content Title	Halogen, Chalcogen, and Pnicogen Bonding Involving Hypervalent Atoms
Licensed Content Author	Steve Scheiner, Jia Lu
Licensed Content Date	May 9, 2018
Licensed Content Volume	24
Licensed Content Issue	32
Licensed Content Pages	11
Type of use	Dissertation/Thesis
Requestor type	Author of this Wiley article
Format	Electronic

Portion	Full article
Will you be translating?	No
Title	The Computational Study about Noncovalent Bonding Systems Involving Halogen, Chalcogen and Pnicogen Bonds
Institution name	Utah State University
Expected presentation date	Aug 2023
Requestor Location	Ms. JIA LU 1273 N 400 E Apt 4 Logan UT 84341 LOGAN, UT 84341 United States Attn: Ms. Jia Lu
Publisher Tax ID	EU826007151
Total	0.00 USD

Terms and Conditions

TERMS AND CONDITIONS

This copyrighted material is owned by or exclusively licensed to John Wiley & Sons, Inc. or one of its group companies (each a"Wiley Company") or handled on behalf of a society with which a Wiley Company has exclusive publishing rights in relation to a particular work (collectively "WILEY"). By clicking "accept" in connection with completing this licensing transaction, you agree that the following terms and conditions apply to this transaction (along with the billing and payment terms and conditions established by the Copyright Clearance Center Inc., ("CCC's Billing and Payment terms and conditions"), at the time that you opened your RightsLink account (these are available at any time at http://myaccount.copyright.com).

Terms and Conditions

- The materials you have requested permission to reproduce or reuse (the "Wiley Materials") are protected by copyright.
- You are hereby granted a personal, non-exclusive, non-sub licensable (on a stand-alone basis), non-transferable, worldwide,

limited license to reproduce the Wiley Materials for the purpose specified in the licensing process. This license, **and any CONTENT (PDF or image file) purchased as part of your order,** is for a one-time use only and limited to any maximum distribution number specified in the license. The first instance of republication or reuse granted by this license must be completed within two years of the date of the grant of this license (although copies prepared before the end date may be distributed thereafter). The Wiley Materials shall not be used in any other manner or for any other purpose, beyond what is granted in the license. Permission is granted subject to an appropriate acknowledgement given to the author, title of the material/book/journal and the publisher. You shall also duplicate the copyright notice that appears in the Wiley publication in your use of the Wiley Material. Permission is also granted on the understanding that nowhere in the text is a previously published source acknowledged for all or part of this Wiley Material. Any third party content is expressly excluded from this permission.

- With respect to the Wiley Materials, all rights are reserved. Except as expressly granted by the terms of the license, no part of the Wiley Materials may be copied, modified, adapted (except for minor reformatting required by the new Publication), translated, reproduced, transferred or distributed, in any form or by any means, and no derivative works may be made based on the Wiley Materials without the prior permission of the respective copyright owner.**For STM Signatory Publishers clearing permission under the terms of the STM Permissions Guidelines only, the terms of the license are extended to include subsequent editions and for editions in other languages, provided such editions are for the work as a whole in situ and does not involve the separate exploitation of the permitted figures or extracts,** You may not alter, remove or suppress in any manner any copyright, trademark or other notices displayed by the Wiley Materials. You may not license, rent, sell, loan, lease, pledge, offer as security, transfer or assign the Wiley Materials on a stand-alone basis, or any of the rights granted to you hereunder to any other person.

- The Wiley Materials and all of the intellectual property rights therein shall at all times remain the exclusive property of John Wiley & Sons Inc, the Wiley Companies, or their respective licensors, and your interest therein is only that of having possession of and the right to reproduce the Wiley Materials pursuant to Section 2 herein during the continuance of this Agreement. You agree that you own no right, title or interest in

or to the Wiley Materials or any of the intellectual property rights therein. You shall have no rights hereunder other than the license as provided for above in Section 2. No right, license or interest to any trademark, trade name, service mark or other branding ("Marks") of WILEY or its licensors is granted hereunder, and you agree that you shall not assert any such right, license or interest with respect thereto

- NEITHER WILEY NOR ITS LICENSORS MAKES ANY WARRANTY OR REPRESENTATION OF ANY KIND TO YOU OR ANY THIRD PARTY, EXPRESS, IMPLIED OR STATUTORY, WITH RESPECT TO THE MATERIALS OR THE ACCURACY OF ANY INFORMATION CONTAINED IN THE MATERIALS, INCLUDING, WITHOUT LIMITATION, ANY IMPLIED WARRANTY OF MERCHANTABILITY, ACCURACY, SATISFACTORY QUALITY, FITNESS FOR A PARTICULAR PURPOSE, USABILITY, INTEGRATION OR NON-INFRINGEMENT AND ALL SUCH WARRANTIES ARE HEREBY EXCLUDED BY WILEY AND ITS LICENSORS AND WAIVED BY YOU.

- WILEY shall have the right to terminate this Agreement immediately upon breach of this Agreement by you.

- You shall indemnify, defend and hold harmless WILEY, its Licensors and their respective directors, officers, agents and employees, from and against any actual or threatened claims, demands, causes of action or proceedings arising from any breach of this Agreement by you.

- IN NO EVENT SHALL WILEY OR ITS LICENSORS BE LIABLE TO YOU OR ANY OTHER PARTY OR ANY OTHER PERSON OR ENTITY FOR ANY SPECIAL, CONSEQUENTIAL, INCIDENTAL, INDIRECT, EXEMPLARY OR PUNITIVE DAMAGES, HOWEVER CAUSED, ARISING OUT OF OR IN CONNECTION WITH THE DOWNLOADING, PROVISIONING, VIEWING OR USE OF THE MATERIALS REGARDLESS OF THE FORM OF ACTION, WHETHER FOR BREACH OF CONTRACT, BREACH OF WARRANTY, TORT, NEGLIGENCE, INFRINGEMENT OR OTHERWISE (INCLUDING, WITHOUT LIMITATION, DAMAGES BASED ON LOSS OF PROFITS, DATA, FILES, USE, BUSINESS OPPORTUNITY OR CLAIMS OF THIRD PARTIES), AND WHETHER OR NOT THE PARTY HAS BEEN ADVISED OF THE POSSIBILITY OF SUCH DAMAGES. THIS LIMITATION

SHALL APPLY NOTWITHSTANDING ANY FAILURE OF ESSENTIAL PURPOSE OF ANY LIMITED REMEDY PROVIDED HEREIN.

- Should any provision of this Agreement be held by a court of competent jurisdiction to be illegal, invalid, or unenforceable, that provision shall be deemed amended to achieve as nearly as possible the same economic effect as the original provision, and the legality, validity and enforceability of the remaining provisions of this Agreement shall not be affected or impaired thereby.

- The failure of either party to enforce any term or condition of this Agreement shall not constitute a waiver of either party's right to enforce each and every term and condition of this Agreement. No breach under this agreement shall be deemed waived or excused by either party unless such waiver or consent is in writing signed by the party granting such waiver or consent. The waiver by or consent of a party to a breach of any provision of this Agreement shall not operate or be construed as a waiver of or consent to any other or subsequent breach by such other party.

- This Agreement may not be assigned (including by operation of law or otherwise) by you without WILEY's prior written consent.

- Any fee required for this permission shall be non-refundable after thirty (30) days from receipt by the CCC.

- These terms and conditions together with CCC's Billing and Payment terms and conditions (which are incorporated herein) form the entire agreement between you and WILEY concerning this licensing transaction and (in the absence of fraud) supersedes all prior agreements and representations of the parties, oral or written. This Agreement may not be amended except in writing signed by both parties. This Agreement shall be binding upon and inure to the benefit of the parties' successors, legal representatives, and authorized assigns.

- In the event of any conflict between your obligations established by these terms and conditions and those established by CCC's Billing and Payment terms and conditions, these terms and conditions shall prevail.

- WILEY expressly reserves all rights not specifically granted in the combination of (i) the license details provided by you and accepted in the course of this licensing transaction, (ii) these

terms and conditions and (iii) CCC's Billing and Payment terms and conditions.

- This Agreement will be void if the Type of Use, Format, Circulation, or Requestor Type was misrepresented during the licensing process.

- This Agreement shall be governed by and construed in accordance with the laws of the State of New York, USA, without regards to such state's conflict of law rules. Any legal action, suit or proceeding arising out of or relating to these Terms and Conditions or the breach thereof shall be instituted in a court of competent jurisdiction in New York County in the State of New York in the United States of America and each party hereby consents and submits to the personal jurisdiction of such court, waives any objection to venue in such court and consents to service of process by registered or certified mail, return receipt requested, at the last known address of such party.

WILEY OPEN ACCESS TERMS AND CONDITIONS

Wiley Publishes Open Access Articles in fully Open Access Journals and in Subscription journals offering Online Open. Although most of the fully Open Access journals publish open access articles under the terms of the Creative Commons Attribution (CC BY) License only, the subscription journals and a few of the Open Access Journals offer a choice of Creative Commons Licenses. The license type is clearly identified on the article.

The Creative Commons Attribution License

The Creative Commons Attribution License (CC-BY) allows users to copy, distribute and transmit an article, adapt the article and make commercial use of the article. The CC-BY license permits commercial and non-

Creative Commons Attribution Non-Commercial License

The Creative Commons Attribution Non-Commercial (CC-BY-NC)License permits use, distribution and reproduction in any medium, provided the original work is properly cited and is not used for commercial purposes.(see below)

Creative Commons Attribution-Non-Commercial-NoDerivs License

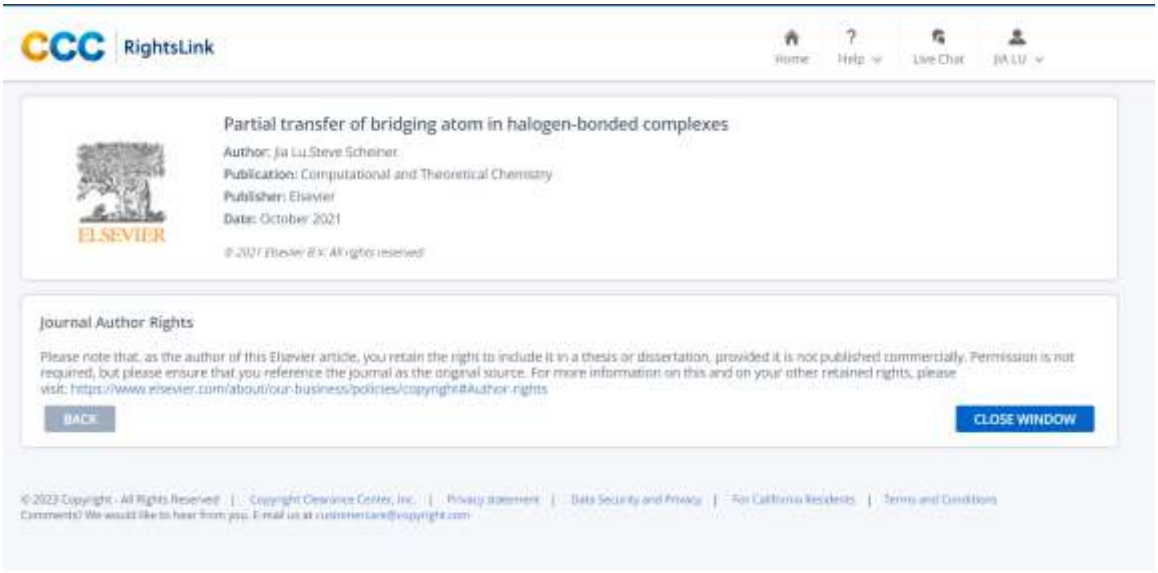
CCC RightsLink
Home
Help
Live Chat
JIA LU
Partial transfer of bridging atom in halogen-bonded complexes
Author: Jia Lu,Steve Scheiner
Publication: Computational and Theoretical Chemistry
Publisher: Elsevier
Date: October 2021
© 2021 Elsevier B.V. All rights reserved
ELSEVIER
Journal Author Rights
Please note that, as the author of this Elsevier article, you retain the right to include it in a thesis or dissertation, provided it is not published commercially. Permission is not required, but please ensure that you reference the journal as the original source. For more information on this and on your other retained rights, please visit: https://www.elsevier.com/about/our-business/policies/copyright#Author-rights
BACK
CLOSE WINDOW
© 2023 Copyright - All Rights Reserved | Copyright Clearance Center, Inc. | Privacy statement | Data Security and Privacy | For California Residents | Terms and Conditions
Comments? We would like to hear from you. E-mail us at customercare@copyright.com


MDPI
Journals
Topics
Information
Author Services
Initiatives
About
Submit
Search for Articles:
Search
Advanced
Information
For Authors
For Reviewers
For Editors
For Librarians
For Publishers
For Societies
For Conference Organizers
MDPI Open Access Information and Policy
Permissions

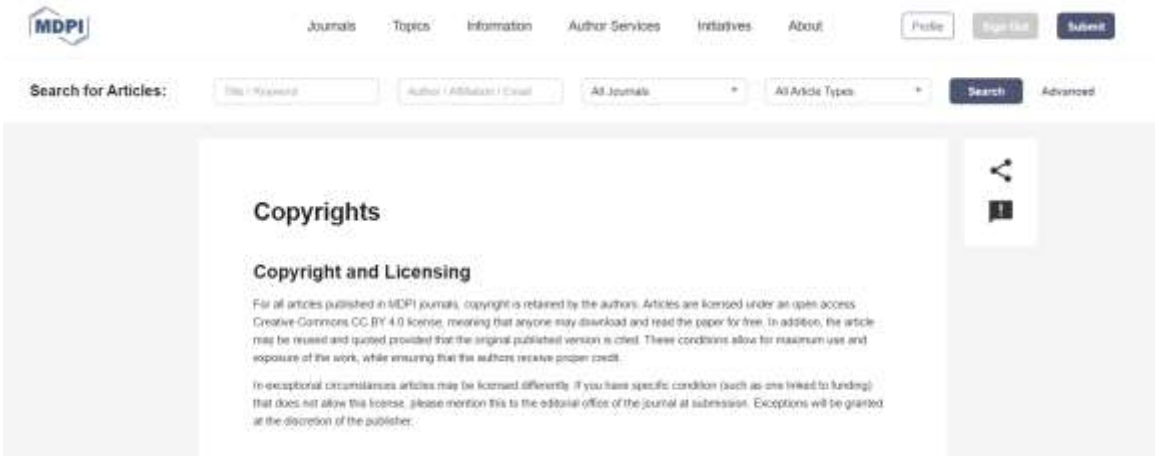
MDPI
Journals
Topics
Information
Author Services
Initiatives
About
Submit
Search for Articles:
Search
Advanced
Copyrights
Copyright and Licensing

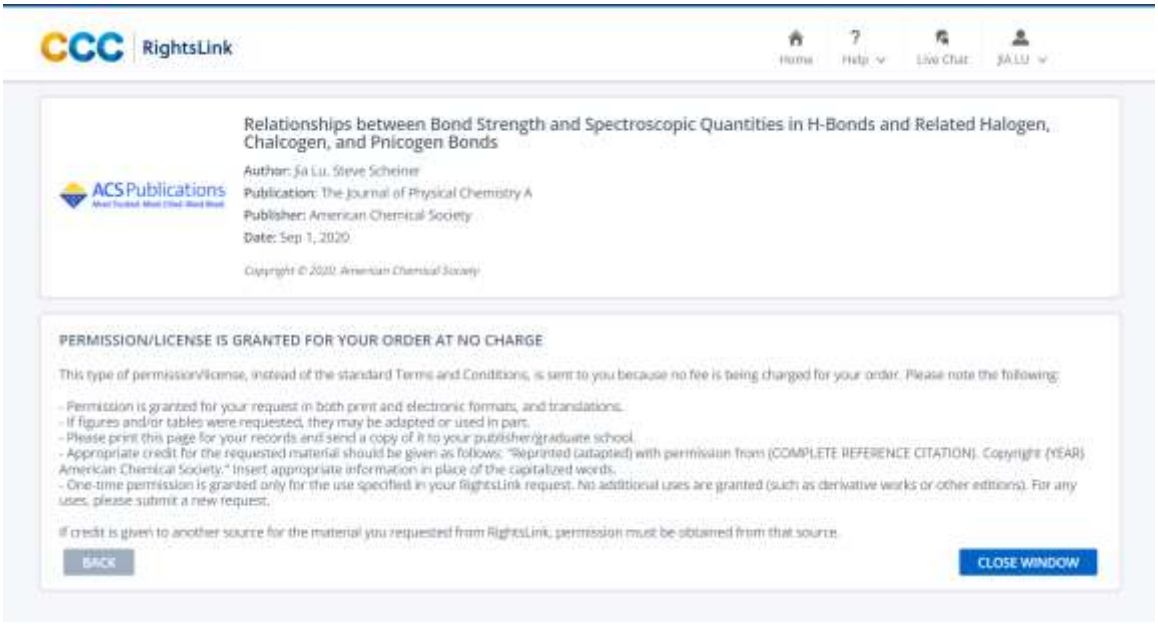

CCC RightsLink

Home Help Live Chat JIA LU

ACS Publications

Relationships between Bond Strength and Spectroscopic Quantities in H-Bonds and Related Halogen, Chalcogen, and Pnicogen Bonds

Author: Jia Lu, Steve Scheiner

Publication: The Journal of Physical Chemistry A

Publisher: American Chemical Society

Date: Sep 1, 2020

Copyright © 2020, American Chemical Society

PERMISSION/LICENSE IS GRANTED FOR YOUR ORDER AT NO CHARGE

This type of permission/license, instead of the standard Terms and Conditions, is sent to you because no fee is being charged for your order. Please note the following:

- Permission is granted for your request in both print and electronic formats, and translations.
- If figures and/or tables were requested, they may be adapted or used in part.
- Please print this page for your records and send a copy of it to your publisher/graduate school.
- Appropriate credit for the requested material should be given as follows: "Reprinted (adapted) with permission from (COMPLETE REFERENCE CITATION). Copyright (YEAR) American Chemical Society." Insert appropriate information in place of the capitalized words.
- One-time permission is granted only for the use specified in your RightsLink request. No additional uses are granted (such as derivative works or other editions). For any uses, please submit a new request.

If credit is given to another source for the material you requested from RightsLink, permission must be obtained from that source.

BACK CLOSE WINDOW

Appendix B. Permission Letters from Coauthors

Jia Lu
Department of Chemistry and Biochemistry
Utah State University
0300 Old Main Hill
Logan, UT 84322-0300

Aug 6, 2023

Prof. Steve Scheiner
Department of Chemistry and Biochemistry
Utah State University
0300 Old Main Hill
Logan, UT 84322-0300
Email: steve.scheiner@usu.edu

I hereby give permission to Jia Lu to reprint the following publications in part or in full in her thesis and dissertation:

1. Lu, J.; Scheiner, S. Partial transfer of bridging atom in halogen-bonded complexes. Computational and Theoretical Chemistry 2021, 1204, 113398.

2. Lu, J.; Scheiner, S. Relationships between Bond Strength and Spectroscopic Quantities in H-Bonds and Related Halogen, Chalcogen, and Pnicogen Bonds. The Journal of Physical Chemistry A 2020, 124 (38), 7716-7725.

3. Lu, J.; Scheiner, S. Effects of Halogen, Chalcogen, Pnicogen, and Tetrel Bonds on IR and NMR Spectra. Molecules 2019, 24, 2822.

4. Lu, J.; Scheiner, S. Comparison of halogen with proton transfer. Symmetric and asymmetric systems. Chemical Physics Letters 2019, 731, 136593.

5. Scheiner, S.; Lu, J. Halogen, Chalcogen, and Pnicogen Bonding involving Hypervalent Atoms. Chem. Eur. J. 2018, 24, 8167-8177.

Sincerely,

Steve Scheiner